Finnmarkian Monazite EMP ages in the Central belt of the Seve Nappe, north Jämtland/south Västerbotten, Sweden

Msc Thesis

Michiel Gademan

Supervisor: Herman Van Roermund

Department of Earth Sciences, Faculty of Geosciences, Utrecht University, Budapestlaan 4, Utrecht, 3508 TA, Netherlands

1 Abstract

In this Msc thesis an age dating project is described on high grade gneisses of the Central Belt of the Seve Nappe Complex, Central Sweden. The age dating is done with an Electron Microprobe applied to monazites. The units dated are the Lillfjället gneiss, Avardo gneiss and the Svartsjöbäcken schist (Western Belt) located in the upper and central parts of the Seve Nappe Complex, Swedish Caledonides, Jämtland, Sweden. The Lillfjället gneiss has a T_0 age of 497.9 +/- 20 Ma, the Avardo gneiss 502.3 +/- 20 Ma and the Svartsjöbäcken schist 491.2 +/- 22 Ma. All Electron Micro Probe (EMP) monazite ages are interpreted to be the result of the same tectonometamorphic event; the Finnmarkian. During the chemical age dating a standard monazite was used with known age of 1125 Ma. The measurements gave a mean apparent age for the standard monazite of 1132.7 Ma +/- 10 Myr. In addition the PT-conditions are determined for the Lillfjället gneiss. This is done by thermobarometry and with the computer program Domino. Calculated PT conditions are 750 – 800 ºC and 9 – 10 kbar for the Lillfjället gneiss. The calculated metamorphic conditions and age data are used to construct a geodynamic model for the area. This model explains the regional tectonometamorphic setting between the Finnmarkian (~500 Ma) and the Scandian (~420 Ma) orogeny resulting in two collisional events with corresponding subduction and eduction in the surrounding area.

2 Index

3 Introduction

Mountain building events are not completely understood. How do they form? What components are involved? What role do microcontinents play? What happens with subducted material?

The plate tectonic theory is generally accepted. Two tectonic plates collide against each other to form a mountain chain. When an oceanic plate collides with a continental plate the oceanic plate subducts beneath the continental plate because of the higher density. The oceanic plate is probably littered with microcontinents as the oceanic plates are today. This means that the microcontinents will also collide with the continental plate during convergence. These collisions will be local and will probably take place at different moments in space and time. Part of the microcontinent may become part of the continental plate during collision, while another part subducts beneath the continental plate. The microcontinents will be deformed and metamorphosed. Part of the subducted microcontinent may return back to the surface after slab break off.

To investigate this, research is done in an old mountain chain where a cross section is exposed through a deeply eroded mountain chain. The mountain chain is called the Scandinavian Caledonides.

The Scandinavian Caledonides is build of different nappe stacks, called allochthons, which have been thrust from east to west, onto the Baltic shield. The nappes can be divided into four different complexes: the Lower, Middle, Upper and Uppermost Allochthons (Roberts & Gee, 1985) (figure 3-1). The Allochthons consists of different rocks with different ages, metamorphic grades and structures. Proposed is that the Allochthons originate due to (at least) three different collisional events called the Finnmarkian orogeny (~500 Ma), the (proposed) Jämtlandian orogeny (454 Ma) (Brueckner & Van Roermund 2004) and the Scandian orogeny (between 430 and 400 Ma) (Brueckner & Van Roermund 2004, Roberts (2003).

This research project will focus on the Seve Nappe Complex (SNC). The SNC is located in N Jämtland and S. Västerbotten, Sweden (figure 3-1). In the seventies and eighties this area is mapped by Dutch geology students of the University of Leiden, the

Netherlands, supervised by H.J. Zwart. The SNC belongs to the Middle Allochthon and is in the west overlain by the Köli Nappe Complex (KNC) which belongs to the Upper Allochthon. In the east the SNC is underlain by the Särv Nappe and other units of the Middle and Lower Allochthon.

The SNC, which is studied, is divided into three different belts: the Western, the Central and the Eastern belts. All belts are north-south running belts on the map with an overall gentle dip to the west. From the structurally higher Western belt to the underlying Central belt the metamorphic grade increases from low amphibolite to upper amphibolite to granulite facies. This metamorphic zoning becomes inverted going to the Eastern belt, which is of a lower grade, amphibolite facies (Zwart 1974, Roermund & Bakker 1984). In the central part of the SNC (in the investigated area) the Western belt is missing due to truncation by the overlying KNC (figure 4-2).

The aim of this project is to date the high grade mineral assemblage in the southern and central part of the Central belt, using the monazite age dating method: i.e. monazites are dated with the Electron Microprobe (EMP). In addition some samples are dated from the Western Belt. The monazite ages will be combined with metamorphic PT conditions to construct a new geodynamic model that can explain the regional geology of the SNC. As such the model will give new insights about the fundamental question whether Caledonian Nappe transport in this part of the Scandinavian Caledonides occurred during one or more orogenic events widely separated in time, and or space, or not. It will also try to explain how different metamorphic units can be located next to each other.

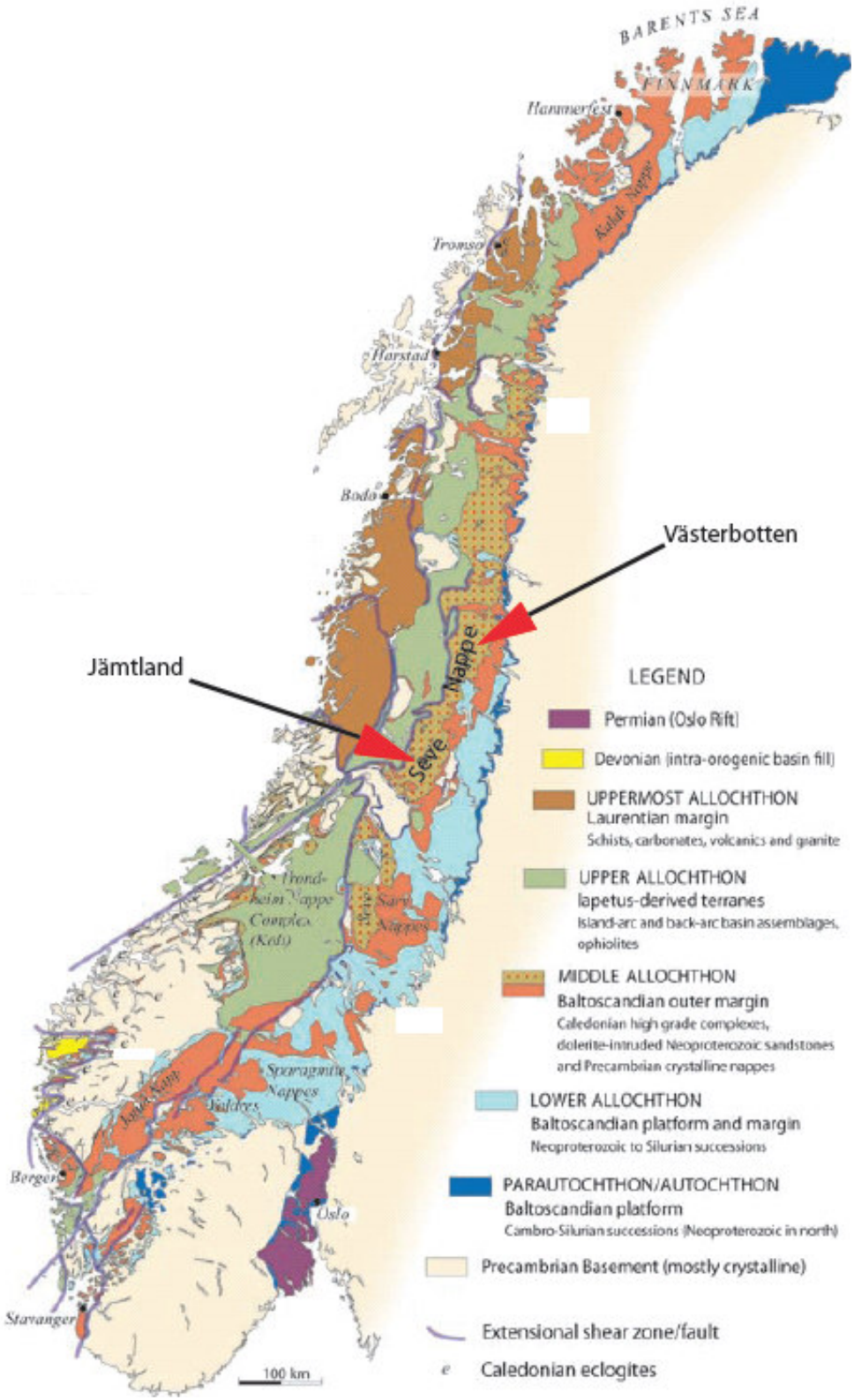

Figure 3-1 Location of the different Allochthons. After Gee et al. 2008.

4 The Caledonian Orogeny

4.1 Baltic shield

The Baltic shield consists of several Precambrian domains formed in Archean-Neoproterozoic. In the Early Archean, microcontinents formed until the first accretionary event, the Svecofennian orogeny (1.75 – 2.0 Ga), in mid Proterozoic time. This orogeny introduced a new stage of crustal formation followed by the Gothian orogeny (1.5 – 1.75 Ga). At this time most of present day Baltica was accreted to form the Baltoscandian platform (Gaál and Gorbatcheb 1987). This period is followed by a quiet period until the Sveconorwegian orogeny (1.25 – 0.9 Ga). The Sveconorwegian period is not a period of accretion and formation of new crust but reworking of the older crust. By 0.9 Ga this period was ended. At the end of this period Baltica formed part of a new supercontinent named Rhodinia, positioned at the lower hemisphere (figure 4-1).

4.2 Caledonian plate configuration

The supercontinent Rhodinia broke up around 750 – 800 Ma (Torsvik & Cocks, 2005), resulting in the formation of several new continents: Laurentia, Baltica, Siberia and Gondwana (figure 4-1a). At ~650 Ma Baltica started to rift away from the remaining parts of Rhodinia (Gondwana) and at ~600 Ma the Iapetus ocean was formed in between Laurentia and Baltica (Cocks & Torsvik, 2006). Convergence starts at ~520 Ma resulting in closure of the Iapetus Ocean and the ultimate collision between Baltica and Laurentia to form Laurussia. The latter collisional events, discussed in more detail below, formed the Caledonides (500 – 380 Ma), in Scandinavian called the Scandinavian Caledonides.

To get a general overview of the plate configuration a reconstruction of Roberts (2003), based on work of Torsvik (1996, 1998) and Torsvik and Cocks (2002), is illustrated in figure 4-1. In the figure the different tectonic events with the corresponding collisions according to Roberts are displayed. Two main collisional events are accepted, the first,

the Finnmarkian event (~500 Ma) where a microcontinent collide with a volcanic arc in the Iapetus Ocean and second the Scandian event (400 – 425 Ma) where Laurentia collide with Baltica (i.e. Brueckner & Roermund, 2004; Roberts 2003). Below different tectonic models are described.

Not relevant here is the discussion whether Baltica rotated anticlockwise or not in the time interval 480 – 440Ma (figure 4-1). One of the models below shows this anticlockwise rotation while the other model does not. This does not result in major differences. The plate configuration below (Roberts 2003; figure 4-1) is based on rotation of Baltica.

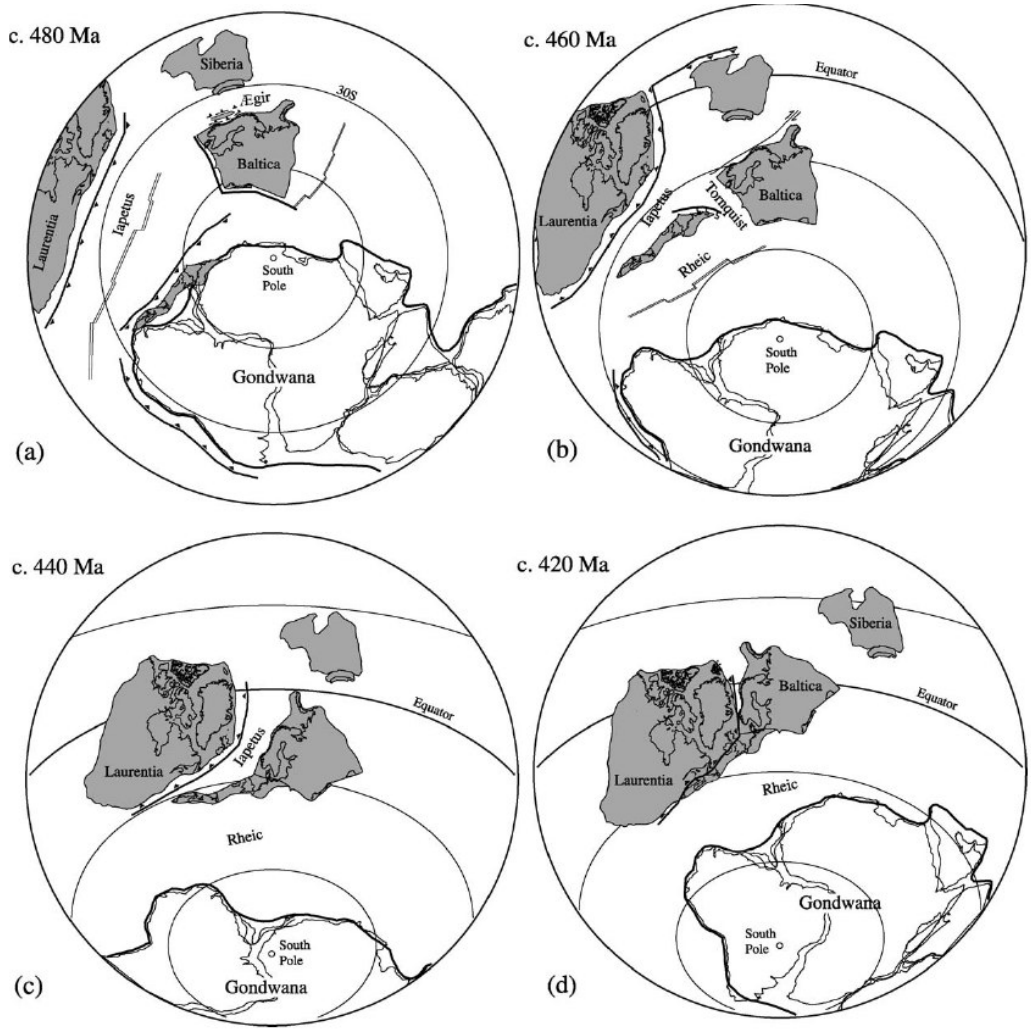

Figure 4-1 Paleomagnetic reconstruction of Roberts (2003), based on work of Torsvik (1996, 1998) and Torsvik and Cocks (2002). Indication of the plate tectonic configuration during collisional events of the Caledonide orogeny.

4.3 Scandinavian Caledonides

The Scandinavian Caledonides are now exposed over a length of 1800 km in western Scandinavia, from Finnmark in northern Norway at 71ºN latitude, southwards through western Sweden and Norway to the Oslo district in Norway at 59 ºN. The mountain chain has a width of at most 300 km and is cut by glacial valleys leaving nice geological cross sections. The Caledonides is build of thrust nappes which were transported eastward. The thrust nappes have metasedimentary and igneous rock types varying from Late Proterozoic through to Devonian age along with pre-Caledonian crystalline basement rocks. The thrust nappes are separated into different units (Allochthons) by Roberts & Gee (1985), called the Lower, Middle and Upper Allochthon. At some locations in the west a fourth unit is identified which is called the Uppermost Allochthon (figure 3-1).

The Lower Allochthon consists of late Proterozoic and Early Paleozoic sediments with very little basement involvement. The metamorphic grade is greenschist or sub-greenschist facies (Roberts & Gee, 1985).

The Middle Allochthon is largely composed of strongly deformed Precambrian crystalline rocks and thick, largely Late Proterozoic, psammites. Some areas are intruded by dolerites. The metamorphic grade of the whole complex varies between middle greenschist to granulite facies (Gee et al, 2010). The SNC belongs to the Middle Allochthon and consists of gneisses and amphibolites with locally eclogites and peridotite bodies.

The Upper Allochthon consists of the Köli Nappe Complex (KNC), which has a low metamorphic grade varying from greenschist to high amphibolite facies (Gee et al, 2010).

The Uppermost Allochthon consists of schists and gneisses with a dominant metamorphic grade of amphibolite facies. Some of the schists and gneisses have pre-Caledonian protoliths age (Roberts & Gee, 1985).

The Autochthon is the Precambrian crystalline basement of the Baltic Shield. The autochthon is overlain by all Allochthons and is still outcropping in the North and East (fig 3-1). The Parautochthon consists of blackshales of Middle to Late Cambrian age. At some places the blackshales cover the crystalline basement and at other places some

sediments are deposited in between. The Parautochthon unit acts as a solethrust over which the Lower Allochthon is transported (Roberts & Gee (1985), Gee et al (2008)).

4.4 Seve Nappe

The SNC was at first classified in the Upper Allochthon because of the metamorphic grade (Roberts & Gee, 1985). More recently the SNC is classified as part of the Middle Allochthon because the Seve Nappe has more affinity with the metasedimentary units of those in the Middle Allochthon (Gee et al. 2008). The Seve Nappe is overlain in the west by the KNC, which belongs to the Upper Allochthon, and is underlain by the Särv Nappe and lower units of the Middle and Lower Allochthons in the east (Zwart, 1974). The difference between the KNC and the SNC is that the KNC is oceanic in origin and the SNC is transitional to continental, this means that this is a transition zone in some way.

The Seve Nappe is subdivided in three belts, the Eastern belt, Central belt and the Western belt (figure 4-2).

The Western belt which overlies the Central belt consists of garnet-micaschist (Svartsjöbäcken schist), and amphibolites with a metamorphic grade which is generally, low-medium amphibolite facies (Zwart (1974), Trouw (1973)). The contact between the Köli sequence and the Svartsjöbäcken schist is tectonic. The Western belt is missing in the south (figure 4-2).

The Central belt consists of kyanite-k-feldspar gneiss (Marsfjället gneiss), quartzo feldspathic gneiss, amphibolites, sillimanite-gneiss (Lillfjället gneiss) and at some places eclogites. The average metamorphic grade of the Central belt is upper amphibolite to granulite facies. The contact between the Western belt and Central belt is badly exposed, so the contact could be gradational or tectonic (Zwart, 1974).

The Eastern belt, underlying the Central belt consists of a large variety of foliated rocks: for example, garnet-mica schists, marbles, kyanite-staurolite schists, quartzo-feldspathic gneisses, amphibolites, quartzites and garnet-biotite rocks (Zwart, 1974; Roermund & Bakker, 1984). The metamorphic grade of the Eastern belt is generally amphibolite facies. An exception is found in the Sjouten unit (figure 4-2) which consists

dominantly of quarto feldspathic rocks with micaschists, eclogite and garnet peridotite. It's a HPT lens but is not further described. The metamorphic contact between the Eastern- and Central belt is usually a mylonite zone, the contact between the Eastern belt and the Särv Nappe is also tectonic.

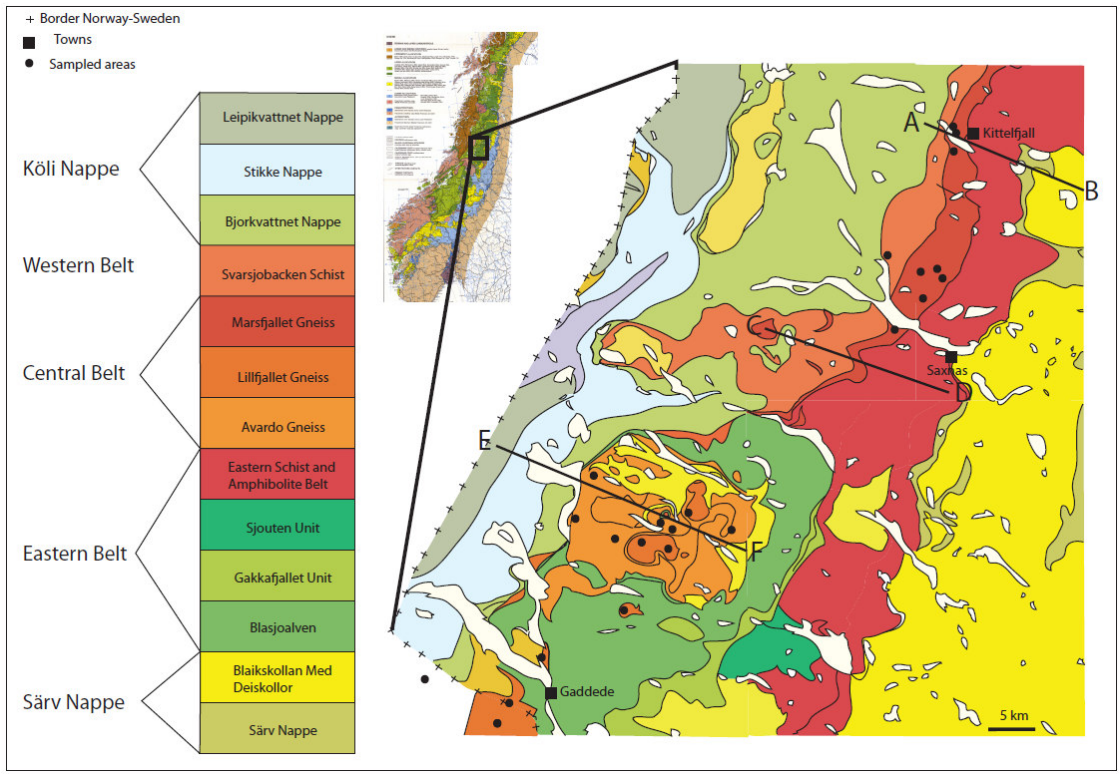

Figure 4-2 Geological map outlining the fieldwork area in North Jämtland and Southern Västerbotten, central Sweden. Dark points indicate areas where samples are taken (see appendix 1.13 for (GPS) location), squares to major towns. Each dark point indicates more than one sample. The lines AB, CD and EF indicate cross sections shown in figure 4-4. Scale ~1:750.000. (Sveriges Geologiska Undersokning, 1991).

The complexity of the Seve Nappe is that the metamorphic grade increases from the Eastern belt upwards to the Central belt and than decreases again to the Western belt, an inversion of the metamorphic grade. Another complexity is that the Central belt can also be subdivided from north to south into three different units having the same metamorphic grade (refers to T) but different metamorphic facies (refers to P) (figure 4-3). The northern part consists of the kyanite-k-feldspar gneisses, called the Marsfjället gneiss.

This is interpreted to originate at medium pressure granulite facies (650 – 1000 °C and 12.5 – 18 kbar) because metabasic rocks are not converted into eclogites: cpx-plag-grt (Trouw, 1973). The middle unit consists of an eclogite bearing gneiss, called the Avardo gneiss. The Avardo gneiss has undergone the highest metamorphic pressure conditions (metabasic rocks are converted into eclogites) (650 – 1000 °C and ≥18 kbar). Most southern the sillimanite gneiss is found, called Lillfjället gneiss. The Lillfjället gneiss has undergone the lowest pressure, (metabasic rocks contain 2 pyr-plag; no garnet) lower granulite facies (650 – 1000 °C and 8 – 12.5 kbar) (figure 4-3).

In figure 4-4 cross sections are shown of the area described above, the exact locations of the cross sections are shown in figure 4-2. The Allochthon stacks are shown with the westward dip in all three profiles. In the profiles are the relative positions shown of the Marsfjället gneiss, Avardo gneiss and Svartsjöbäcken schist. The Lillfjället gneiss is located more to the south of the profiles. To the south the Western belt containing the Svartsjöbäcken schist disappeared.

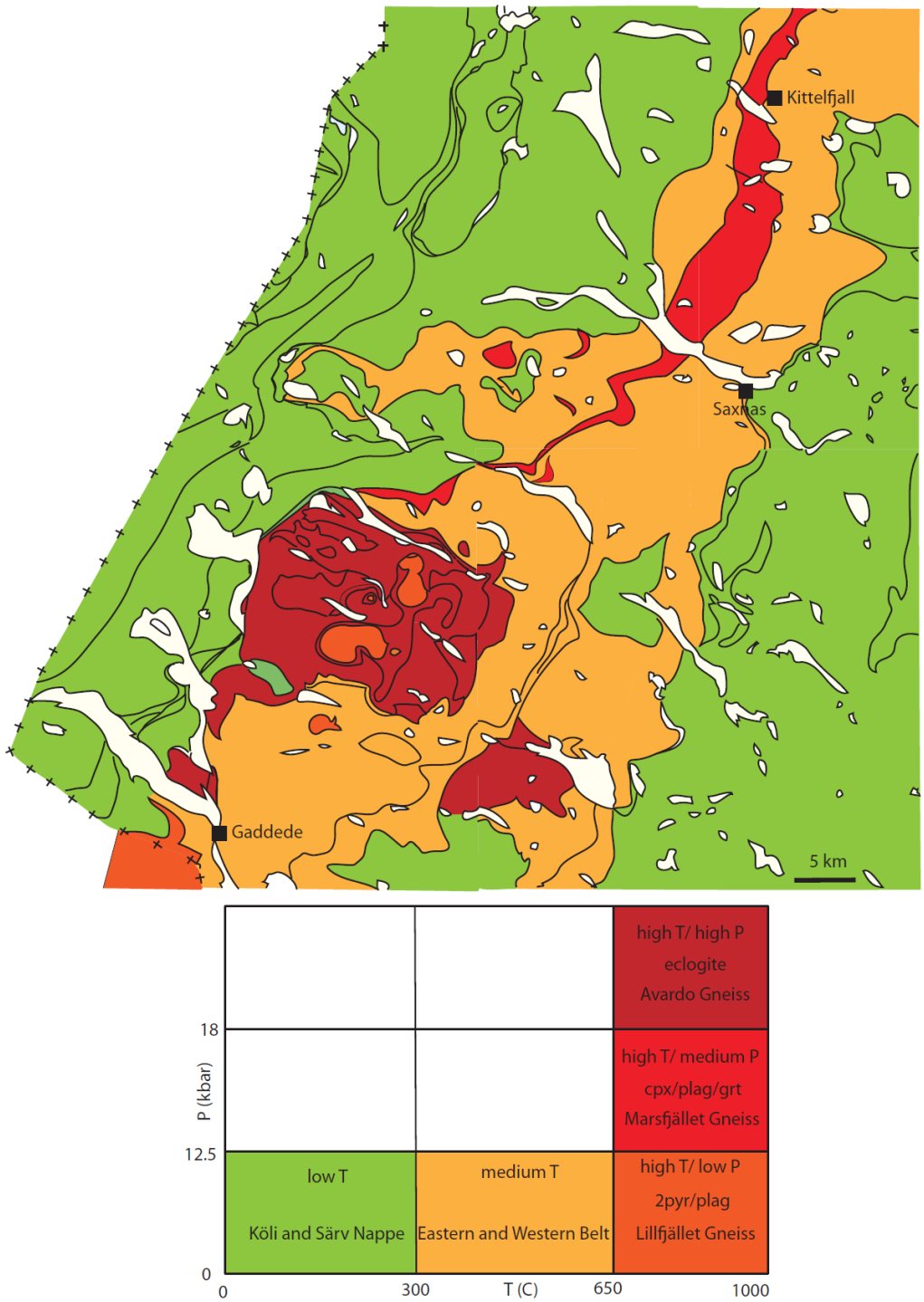

Figure 4-3 Metamorphic facies map. The Central belt is subdivided in three different zones; high pressure, medium pressure and low pressure units. The eastern and western belt is indicated as medium temperature and low pressure. The Koli Nappe and Lower Nappes are indicated as low temperature and low pressure. The high T/high P area in the south east is not the Avardo gneiss but another HP tectonic lens positioned in the Eastern belt; Tjelike.

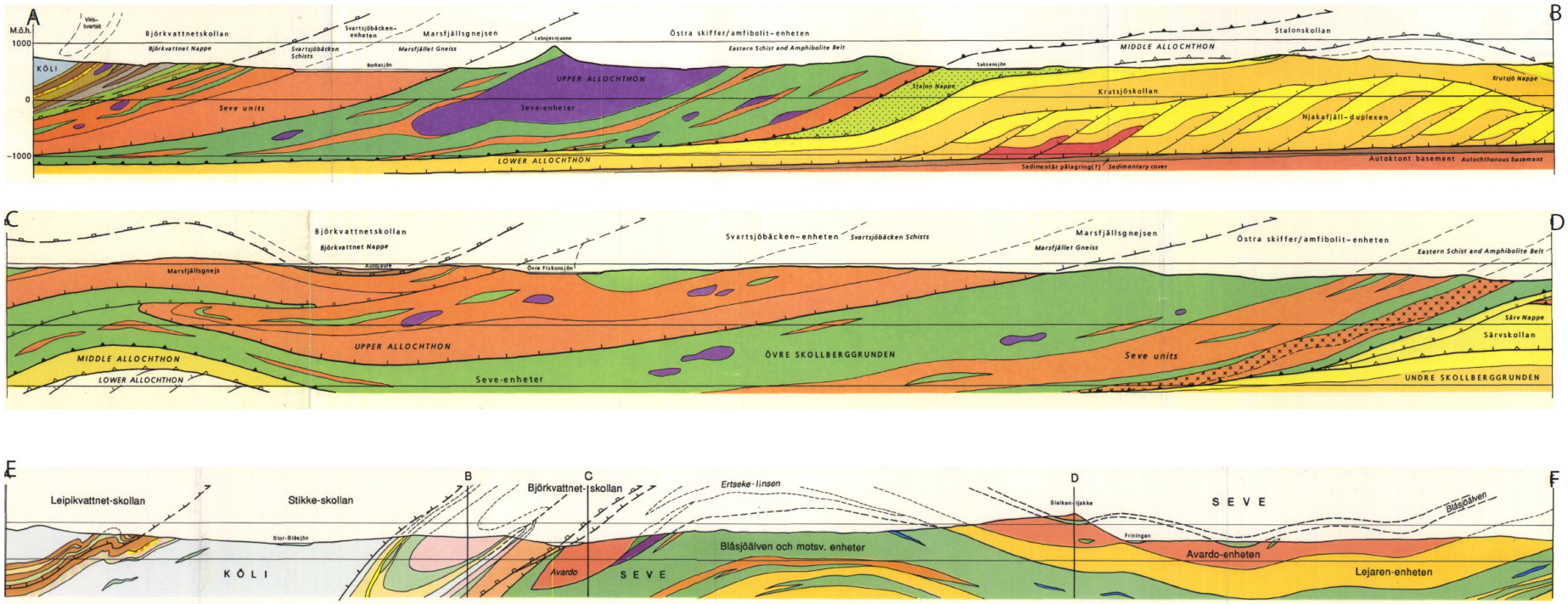

Figure 4-4 East-west cross sections through the Seve Nappe. Locations of profiles AB, CD and EF are indicated in figure 4-2. In these cross sections the Seve Nappe is still classified as Upper Allochthon (Sveriges Geologiska Undersokning, 1991).

4.5 Recent plate tectonic models for the formation of the Scandinavian Caledonides

Brueckner & Van Roermund (2004) have recognized four orogenic events for the formation of the Scandinavian Caledonides i.e.; the two classic events Finnmarkian (~500 Ma) and Scandian (400 – 425 Ma), the Jamtländian (~454 Ma) and a simultaneous fourth event that occurred along the Laurentian-Iapetus margin (western Iapetus). The model is based on what is called dunk tectonics: each orogenic event involves an initial collision between an oceanic and a continental plate (followed by (micro) continent-continent collision). First the undergoing plate is subducted (deep) into the mantle. This is caused by slab pull generated by the denser oceanic lithosphere. The slab pull is sufficient to pull subcontinental lithosphere and continental crust into the mantle. Finally the slab pull is balanced by the positive buoyancy of the continental crust. When the forces are balanced the subducting oceanic slab breaks off (i.e. Wortel & Spakman, 2000). The oceanic lithosphere will sink deeper into the mantle while the continental crust tends to move upwards (eduction/exhumation) (figure 4-5). This buoyancy driven eduction/exhumation can bring the metamorphosed continental crust back to the surface i.e. to subcrustal levels. Dunk tectonics is a subduction/eduction model. The continental crust may contain, after ultra high pressure (UHP) conditions, coesite and microdiamands. The latter may be replaced by lower pressure minerals during exhumation/eduction. Dunk tectonics can also explain the introduction of mantle wedge peridotites (Van Roermund, 2009). Both index minerals coesite and microdiamands thus indicate how deep continental subduction is, and refer to UHP metamorphic conditions. This is however one possible scenario referring to the deepest subduction depths reported so far; the slab can also ‘break’ off at lower subduction depths so the metamorphism of the subducted continental crust will be of lower metamorphic grade.

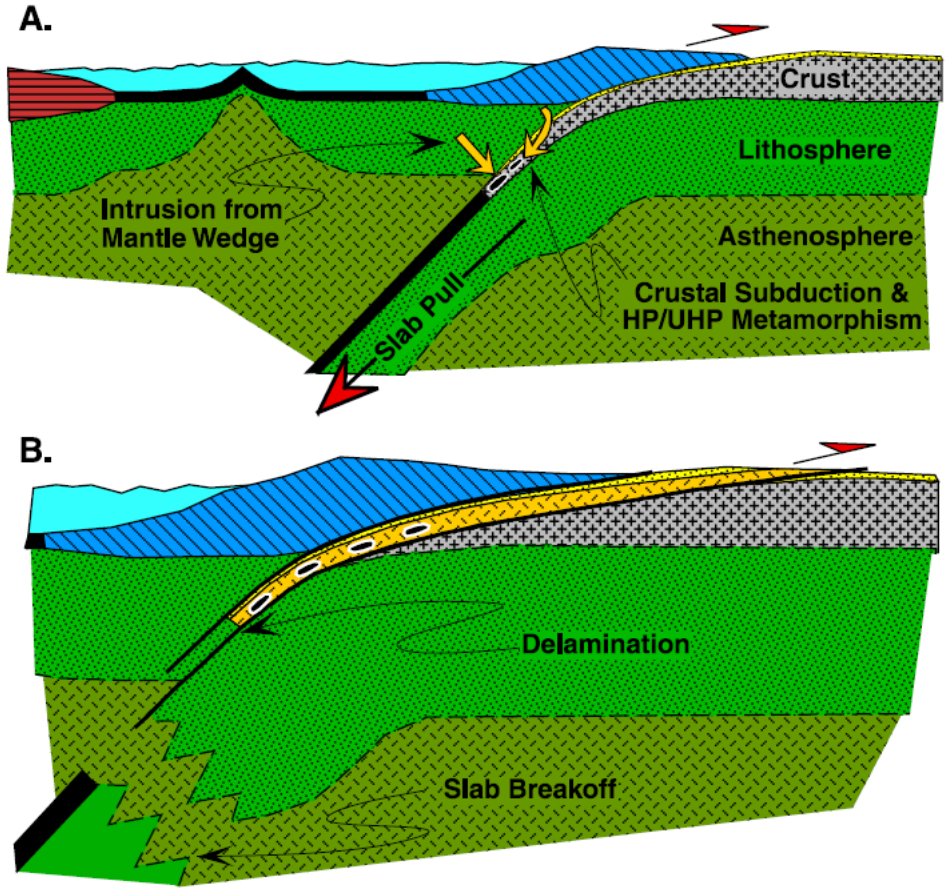

Figure 4-5 Simplified subduction/eduction model for an arc-continent collision. a) Subduction of oceanic lithosphere with continental crust. In additions intrusion from mantle wedge takes place. b) Slab break off, oceanic lithosphere moves downwards, continental crust upwards. After Brueckner & Van Roermund 2004.

Multiple subduction/eduction events are forming the backbone of the model of Brueckner & Van Roermund (2004). This should not be surprising if the Iapetus Ocean or Ægir Sea were as littered with microcontinents and arcs as the Pacific Ocean is today. If this is the case multiple subduction/eduction events could have occurred at the same moment in time but at different locations. The model used by Brueckner & Van Roermund (2004) illustrated in figure 4-6A, consists of the following components: A. Baltica; B. an ocean of unknown width; C. a microcontinent; D. eastern Iapetus; E. Virisen Arc; F. western Iapetus; G. Laurentia. All components were formed during the break-up of Rhodinia except for the Virisen arc.

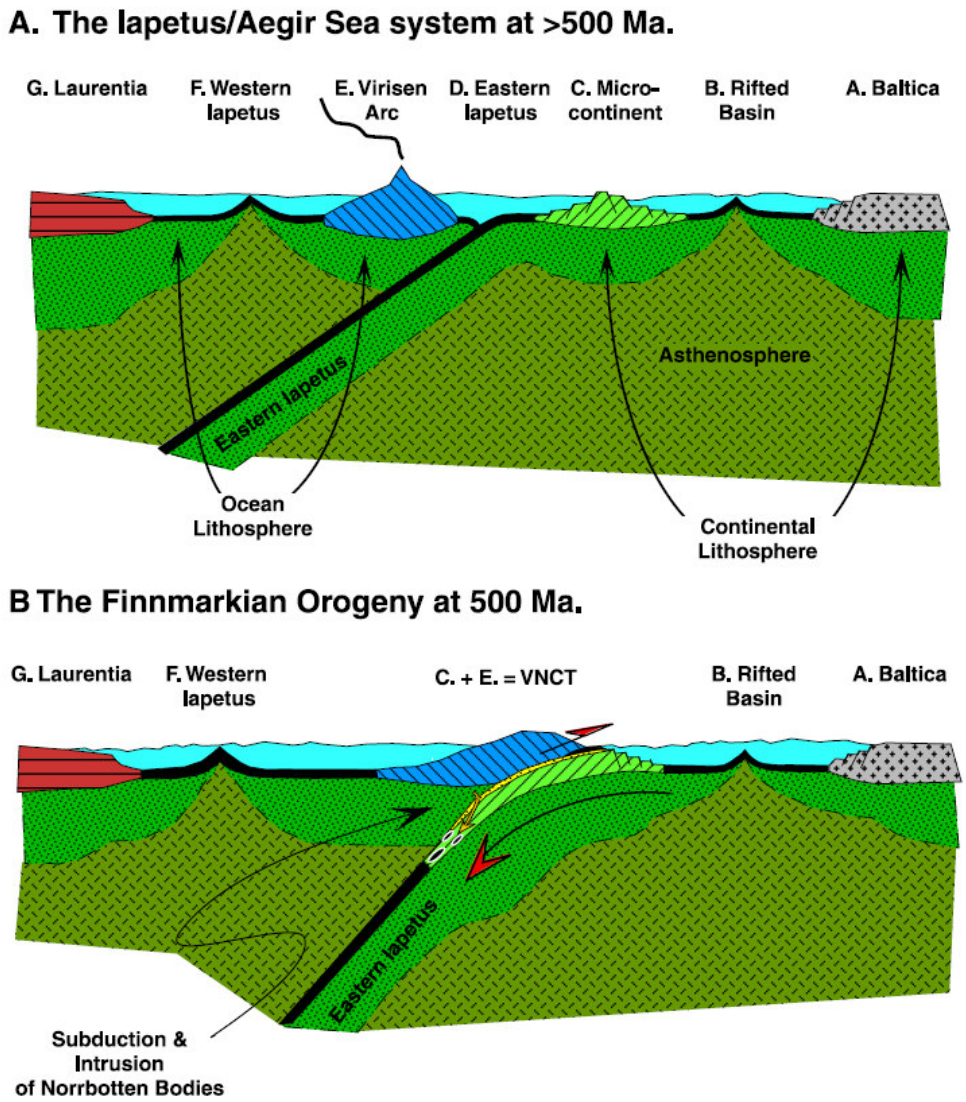

Figure 4-6 Subduction/eduction model. a) Original components of the model after Brueckner & Van Roermund (2004). b) Subduction of the microcontinent under the Virisen arc to eclogite facies and introduction of the subduction zone peridotite from the overlying mantle wedge. VNCT = Virisen/Norbotten Composite Terrane. After Brueckner & Van Roermund (2004).

During the Finnmarkian orogeny a microcontinent and oceanic plate (Eastern Iapetus) is pulled down below the Virisen Island Arc, an island arc formed during closure of central Iapetus (now part of the lower Köli Nappe) (figure 4-6 B). Fragments of the mantle became incorporated into the subducting slab and were carried deeper into the mantle by the subducting slab. All rocktypes (peridotite, metabasic rocks and continent basement gneiss) underwent HP metamorphism to form garnet-pyroxene-olivine

assemblages in the peridotite body, eclogites in the metabasic rocks (Van Roermund, 1989) and kyanite-k-feldspar assemblages in the gneisses. Then after the weight of the subducted oceanic lithosphere is over compensated by the buoyancy force of the subducted continental crust slab brake off occurred. The slab brake off is followed by eduction of the continental plate to subcrustal levels.

After the Finnmarkian orogeny the Virisen/Norbotten Composite Terrane (VNCT) was still separated by Baltica by an ocean of unknown width (figure 4-6b). Continued converging between 500 and 454 Ma resulted in subduction of Baltica beneath the VNCT, called the Jamtländian orogeny (figure 4-7 A).

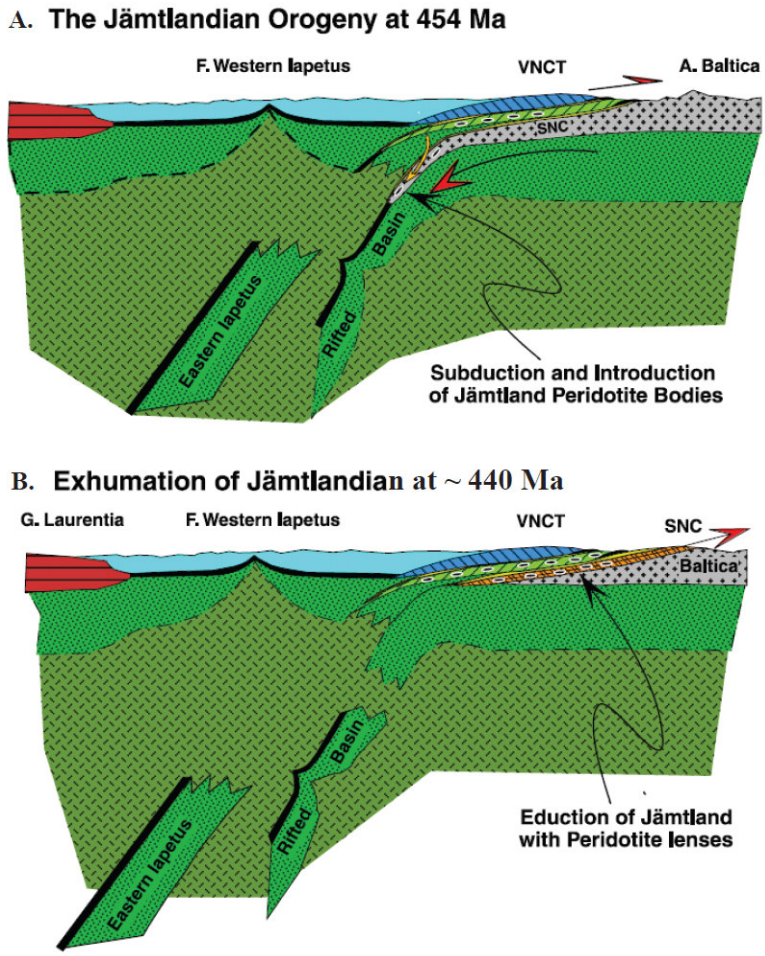

Figure 4-7 Subduction/eduction model of the Jamtländian orogeny. A) Baltica subducts beneath the VNCT to "eclogite facies". In addition insertion of peridotite with subcontinental affinity from the mantle wedge into the subducted crust takes place. B) Eduction of the HP Jamtländian terrane, during which it becomes emplaced further eastward over the Baltic Shield. SNC = Seve Nappe Complex. After Brueckner & Van Roermund (2004).

Similar to the Finnmarkian orogeny peridotite may be inserted in the subducted continental crust but with the difference that in this case the mantle wedge consists of subcontinental lithosphere. This peridotite body is metamorphosed to “eclogite facies” together with the host rock to form garnet peridotite. Then it educts back again (to subcrustal levels) at 440 Ma where it is emplaced on the Baltic Shield (figure 4-7 B).

The Iapetus is still closing between 454 Ma and 425 Ma, resulting in the subduction of western Iapetus (figure 4-7a) under Laurentia. At around 430 Ma Laurentia starts to collide with Baltica and Baltica starts to subduct beneath Laurentia (figure 4-8 A) resulting in the Scandinavian orogeny. During the Scandian earlier Nappe complex can be transported further to the east.

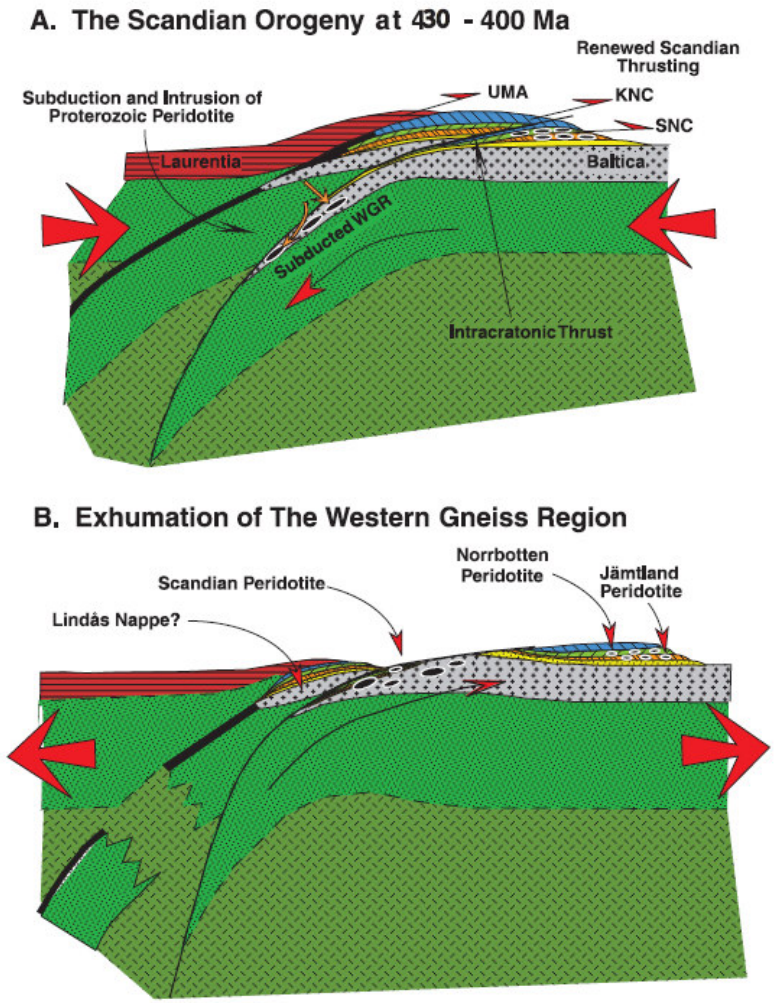

Figure 4-8 Subduction/eduction model for the Scandian orogeny. A) Collision between Laurentia and Baltica causing eastward thrust motions between earlier boundaries and the emplacement of the

Uppermost Allochthon on top of the other Allochthons and subduction of the Western Gneiss Region (WGR). B) Post-Scandian exhumation of the WGR caused by extension of the Scandinavian Caledonides. UMA = Uppermost Allochthon. After Brueckner & Van Roermund (2004).

During the Scandian Laurentia is thrusted over Baltica to form the Uppermost Allochthon above KNC. The Scandian orogeny also caused further eastward thrust motions along reactivated older boundaries (i.e. between KNC and SNC) and subduction of the Western Gneiss Region (WGR). This subduction stage is also considered to involve peridotite emplacement into the subducting slab. The peridotite could be Archean-Proterozoic in age with Laurentian or Baltic affinity. Then the WGR educts/exhumes back to the surface, first by buoyancy (eduction) subsequently followed by Post-Scandian extension related to final collapse of the orogen (figure 4-8 B).

The second model is the model of Roberts (2003). Roberts's model starts with the Finnmarkian orogeny (~520 – 500 Ma) using another configuration: Baltica collided with Siberia with the Ægir Sea in between containing a magmatic arc under which Baltica subducts (figure 4-9). The subduction of Baltica beneath the magmatic arc undergoes "eclogite facies" metamorphic conditions. This is followed by rapid eduction/exhumation and emplacement of the nappes on the Baltica Shield.

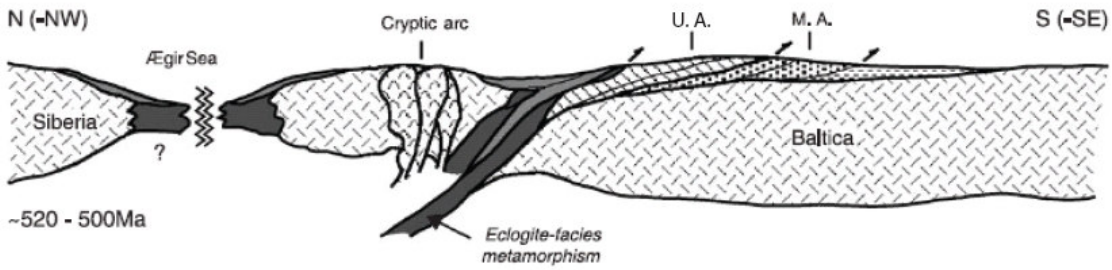

Figure 4-9 Schematic configuration of the Finnmarkian event. The subducting plate underwent "eclogite facies" conditions; this was followed by rapid exhumation and emplacement of Finnmarkian nappes. UA = Upper Allochthon; MA = Middle Allochthon. After Roberts (2003).

The next event is the Trondheim event (480 – 475 Ma) which is especially recognized in the area around Trondheim (Norway) more south than the cross-sections discussed

above. A microcontinent, rifted off from Baltica in earlier times, causes oceanward subduction and obduction of ophiolitic assemblages (figure 4-10). The subducting slab undergoes at least blueschist metamorphic conditions. In this time Baltica started to face Laurentia.

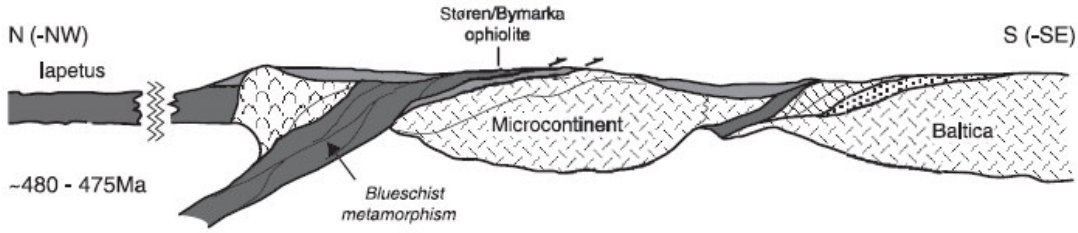

Figure 4-10 Schematic configuration of the Trondheim event. Oceanward subduction, to at least blueschist metamorphic conditions, along a microcontinental edge that is rifted off of Baltica in earlier times. Also obduction of ophiolites. After Roberts (2003).

The Taconian event (~470 – 450 Ma) is an event that is recognized at the other side of the Iapetus Ocean where Laurentia collides with a volcanic arc complex. This is now recognized in the Uppermost Allochthon and to some extent within the Köli Nappe. The subduction is again oceanward so to the (E)SE instead of N(NW) (figure 4-11).

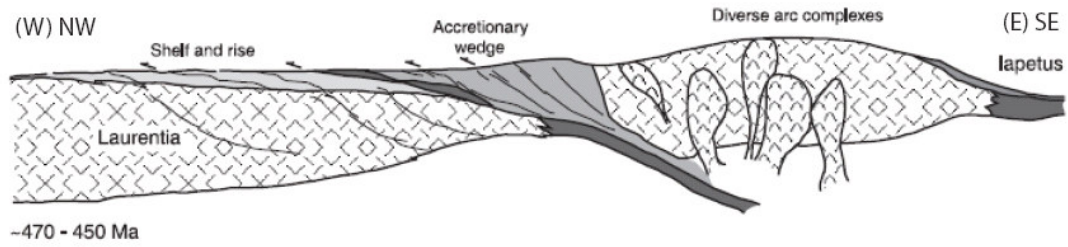

Figure 4-11 Schematic configuration of the Taconian event. Laurentia collides with a volcanic arc which results in an accretionary wedge in between. After Roberts (2003).

The Scandian orogenic event (~430 – 400 Ma) represents the final collision between Laurentia and Baltica (figure 4-12). The subduction goes to ultra high pressure conditions, some microdiamonds are found. During this collision the final nappe geometry becomes recognizable. The nappes are thrusted above each other to form the

Lower, Middle, Upper and Uppermost Allochthons. At the side of Laurentia the Appalachians and Irish and Scottish Caledonides formed. Both subduction and exhumation were relatively fast processes.

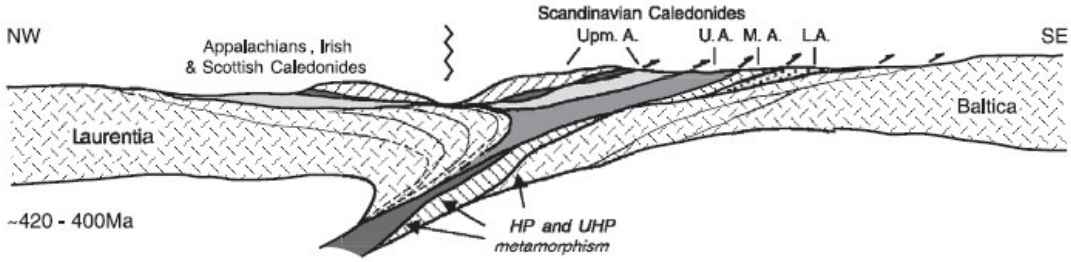

Figure 4-12 Schematic configuration of the Scandian event. Baltica and Laurentia collide to form the Scandinavian Caledonides. Baltica (with earlier nappe complexes) subducts beneath Laurentia to eclogite facies depth. During rapid exhumation, numerous thrust sheets were emplaced onto Baltica and partly above earlier nappes. LA = Lower Allochthon; MA = Middle Allochthon; UA = Upper Allochthon; UpmA = Uppermost Allochthon. After Roberts (2003).

Exhumation of Baltica is illustrated in figure 4-13. In figure 4-13a Baltica is still at 100 km depth. In figure 4-13b Baltica is pulled out of the mantle by a process called extension by Roberts (horizontal distance increases in figure 4-13). Exhumation/eduction is however interpreted as a combination of buoyancy forces and extension. In 4-13c this is followed by crustal collapse. Crustal collapse continues into the Late Devonian or even the Early Carboniferous resulting in exhumation of the eclogites towards the surface.

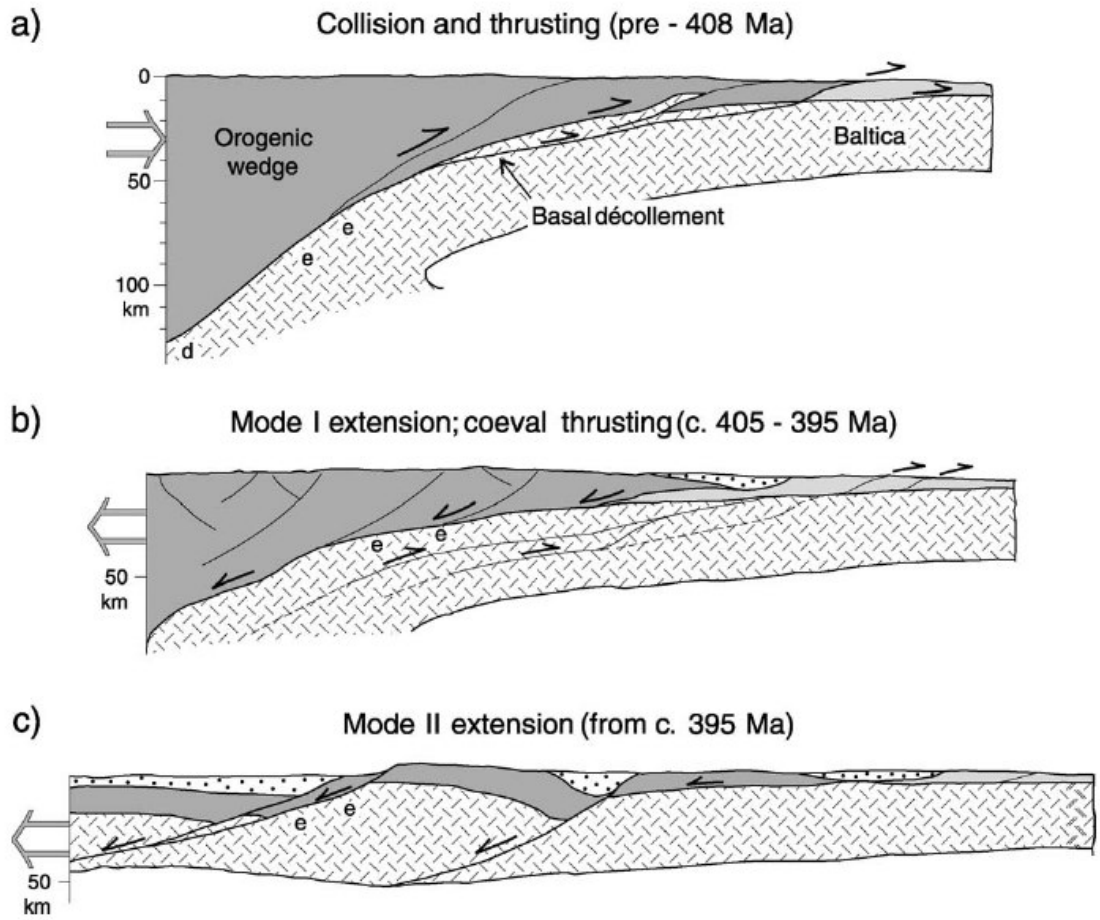

Figure 4-13 Simplified model of post-Scandian extension. a) Situation during the Scandian orogeny. b) Post Scandian extension; orogenic collapse. c) Crustal collapse, extensional detachments with continuing Devonian deposition. The extension continued into Late Devonian and even possible Early Carboniferous time. e = formation of eclogite; d = formation of microdiamond. After Roberts (2003). Earlier nappes are ignored.

5 Methods

In this section different methods are described that are used for the results presented in the following chapters (chapter 6-9).

5.1 Samples

Topographical and geological maps are used to decide where to collect samples in the Southern part of the Central belt (figure 3-1). From all place throughout the Central belt gneisses were taken. The samples were taken as much as possible from different areas of the Avardo- and Lillfjället gneiss. No loose boulders were taken. The samples are numbered 1 to 73, when more than 1 sample is taken from the same location it is numbered with a,b,c etc. The strike and dip is measured and the direction is put on the sample with a markerpen so the thin section could be sawed perpendicular to the foliation. The exact location of the samples was measured by GPS and put on the map later (figure 4-2). Not all collected samples are used for EMP and XRF analysis. Thin sections were only made from samples 24, 24b, 29, 30, 33, 34, 37b, 37c, 37d, 38, 40, 42, 43, 44, 47, 48, 49b, 50, 51b, 52, 52d, 54, 55b, 60, 61, 64, 65, 66, 68, 69, 69II, 70 and 73b (which are all digitalized by scanner (appendix 1.2 – 1.4)). All these samples are analyzed for monazites but monazites are only found in samples 24, 24b, 29, 30, 37d, 40, 42, 43, 44, 51b, 52, 52c, 54, 55b, 61, 64, 65, 66, 68, 70 and 73b (appendix 1.2 – 1.4). Sample 42 and 54 were used for XRF analysis of the bulk rock and the exact mineral chemistry in the samples is examined with the Electron Microprobe (EMP).

5.2 Sample preparation

Samples were collected from locations described above (figure 4-2 and appendix 1.13). Then the selected samples were sawed to prepare thin sections which can be used under the optical and electron microscopes. Before using the EMP thin sections are studied under an optical microscope to analyze the mineral content. Hereafter the thin sections are carbon coated so the thin section will conduct electrons. Then the thin sections are put under the EMP to search for monazites using the backscatter electron (BSE) imaging technique.

The EMP at the Institute for Earth Sciences in Utrecht is a JEOL JXA-8600 Superprobe equipped with an energy dispersive detection system and five wavelength dispersive spectrometers (WDS).

In this chapter the analytical techniques that are used are described. The techniques used are: optical microscopy, electron microprobe, XRF and Domino.

5.3 Electron Microprobe

A selection of the best samples, well distributed over the whole area (figure 4-1), is used for thin section preparation. All thin sections are first analyzed with the optical microscope and then with EMP. With optical microscopy the dominant mineral assemblage is determined. Then the samples are put under the EMP to search for monazites. The best monazites are analyzed for age dating (for detailed description see appendix 1.5 and references of Cocherie et al (1998), Montel et al (1996)). The ages are calculated according to the method of Suzuki & Adachi (1991). EMP monazite analyses are checked for their reliability; if not reliable they are discarded. Monazite EMP analyses are reliable when the sum of the measured element oxides is between 96 - 101 %, the U, Th and Pb values are consistent with the other measurements and the EMP analysis is performed on the monazite itself and not another mineral next to it (SiO_2 goes up; P_2O_5 goes down). Finally a monazite with known age was used, a so called 'standard monazite'. At the beginning and at the end of any monazite analyses session this standard monazite is measured; two lines of 15 measurements. When the mean apparent age of the standard monazite, measured before and after each monazite measurement session, is equal and the age is within 1125 +/- 10 Ma the conditions during the monazite measurement session is interpreted to have operated well.

The EMP was also used to determine mineral chemistry (Reed, 1996). Different kinds of minerals (garnet, biotite, plagioclase and white mica) are analyzed for the exact chemistry. With this mineral chemistry it is possible to determine end member compositions. This information in combination with the computer program Domino (Wei and Powell 2004, 2005) it is possible to determine the PT condition, which is described below.

5.4 X-ray Fluorescence

Representative samples (sample 42 and 54) are crushed to a homogeneous grainsize of ~73 micrometers. This powder is compressed to a tablet which is than analyzed with X-ray fluorescence (XRF). This technique is used to determine the bulk rock chemistry of the samples. Details of this technique are described by Jenkins (1988). Results presented in appendix 1.6.

5.5 Domino

The Domino/Theriak software of de Capitani and Brown (1987) (hereafter simply called Domino) calculates from the given bulk rock chemistry all possible mineral assemblages with corresponding reaction lines presented in a pressure temperature (PT) diagram. When the program has finished the diagram, the mineral assemblage can be compared with the mineral assemblage determined in the hand samples and under the microscope. When the mineral assemblages from the hand samples and microscope overlap, the PT field is found in which the mineral assemblage is formed. This field is further subdivided using detailed mineral chemistry (called 'isoploths'). These are compared with the mineral assemblages found by detailed mineral analysis with the EMP. The intersection between the results of the mineral chemistry determination and the isoploths are the real PT condition during which the mineral assemblage was formed. For limitations of the Domino program see detailed information of Wei and Powell (2004, 2005).

There are some limitations in the program which should be taken into account. All mineral calculations are based on set mineral formulas. For example garnet; only three end-members are put in the program, pyrope ($Mg_3Al_2Si_3O_{12}$), almandine ($Fe_3Al_2Si_3O_{12}$) and grossular ($Ca_3Al_2Si_3O_{12}$). This means that the Mn, which is present in the samples according to the XRF measurements, is not put into garnet as expected. The Mn endmember of garnet (spessartine) is not taken into account. Since there is no place for Mn in all other minerals present in the samples the program puts Mn in the olivine end-member tephroite (Mn_2SiO_4). Tephroite is highly unlikely to form in a felsic environment so could be discarded. There is only one way to take care that no tephroite forms and that is to neglect the Mn input but without the Mn there is relatively too much Si and O. Herefore is not compensated.

The same reasoning for Ti. Ti is not taken into account by biotite while biotite contains a certain amount of Ti. All Ti is put into rutile and ilmenite. These minerals are present in the rock but not in the amounts given by Domino.

Another problem that should be thought of beforehand is the amount of O and H put into the program. O and H should be put into the program because mica's contain OH-groups. Since the host rock is gneiss, which contain water to some extend, water is expected to be present at the chosen pressure temperature range. For the program it does not matter how much free water is available 1 molecule or liters of water. Therefore I chose to put a lot of water into the program to be sure that there is free water available all over the pressure temperature range. Afterwards the ratio between O and H should be tested (figure 5-1). This is done in such way that there is no O_2 or H_2 left.

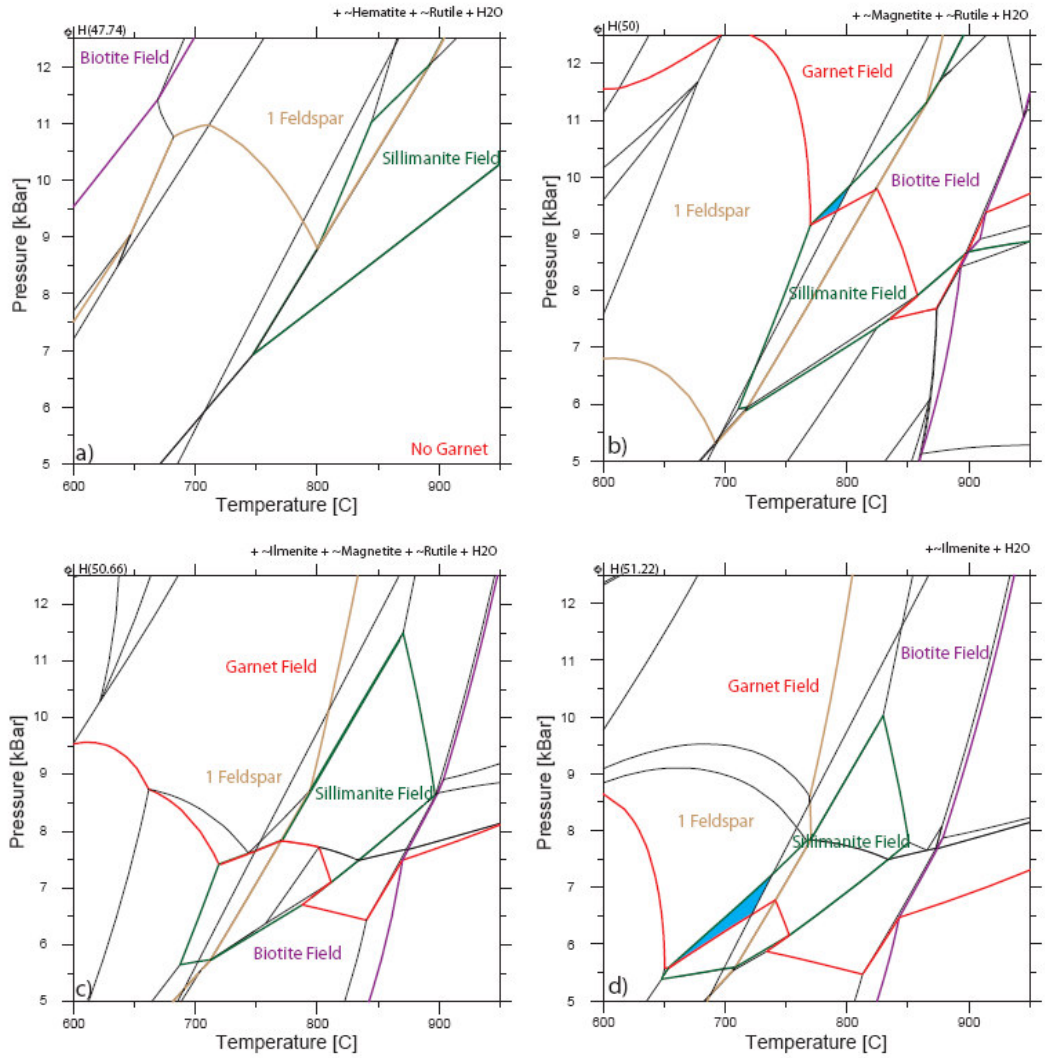

Figure 5-1 Difference in ratio between O and H with the resulting differences in pseudosections. a) shows the maximum OH ratio without free O_2. b) and c) show expected ratios, somewhere in between the maximum and minimum ratios. d) shows the minimum OH ratio without free H2. Blue area indicates the PT area of the mineral assemblage found.

5.6 Statistical curves on age analyses

The age curves plotted in the result section (chapter 8) are performed using the Microsoft Excel add-in isoplot; a geochronological toolkit for Microsoft Excel by Kenneth R. Ludwig, 2003. The uncertainty range (which is necessary to make the plot) used is the uncertainty range given in the monazite program (developed at the EMP lab of the

Utrecht University, further described below). For more info of this program see K.R. Ludwig (1993).

5.7 Calculations

In this section all calculations that are used are described. Numbers presented in the results section (chapter 8) are based on these calculations.

5.7.1 Age dating theory with EMP

The ages of monazites can be calculated from the U/Th/Pb concentrations, measured with the EMP. These ages are calculated using the program developed at the EMP lab at Utrecht University. This program uses the following calculations.

To calculate the apparent age of monazites out of a certain element concentration the following formulas are used, following the method of Suzuki and Adachi (1990).

$$\frac{PbO}{W_{Pb}} = \left[\frac{ThO_2}{232}\cdot\left(e^{(\lambda_{232}\cdot t)}-1\right)\right]+\left[\frac{UO_2}{W_U}\cdot\left(\frac{e^{(\lambda_{235}\cdot t)}+137.88\cdot e^{(\lambda_{238}\cdot t)}}{138.88}-1\right)\right] \qquad (1)$$

Where W_{Pb}, W_{Th} and W_U are the molecular weights of respectively Pb, Th and U. λ_{232}, λ_{235} and λ_{238} are the decay constants of respectively Th^{232} (4.95E-11/year), U^{235} (9.85E-10/year) and U^{238} (1.55E-10/year). PbO, ThO_2 and UO_2 are the oxide weight percentages found in the monazite. These values allow calculating the apparent age t_0 of every single spot analysis.

The mean apparent age of all spot analyses, t, may not be the same as the isochron age, T_0. For the latter age method the total amount of UO_2 is converted to ThO_2 in such way that the final amount of radiogenically produced PbO remains the same. This amount of ThO_2 is added to the measured amount of ThO_2. This new amount of ThO_2 is represented by ThO_2*, see calculation (2) below.

$$ThO_2^{*} = ThO_2 + \frac{UO_2\cdot W_{Th}}{W_U\left(e^{(\lambda_{232}\cdot t)}-1\right)}\cdot\left(\frac{e^{(\lambda_{235}\cdot t)}+137.88\cdot e^{(\lambda_{238}\cdot t)}}{138.88}-1\right) \qquad (2)$$

Substituting (2) in equation (1) gives:

$$\frac{PbO}{W_{Pb}} = \frac{ThO_2^{*}}{W_{Th}}\left(e^{(\lambda_{232}\cdot t)} - 1\right) \quad (3)$$

ThO_2* can be plotted against PbO which should theoretically result into a straight line through the origin called the isochron age (T_0). The "best fit" age can be found when all points are plotted in one single diagram. If this is not the case the statistically best fit line is chosen. The latter line, when forced through the origin corresponds to the geometry that there is no initial Pb present in the monazite. The line is represented by formula (4)

$$PbO = a \cdot ThO_2^{*} + b \quad (4)$$

Where a is the slope of the line and b is the intercept. As explained above b should be 0 to find T_0. Substituting the slope into the formula gives the formula for the apparent isochron age:

$$T_0 = \frac{1}{\lambda_{232}} \cdot \ln\left(\frac{W_{Th}}{W_{Pb}} \cdot \frac{PbO}{ThO_2^{*}}\right) + 1 \quad (5)$$

When b is not 0, T is calculated (not T_0), corresponding to a situation in which the line is not forced through the origin.

5.7.2 Age calculations

There are different ways to express the ages of monazites. This can be expressed as t, T(0) and T. All three ages are given in the results section.

t is the mean apparent age. This is the average of all ages.

T(0) is the age that corresponds with the best fitting line which goes through the origin (in a graph PbO vs. ThO_2^{*}). This is used because of the assumption that there is no initial PbO in the sample. The slope of the best fitting line is put in the formula from a PbO/ThO_2^{*} vs. age graph (figure 5-2). This best fitting line corresponds to the y value in the PbO/ThO_2^{*} vs. age graph. The x value gives the belonging age.

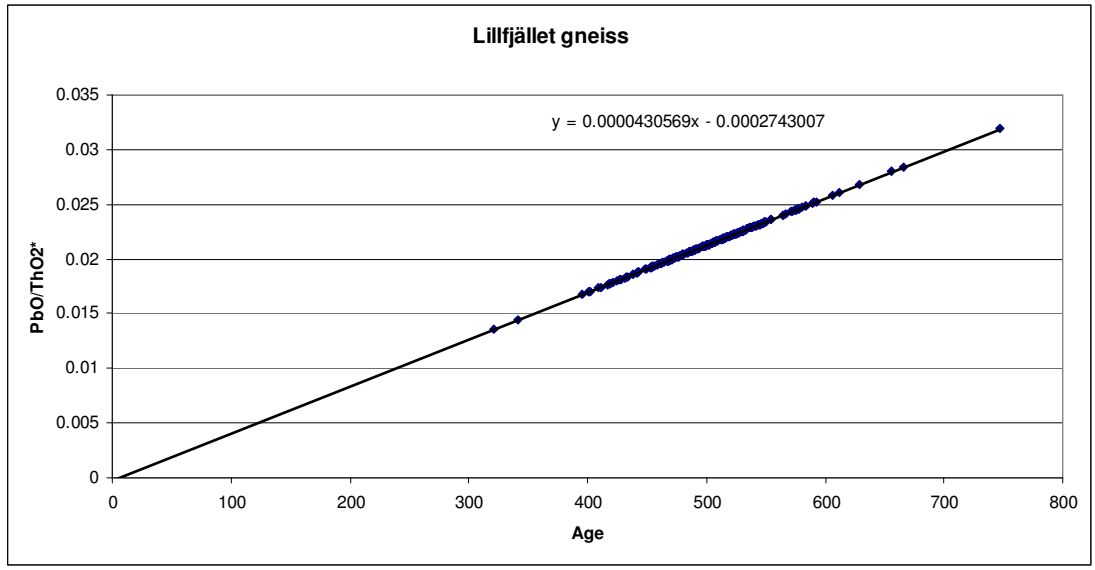

Figure 5-2 PbO/ThO_2^* vs. age graph. If the slope (y in formula), from the PbO vs. ThO_2^* (T or T_0), is put into the formula given in the figure the corresponding age can be calculated (x in formula). The formula is the slope of the line in the graph.

T is calculated in the same way but with another slope. For T the best fitting line is taken, which will probably not go through the origin. This slope is put into the same formula.

To check the reliability of the ages, r^2 is calculated. r^2 is calculated with the Excel function linest.

5.7.3 Backscatter coefficients

The backscatter coefficients are calculated to interpret differences in gray shading (black/white) of the monazites in BSE images taken with the EMP. It is also calculated because not all BSE images of the monazites are taken under the same BSE contrasts on the EMP.

The backscatter coefficients are calculated by:

$\eta^* = -0.0254 + 0.0162.Z^* - 1.86 \times 10^{-4} Z^{*2}$ and

$Z^* = \sum c_j Z_j$

$\eta^* = \sum c_j . \eta_j$

Where η^* is the weighted mean backscatter coefficient, c_j is the mass fraction (wt%), Z^* is the mean atomic number, Z_j is the atomic number of the specific element and η_j is the

backscatter coefficient of the element. The backscatter coefficients are first calculated for all single elements using:

$\eta = -0.0254 + 0.0162.Z - 1.86 \times 10^{-4} Z^2$

Where η is the backscatter coefficient of the element and Z the atomic number. To use this calculation the sum of all element compounds should be put to 100%. For monazites the backscatter coefficient should be around 0.24. When this is not the case there is something wrong with the calculation or the mineral is not a monazite.

5.7.4 End member calculations

The end members of garnet (pyrope ($Mg_3Al_2Si_3O_{12}$), almandine ($Fe_3Al_2Si_3O_{12}$) and grossular ($Ca_3Al_2Si_3O_{12}$)) are distinguished by the elements Mg, Fe^{2+} and Ca. To calculate the relative abundance of pyrope in comparison with almandine and grossular the Mg amount in the SFU can thus be taken and is divided by the sum of Mg, Fe^{2+} and Ca. Thus:

$$\frac{Mg}{Mg + Fe^{2+} + Ca} = \text{relative amount of pyrope}$$

In the same way the end members are calculated of all other minerals.

5.7.5 Pressure/temperature calculations

Another way to determine the metamorphic conditions is by using thermobarometry. For this method the mineral chemistry should be analyzed by EMP. The most popular thermometer is the garnet-biotite thermometer from Ferry and Spear (1978).

$$T(°C) = \left\{ \frac{(2089 + 9.56P(kbar))}{2.868 - \ln K_D} \right\} - 273 \qquad \text{Where} \qquad K_D = \frac{(Fe/Mg)^{Bt}}{(Fe/Mg)^{Grt}}$$

Where Fe and Mg are the element concentrations in respectively garnet and biotite.

This should be restricted, according to Ferry and Spear (1978), to:

$$\frac{(Ca + Mn)}{(Ca + Mn + Fe + Mg)} = 0.2 \qquad \text{for garnet and:}$$

$$\frac{(Al^{VI} + Ti)}{(Al^{VI} + Ti + Fe + Mg)} \leq 0.15 \qquad \text{for biotite.}$$

Where Al^{VI} is half of the total Al -1. According to the last restriction this thermometer can not be used in this thesis because:

$$\frac{\left(Al^{VI} + Ti\right)}{\left(Al^{VI} + Ti + Fe + Mg\right)} \approx 0.3$$ (data set used shown in appendix 1.12).

6 Monazites

In this chapter the properties of monazites are described and discussed.

6.1 Crystal chemistry

Monazite belongs to the Orthophosphate mineral group. Orthophosphates have an idealized formula $A(PO_4)$. The oxygen atoms are located at the corners of each $[PO_4]$ tetrahedron while the A-cations keep the different tetrahedron together. Other members of the orthophosphates group are apatite and xenotime. Monazite and xenotime have both the same structural formula $[REE(PO_4)]$ but a different mineral structure. Monazite has a monoclinic and xenotime a tetragonal crystal system. Another difference is that the cations in monazite consist of the Light Rare Earth Elements (LREE) while xenotime consists of the Heavy Rare Earth Elements (HREE) and Yttrium (Y). This difference in cation content also explains the difference in mineral structure; monoclinic crystal systems occupy more space than the tetragonal crystal system. LREE are bigger than the HREE, which is the reason for the difference in volume between the two crystal structures. Cation substitution can take place in monazites; one REE can be substituted by another REE (or Y). Monazites always contain a small percentage of HREE (Williams et al. 2007).

6.2 Chemical zoning

Chemical zoning in monazites is caused by various cation substitution reactions. Below the most common cation substitution reactions are described.

One substitution reaction occurring in the A-site of monazite is the next reaction:

$$2REE^{3+} \longleftrightarrow Ca^{2+} + Th^{4+} \qquad (1)$$

This substitution produces the end member brabantite $[Ca,Th(PO_4)_2]$ in the ternary system that also includes monazite (figure 6.1). Cheralite, a more general form of the Th end member $[M^{2+},Th(PO_4)_2]$, can contain a lot of other cations such as Sr, Pb and Ba together with Th. The cheralite substitution can contain some U, although there is no U

end member. The Th/U ratio is always > 1.0 (Williams et al. 2007). Radiogenic Th and U will produce radiogenic Pb, so radiogenic Pb will be introduced in the monazite solid crystal structure after time. Non radiogenic Pb^{204} is not compatible in monazite (Parrish, 1990). Therefore it is correct to state that no non-radiogenic Pb is incorporated in monazite if used for chemical U/Th/Pb dating (Suzuki and Adachi, 1991). Another assumption for radiogenic U/Th/Pb dating is that monazite behaves as a closed system. This is valid because monazite is commonly concordant (Parrish, 1990). Radiogenic Pb will be incorporated in the monazite crystal lattice and the concentration will increase with time. This new radiogenic Pb^{2+} will substitute in the monazite crystal lattice for Th^{4+}. In an ideal formula (all A sites filled) this will ultimately result in a charge imbalance (Williams et al. 2007).

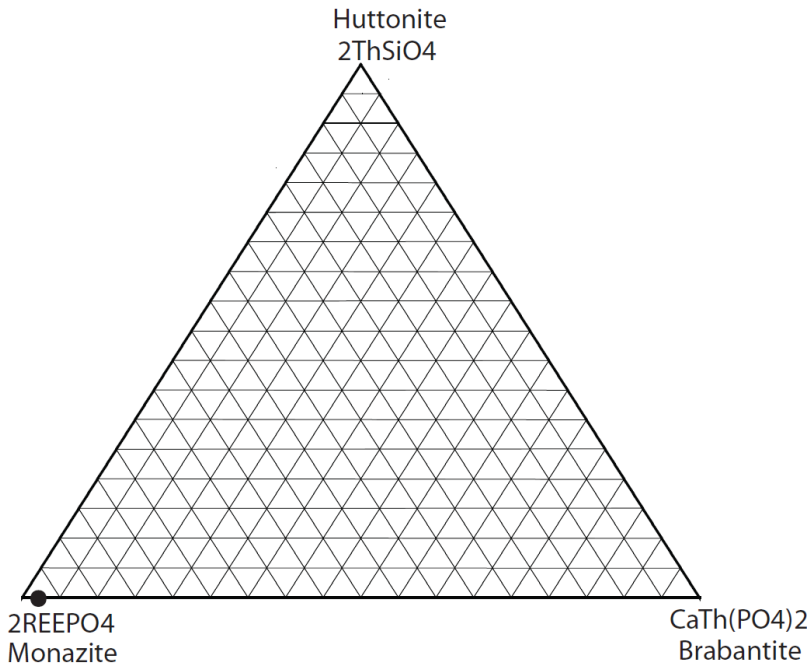

Figure 6-1Monazite end member diagram. Black spot indicate the monazite composition found in the monazites taken from the Lillfjället gneiss, Avardo gneiss and Svartsjöbäcken schist.

A second exchange reaction is:

$$P^{5+} + REE^{3+} \longleftrightarrow Si^{4+} + Th^{4+} \qquad (2)$$

This substitution produces huttonite ($ThSiO_4$) the other end member in the ternary system of monazite (figure 6-1). Huttonite has a monoclinic crystal structure just like monazite and brabantite. The substitution reaction occurs in high temperature metamorphosed and

igneous rocks. A solid solution between huttonite and monazite is not seen often in natural samples (Förster and Harlov, 1999).

Cation Substitution reactions are the reason for different kinds of (chemical) zoning as can be seen in BSE images (figure 6-2). There are different kinds of zoning: i.e. concentric growth zoning, sector zoning and more complex zoning patterns with interfingered domains and zones which cross-cut primary zoning. Some striking examples of zoning in monazites were found in the Central belt, Seve Nappe, Sweden and illustrated in figure 6-2. Concentric zoning (figure 6-2a) reflects an evolution in the composition of the melt/liquid and the composition of the crystallizing monazite. Concentric zoning is typically the result of brabantite or huttonite substitution reactions (Williams et al. 2007). Sector zoning (figure 6-2b) is the result of the preference for a crystal face by some elements (Cressey et al. 1999). The more complex zoning patterns (figure 6-2 c-f) are the result of a combination between the two zoning types or reflect different kinds of metamorphic overgrowth.

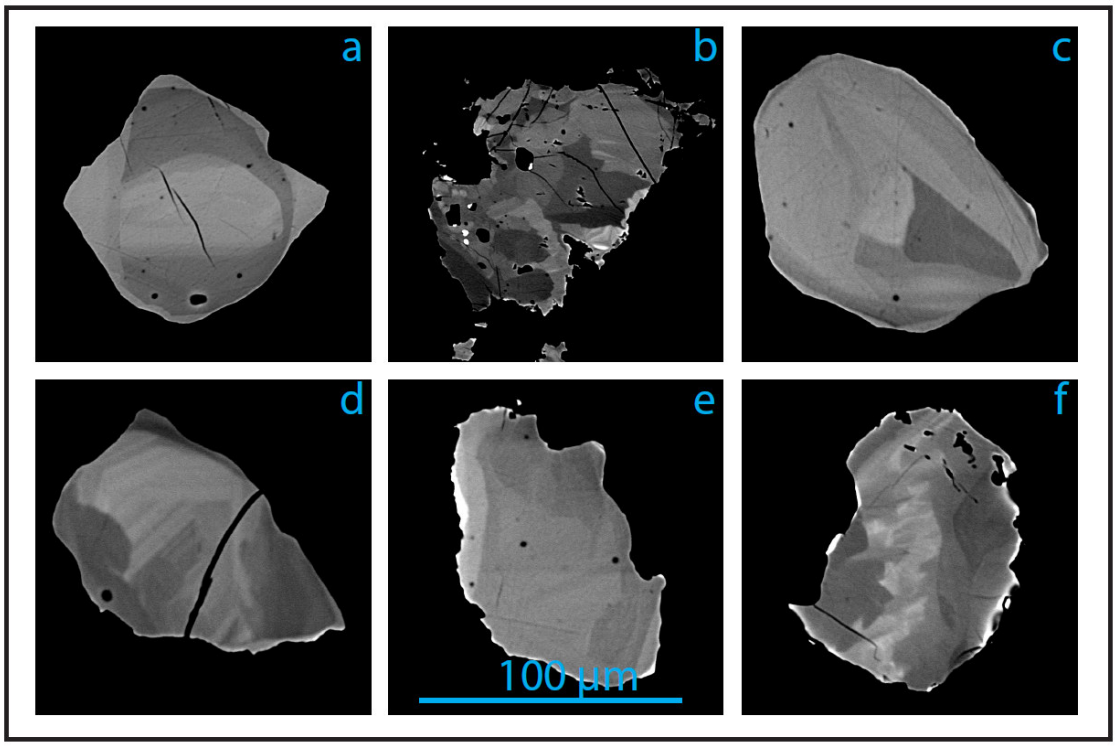

Figure 6-2 Back scatter electron (BSE) images of zoning in monazites from samples of the Central belt, Seve Nappe, Sweden. (a) Example of concentric zoning (b) sector zoning (c-f) more complex zoning. Scale size of the monazite is about 100 µm.

6.3 Uncertainties with EMP analyses

In this paragraph uncertainties in element concentrations, measured with the EMP, are discussed.

To measure the element intensities with the EMP, the background is measured on both sides of the peak to be able to correct for the background by linear interpolation. The background is not always equally large on both sides of the peak which means that there is an uncertainty in the outcome of the concentration measured. This uncertainty is neglible for the major elements with peak/background ratios in the range of 10-100, but not for the trace elements when the peak/background ratio decreases to 1-3. This uncertainty should be as low as possible, which means that the background should not be influenced by other (second or third order) peak interferences corresponding to other trace elements. This is especially important for the peak positions of the elements U/Th/Pb since the ages are calculated using these element intensities. The EMP has taken this into account as good as possible. However there is variable background intensity around the PbMα peak. The most stable background positions are chosen despite the fact that the background position is higher on one side of the PbMα peak in comparison with the other side. This means that there is an uncertainty in the Pb concentrations especially when very low Pb concentrations are measured. The real Pb concentration is probably higher than measured by the EMP, which means a younger age.

Another uncertainty is that some peak interferences will overlap with each other. This is also the case with the PbMα peak (the Pb peak measured) which interferes with the YLγ peak or the ThMζ (Figure 6-3a; Williams et al. 2005). This means that the real concentration for Pb is lower than measured with the EMP, which means an older age. This is opposite to the other correction mentioned above. The same interference as Y has on Pb has Th on U. Several Th peaks overlap with the UMβ peak measured (Figure 6-3b). Th influences both the peak and the background of UMβ. This also results in inaccuracy in age but the effect is not so large since the U and Th concentrations are added by the method described above of Suzuki and Adachi (1991).

High wavelength measurements have a background intensity that is curved. This is another problem determining the exact concentration of Pb. Linear extrapolation should not be used to obtain the best result for the concentrations of trace elements for high

wavelength measurements but exponential regression should be used. This is also the case for Th and U which will partially cancel the inaccuracy in Pb concentration. Since the Pb concentration is lower in comparison with Th and U it will typically result in the largest error and an underestimation of the age (Jercinovic & Williams 2005).

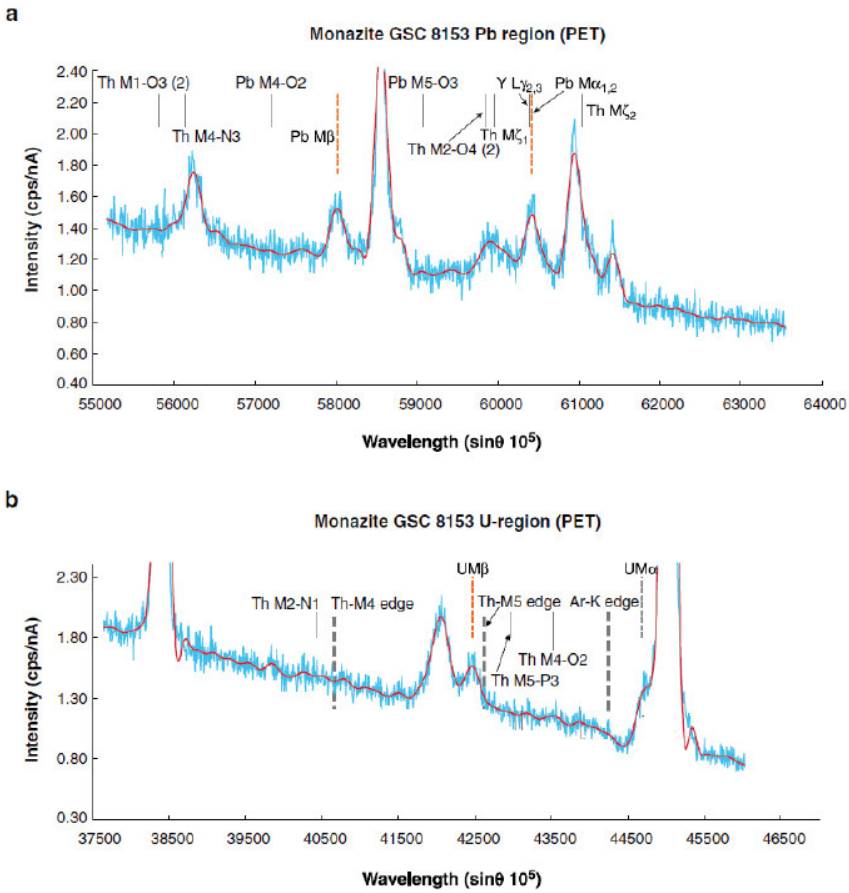

Figure 6-3 Examples of wavelength scans of natural monazites. a) Shows the peak overlap of PbMα with YLγ. b) Shows the overlap of ThMγ with UMβ. After Williams et al 2007.

All errors described above are the reason for the distribution and uncertainties in age. Especially the low concentration of Pb in the samples is crucial in the error of the age. This is compensated by the number of measurements taken which means that the average in age must be correct.

Monazite forms at amphibolite grade and higher. There are some monazite-in reactions. Most common is the breakdown of allanite to monazite at approximately 550ºC (Wing et

al. 2003). Another suggested breakdown is the breakdown of garnet near the staurolite-in isograd (Pyle & Spear, 1999). Since monazite is zoned, it could mean that there are more chemical reactions involved. Different metamorphic zones could mean different monazite-in reactions. So both reactions could occur in different phases. In the case of the monazites of the Seve Nappe there is no clue which reaction is involved.

Garnet and monazite are the major repositories of HREE and Y after xenotime breakdown. When monazite contains relatively a lot of HREE and Y it could mean that it started to grow before the garnet started to grow. Since Y is measured with the EMP this could give some indications about the moment of growth of monazite relative to garnet. When xenotime breaks down both garnet and monazite can grow (Pyle & Spear, 1999). Once xenotime is depleted, monazite and garnet are on the opposite side of the reaction since they represent the two dominant sinks for Y (Williams et al. 2007). Garnet can breakdown during a prograde and retrograde event.

7 Deformation

In this chapter the lithology, structures and mineral parageneses are described of the Lillfjället gneiss.

7.1 Lithology

The Lillfjället gneiss is earlier described as a sillimanite bearing gneiss. This mineral distinguishes the Lillfjället gneiss from the Marsfjället gneiss which has kyanite-k-feldspar assemblages instead of sillimanite-k-feldspar. The Lillfjället gneiss mainly consists of the minerals: sillimanite, garnet, biotite, muscovite, plagioclase and quartz. These minerals are recognized both in the field and in thin sections (figure 7-1 and figure 7-2, appendix 1.2). All these minerals (excluding quartz) have a relatively high Al-content and low Ca-content. This is an indication that the original rock was probably pelitic to quartzofeldspatic (also saturated in quartz) in composition, which means derived from clay-rich sedimentary rock (Bucher & Frey 2002).

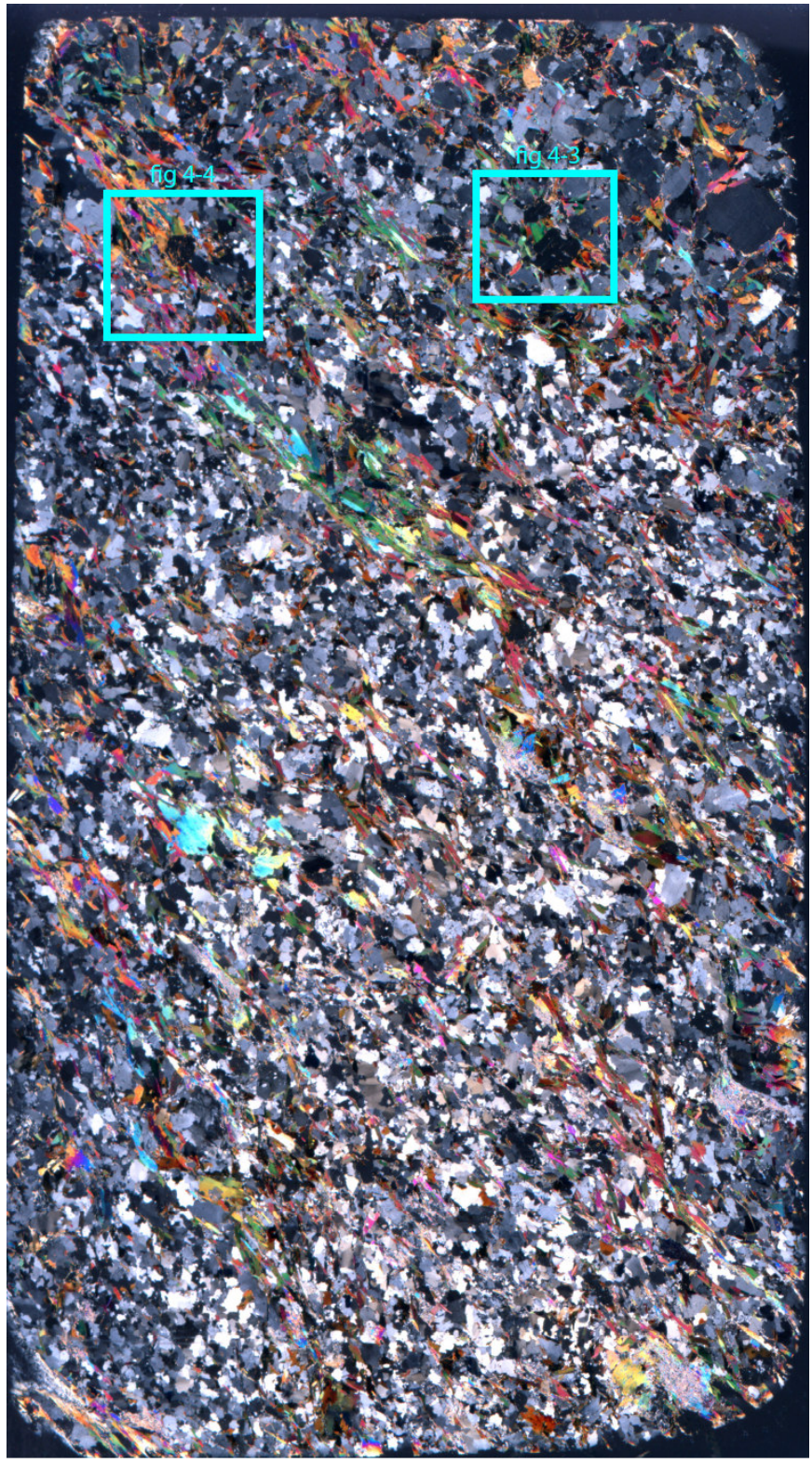

Figure 7-1 Digital scan of thin section 42 with the aid of two crossed polarized filters. Blue squares indicate position of Electron Microprobe images illustrated in figures 7-3 and 7-4.

Figure 7-2 Digital scan of thin section 54 with the aid of two crossed polarized filters. Blue squares indicate position of Electron Microprobe images illustrated in figures 7-5 and 7-6

7.2 Structures

In this paragraph the structures are described which are mainly found in thin sections. Samples 40, 44, 54, 55, 70 and 73 (appendix 1.2) are examples of thin sections which are taken perpendicular to the foliation. All other thin sections have another angle with the foliation.

There are samples that show a more pronounced foliation than other samples. Sample 54 is an example with a pronounced foliation (figure 7-2). The minerals are relatively smaller and more elongated in comparison with other samples, for example sample 42 (figure 7-1). This is caused by post-crystalline strain. Sample 42 is not taken perpendicular to the foliation, but the foliation seems to be less pronounced. The quartzo-feldspatic minerals seem more rounded than the mica's.

In sample 54 some mica fish are recognized. The mica fish are group 1 or group 3 type mica fish (ten Grotenhuis et al, 2002). Group 1 mica fish have attained their apparently stable inclined position by back rotation from an original stable position; the lens shape can be explained by removal due to recrystallisation. Group 3 mica fish can be attained by slip on (001), starting from a position parallel to the foliation.

7.3 Mineral parageneses

Not all minerals originate from the same metamorphic event. This is recognized by two different sizes and thus different generations of muscovite and biotite. This is clearly recognized for muscovite in sample 54 (figure 7-2), in the upper left corner a big muscovite crystal can be seen that is not aligned with the foliation. This indicates muscovite overgrowth. Also for the biotites it can be seen in the thin section of sample 43 (see appendix 1.2) that there are two different grain sizes/shapes. It is also seen in the images taken with the EMP. In figure 7-4 there are big biotite crystals in the upper left corner while the other biotites are much smaller (more crystallized).

All garnets in both samples (especially sample 54) are rounded porphyroblast in a finer grained matrix (figure 7-2; also samples 44 and 70; appendix 1.2). In sample 40 the garnets are much bigger than in the other samples and the foliated minerals curls around the garnets (appendix 1.2). The garnets also show cracks and do have inclusions of, for example, plagioclase. The brittle behavior of garnet means that the deformation occurred

at temperatures lower than the brittle ductile transition zone of garnet (600-800 ºC) (Voegelé et al. 1998b; Wang and Ji 1999). The small muscovites curl around the garnet, which is better seen in sample 54 than in sample 42. This is due to the more pronounced foliation in sample 54.

With the electron microprobe (EMP) it is possible to see all minerals in more detail (see figures 7-3, 7-4, 7-5 and 7-6). The locations of the BSE images are shown in the scans of the thin sections in figures 7-1 and 7-2. As mentioned earlier in figure 7-4 two generations of biotite are recognized. In figure 7-5 it is seen that the biotite curls around the garnet. Figure 7-6 shows the alignment of biotite and muscovite in more detail while plagioclase has a more random orientation. In figure 7-6 recrystallization of plagioclase can be seen in detail. Just right of the garnet some subgrains are seen in the plagioclase. These subgrains are more rounded and less deformed. This is to some extent also seen in the EMP image of sample 42 (figure 7-4 right upper corner) and is clearly seen in the thin section of sample 42 (figure 7-1). The cloud-like shapes are an indication for this recrystallization.

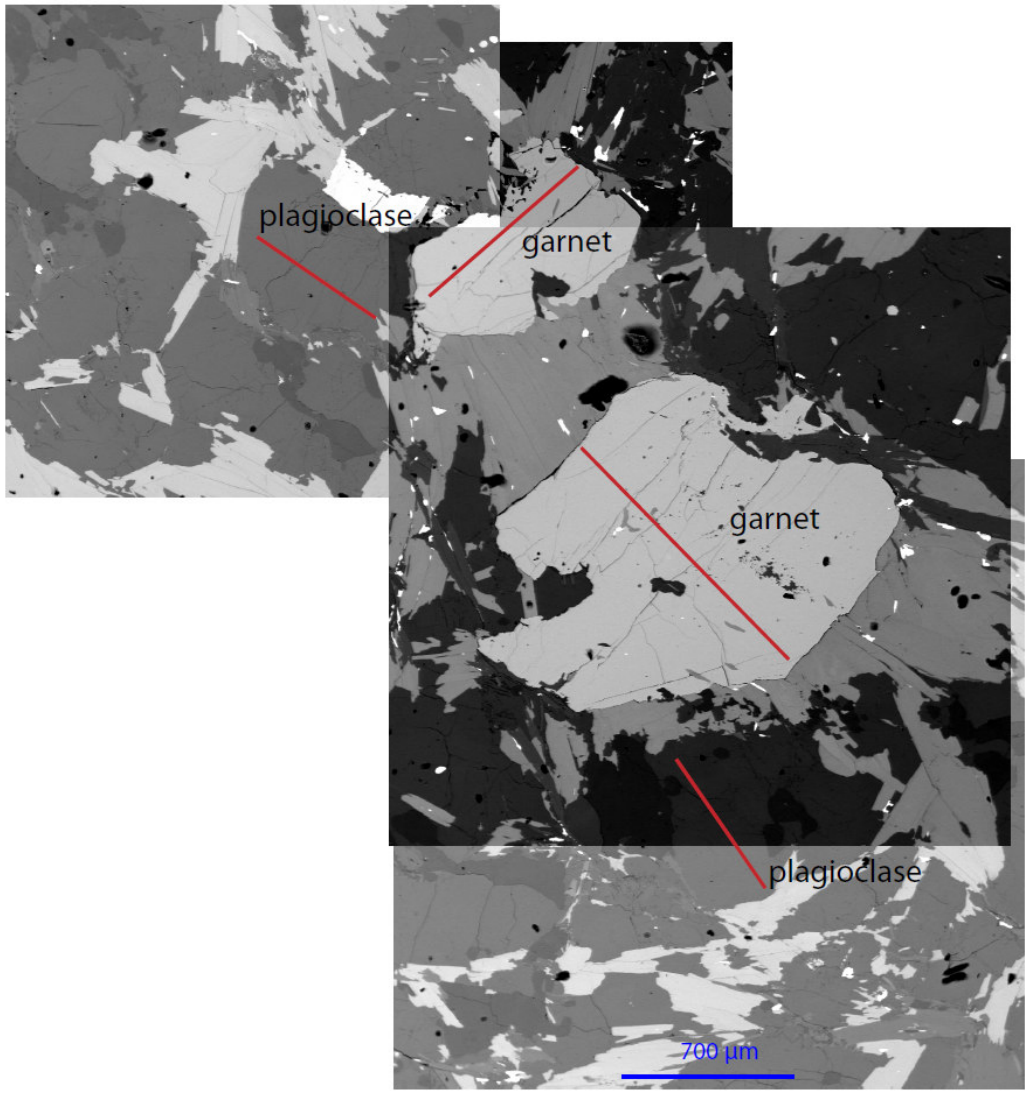

Figure 7-3 Electron Microprobe (EMP) images of sample 42. Red lines indicate lines where spot analyses are taken to analyze the mineral assemblage. Color variations are due to compilations of several images with other contrast adjustments. Different contrast images are taken to see the analyzed mineral best.

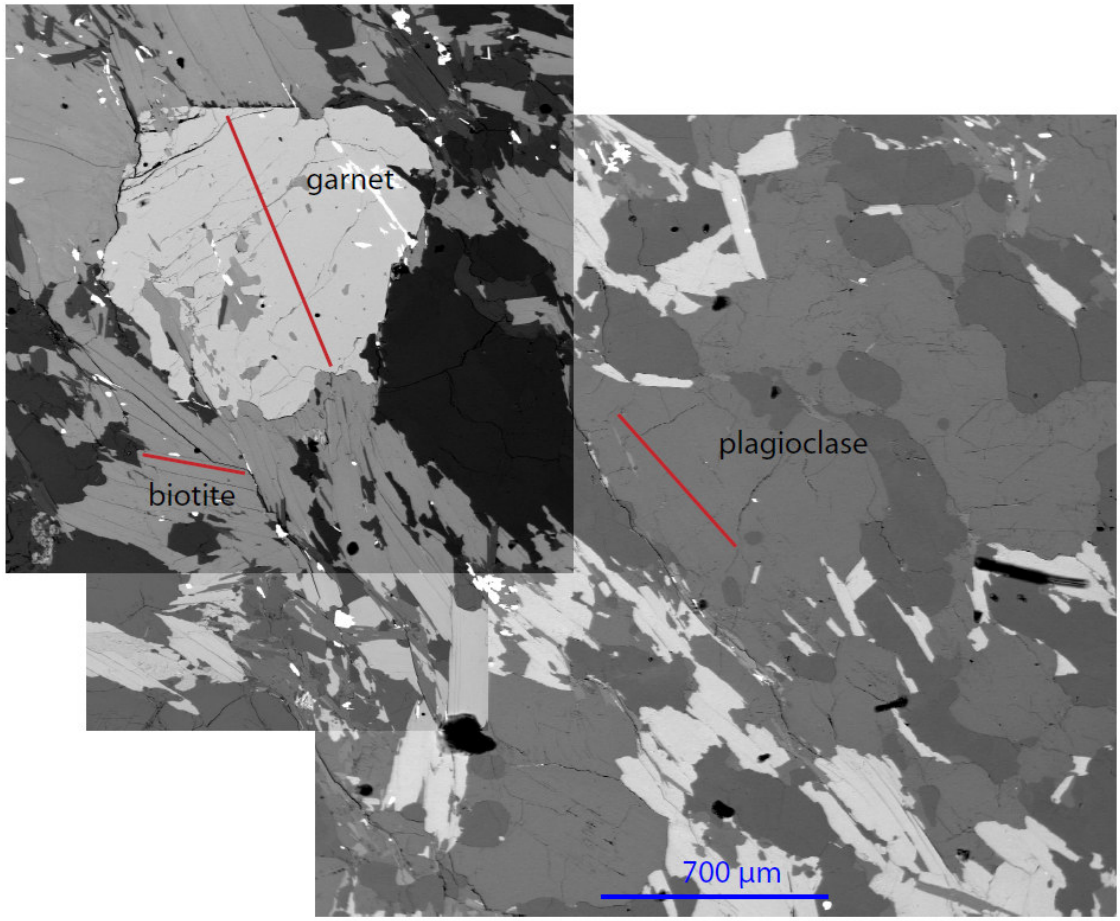

Figure 7-4 Electron Microprobe (EMP) images of sample 42. Red lines indicate lines where spot analyses are taken to analyze the mineral assemblage. Color variations are due to compilations of several images with other contrast adjustments. Different contrast images are taken to see the analyzed mineral best.

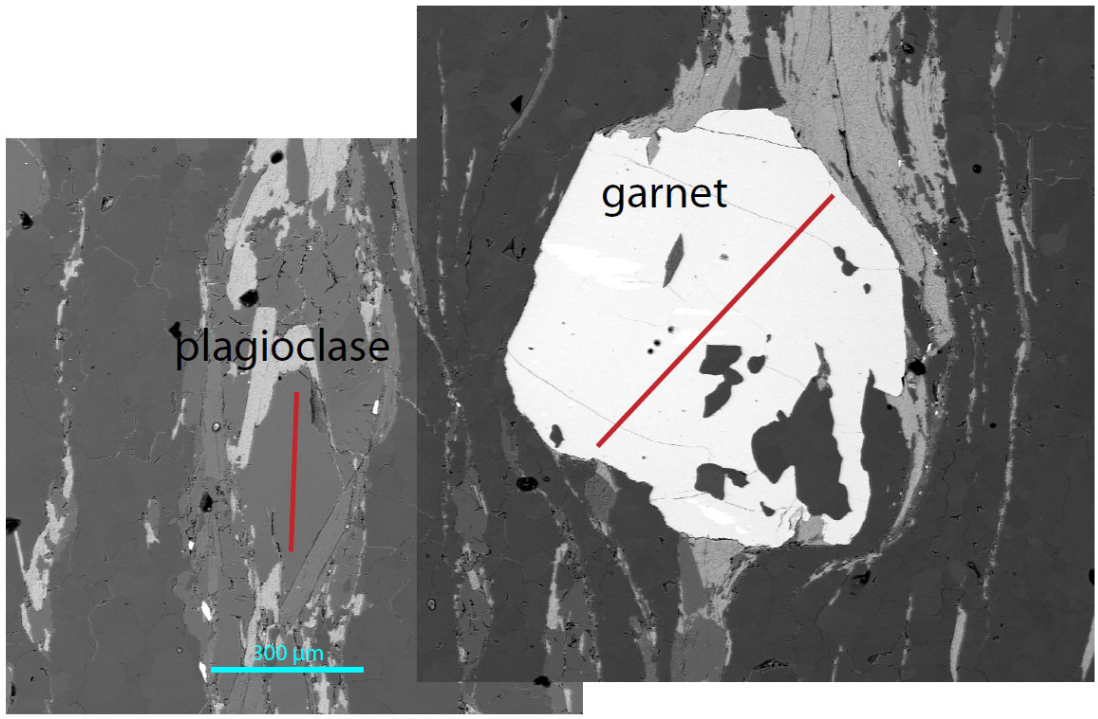

Figure 7-5 Electron Microprobe (EMP) images of sample 54. Red lines indicate lines where spot analyses are taken to analyze the mineral assemblage. Color variations are due to compilations of several images with other contrast adjustments. Different contrast images are taken to see the analyzed mineral best.

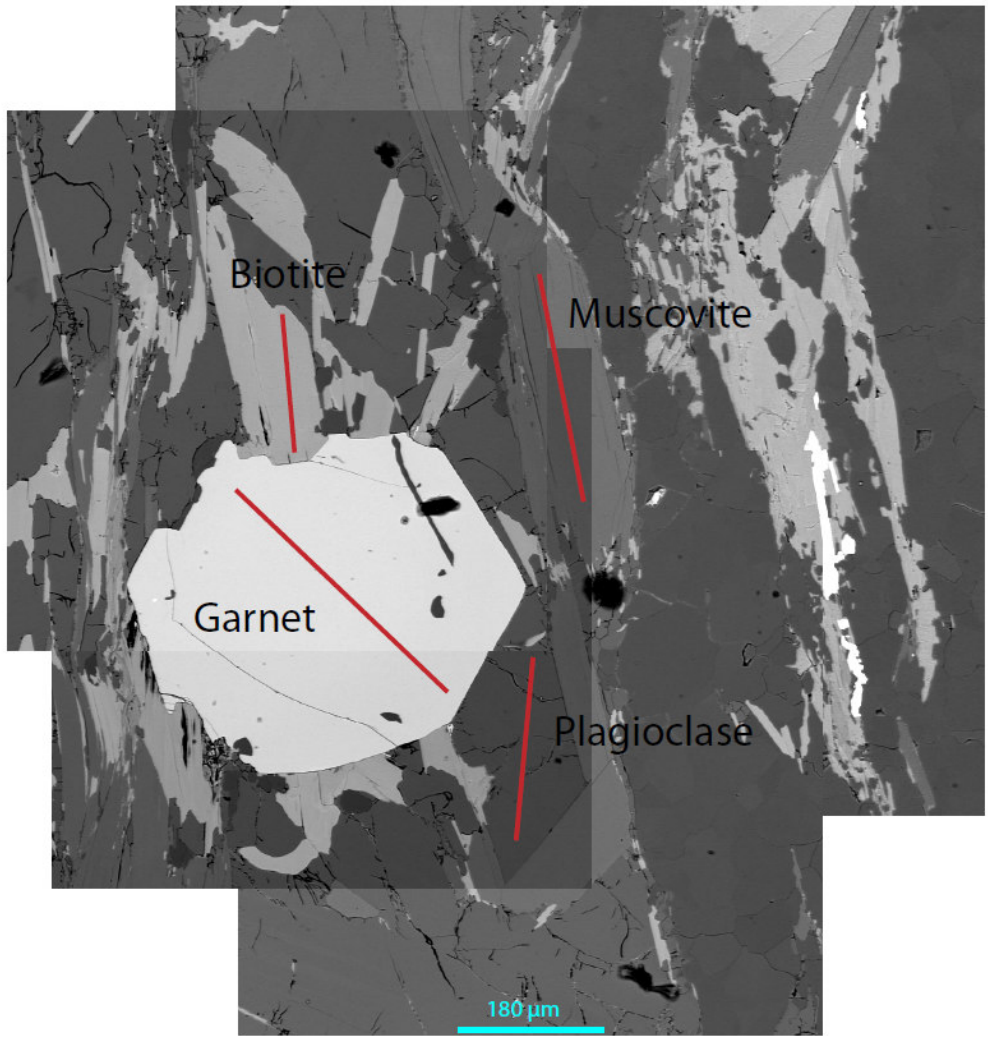

Figure 7-6 Electron Microprobe (EMP) images of sample 54. Red lines indicate lines where spot analyses are taken to analyze the mineral assemblage. Color variations are due to compilations of several images with other contrast adjustments. Different contrast images are taken to see the analyzed mineral best.

7.4 Petrogenetic diagram

All these observations; two generations biotite and muscovite and recrystallized plagioclase, indicate that there are two mineral assemblages. The first assemblage M1 consists of: garnet, muscovite, biotite, sillimanite and plagioclase. The second mineral assemblage recognized consists of: small biotites and muscovite and the recrystallisation of plagioclase. This results in the petrogenetic diagram shown in figure 7-7.

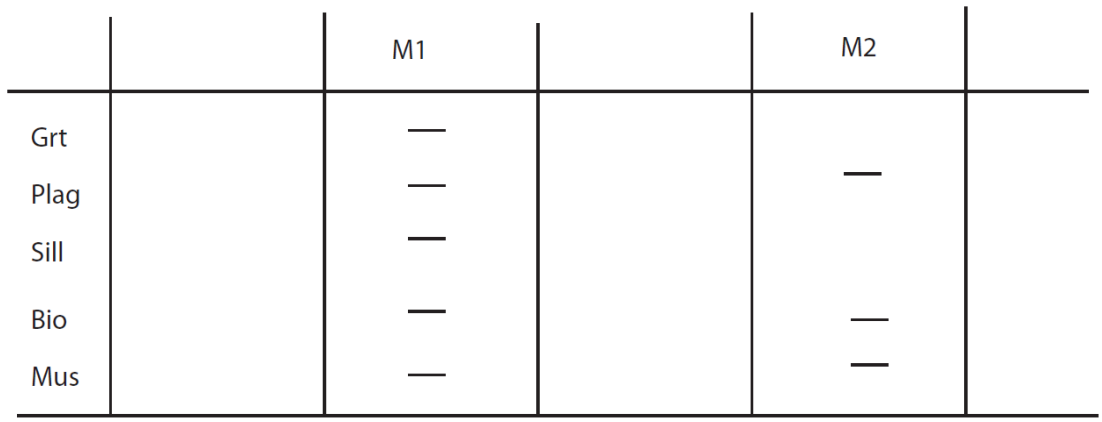

Figure 7-7 Petrogenetic diagram of the Lillfjället gneiss.

Both mineral assemblages could be from the same age. Whether M1 and M2 belong to the same tectonometamorphic event is further discussed below.

8 Results

8.1 EMP Monazite Age Dating

In this chapter all data will be presented obtained by the EMP monazite age dating method (chapter 5). The three tectonometamorphic units (Lillfjället-, Avardo gneiss and Svartsjöbäcken schist) are presented separately followed by a discussion of the results. All the output files are presented in appendix 1.8 – 1.10 and the calculations methods are described in the method section (chapter 5).

8.1.1 Lillfjället gneiss

Monazites from the Lillfjället gneiss were dated by EMP (see appendix 1.8 for data from EMP). In total 204 analyses are performed on 24 different monazites from 12 different thin sections (appendix 1.2). The outcome of the EMP analyses is plotted against number in figure 8-1.

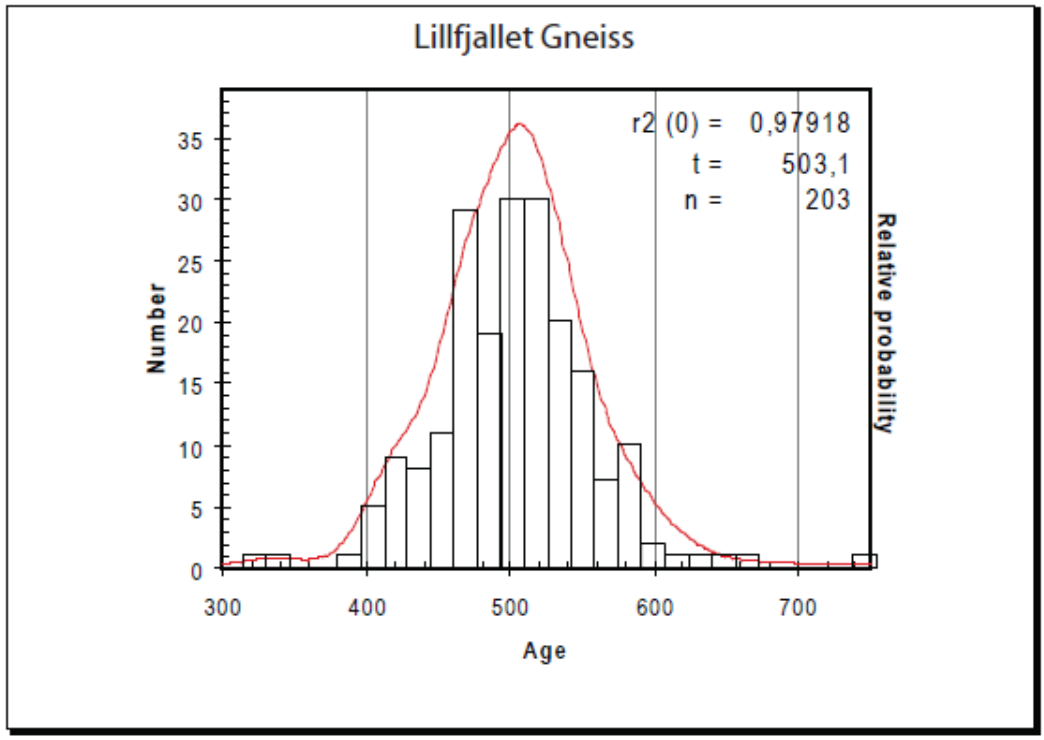

Figure 8-1 Cumulative EMP Monazite age diagram of the Lillfjället gneiss. The peak of the probability curve corresponds to the mean apparent age (t). Also r^2 and number of analyses (n) are given.

The mean apparent age (t) is 503.1 +/- 20 Ma. The uncertainty interval is calculated with the monazite program developed at the EMP lab of Utrecht University. It has an r^2 value of 0.97918, which means that the ages belong to the same data set; the same tectonometamorphic event. Two lines are plotted in figure 8-2 (based on methods described in chapter 5). One line is the best fit (black line) and the other the best fit through the origin (red line). These lines are used to calculate T and T_0 (details in chapter 5). The red line gives the age (T_0) assuming no initial Pb was present; it shows a steeper slope which means an older age than the black line (T). Resulting in T_0=497.9 +/- 20 Ma, T=454.9 +/- 20 Ma.

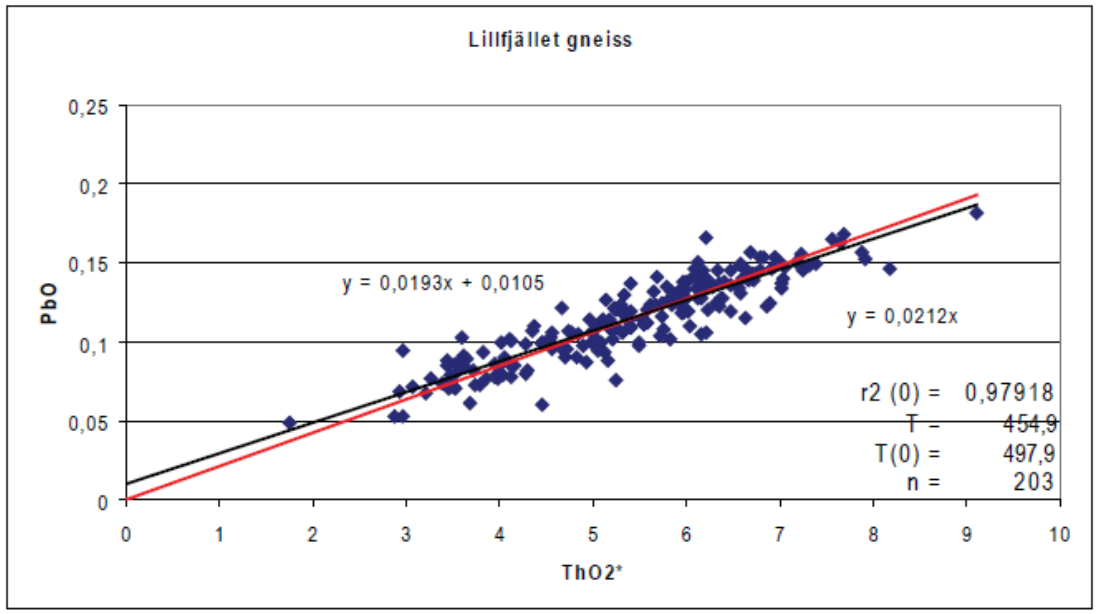

Figure 8-2 Isochron plot of the Lillfjället gneiss with corresponding ages, number of measurements and certainty level. Formulas correspond to the corresponding trend lines.

The monazites from the Lillfjället gneiss are found as inclusions in several M1 minerals such as quartz, garnet, muscovite, biotite and plagioclase (appendix 1.2). There are also some monazites found in M2 minerals such as biotite and plagioclase. All monazites in both mineral assemblages give the same age; T_0 = 497.9 +/- 20 Ma.

8.1.2 Avardo Gneiss

EMP analyses are performed on monazites of the Avardo gneiss (results are listed in appendix 1.9; Avardo gneiss p. 71-76). From the Avardo gneiss there are 153 analyses performed on 13 monazites from 7 different locations. The outcome is plotted against number in figure 8-3.

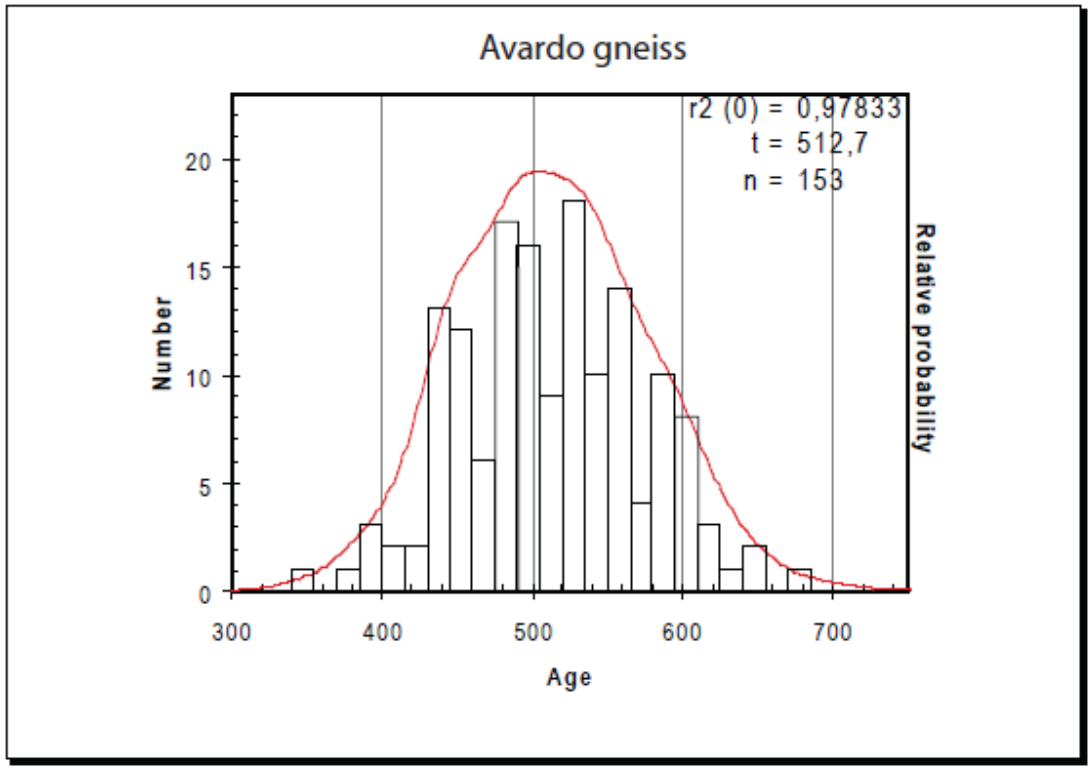

Figure 8-3 Cumulative EMP Monazite age diagram of the Avardo gneiss. The peak of the probability curve corresponds to the mean apparent age (t). Also r^2 and number of analyses (n) are given.

The Avardo gneiss has a mean apparent age of 512.7 +/- 20 Ma. The curve is wider and the number of analyses is less than for the Lillfjället gneiss. It has an r^2 value of 0.978 (figure 8-4). Two lines are plotted in figure 8-4 (based on methods described in chapter 5). The red line gives the age (T_0) assuming no initial Pb was present; it shows a steeper slope which means an older age than the black line (T). Resulting in T_0=502.3 +/- 20 Ma, T=409.3 +/- 20 Ma.

The monazites of the Avardo gneiss are found as inclusions in muscovite, biotite and quartz (appendix 1.3), all belonging to both the M1 and M2 mineral assemblage. The

mineral assemblage should have (at least) the same age as the monazites; T_0=502.3 +/- 20 Ma.

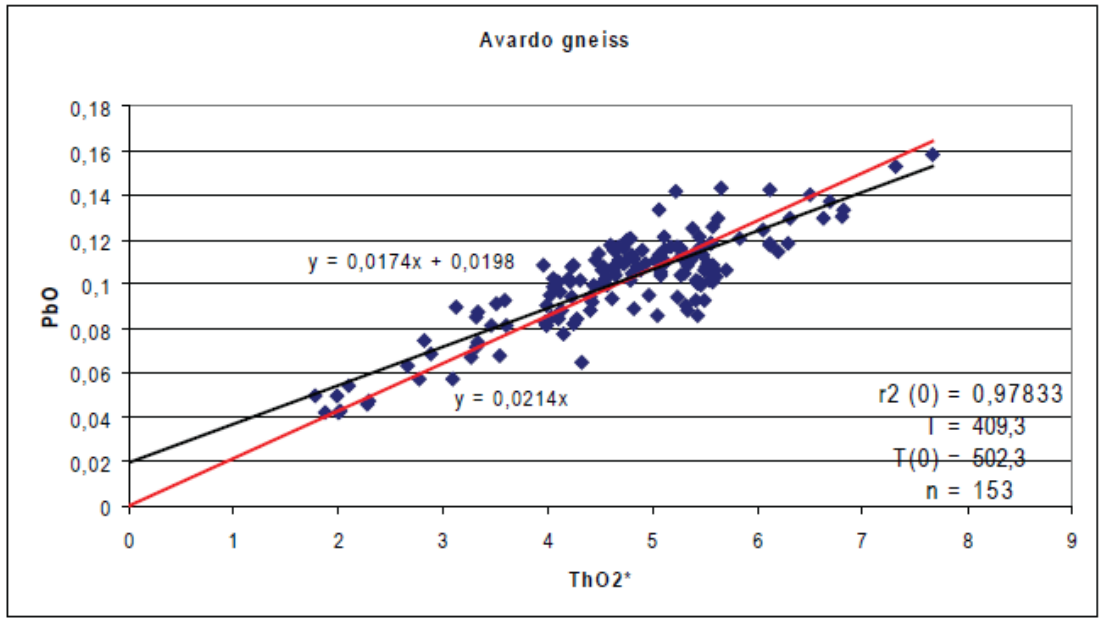

Figure 8-4 Isochron plot of the Avardo gneiss with corresponding ages, number of measurements and certainty level. Formulas correspond to the corresponding trend lines.

8.1.3 Avardo + Lillfjället gneiss

Assuming that the monazites where formed during the same tectonometamorphic event with the same age, the age results of both Avardo and Lillfjället gneiss can be added together in a single graph (figure 8-5).

The total EMP monazite age diagram (figure 8-5) illustrates the results of both tectonometamorphic units. The combined data of the Avardo and Lillfjället gneiss results in a mean apparent age of 507.2 +/- 19 Ma (figure 8-5). Whether this is allowed is discussed below. According to the r^2 value it is allowed (figure 8-5). Two lines are plotted in figure 8-6 (based on methods described in chapter 5). The red line gives the age (T_0) assuming no initial Pb was present; it shows a steeper slope which means an older age than the black line (T). Resulting in T_0=499.5 +/- 19 Ma, T=439.5 +/- 19 Ma.

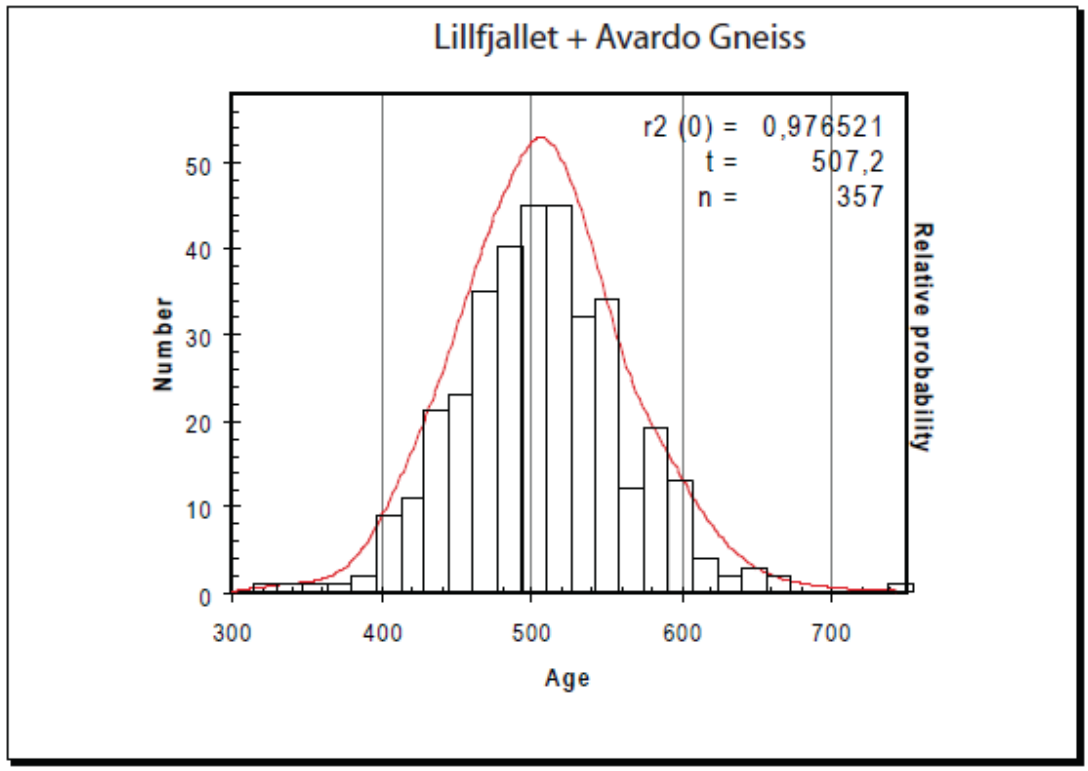

Figure 8-5 Total Cumulative EMP Monazite age diagram of the Lillfjället and the Avardo gneiss. The peak of the probability curve corresponds to the mean apparent age (t). Also r^2 and number of analyses (n) are given.

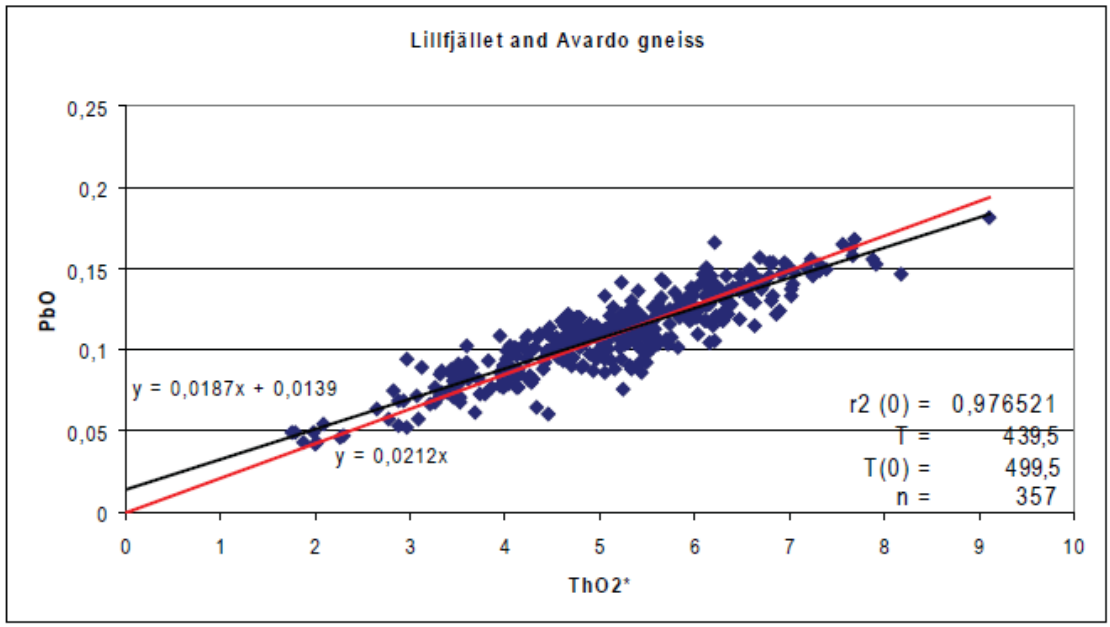

Figure 8-6 Total isochron plot of the Lillfjället and the Avardo gneiss with corresponding ages, number of measurements and certainty level. Formulas correspond to the corresponding trend lines.

8.1.4 Svartsjöbäcken schist

EMP analyses were performed on monazite from the Western belt (see appendix 1.10 for EMP analyses data). Some collected samples of the Svartsjöbäcken schist contain monazites. In total 19 analyses are performed divided over 9 monazites from 1 location (figure 8-7).

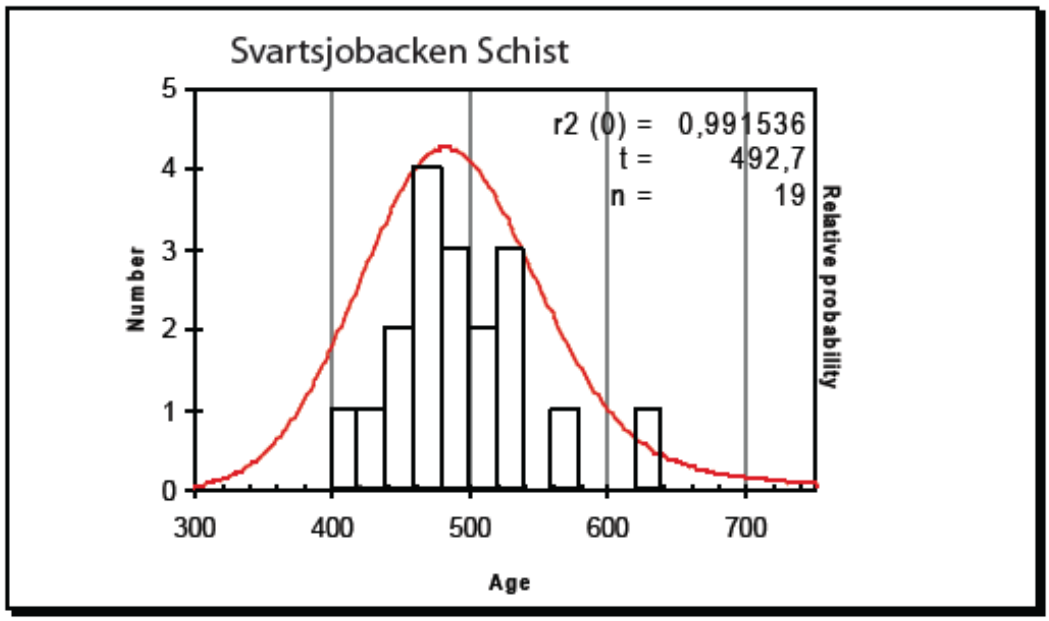

Figure 8-7 Cumulative EMP Monazite age diagram of the Svartsjöbäcken schist. The peak of the probability curve corresponds to the mean apparent age (t). Also r^2 and number of analyses (n) are given.

This results in a mean apparent age (t) of 488,8 +/- 22 Ma (figure 8-7; see appendix 1.4 for the monazites). The r^2 value indicates an almost complete fit; 0.992 (figure 8-8). Two lines are plotted in figure 8-8 (based on methods described in chapter 5). The red line gives the age (T_0) assuming no initial Pb was present; it shows a steeper slope which means an older age than the black line (T). Resulting in T_0=491.2 +/- 22 Ma, T=473.1 +/- 22 Ma.

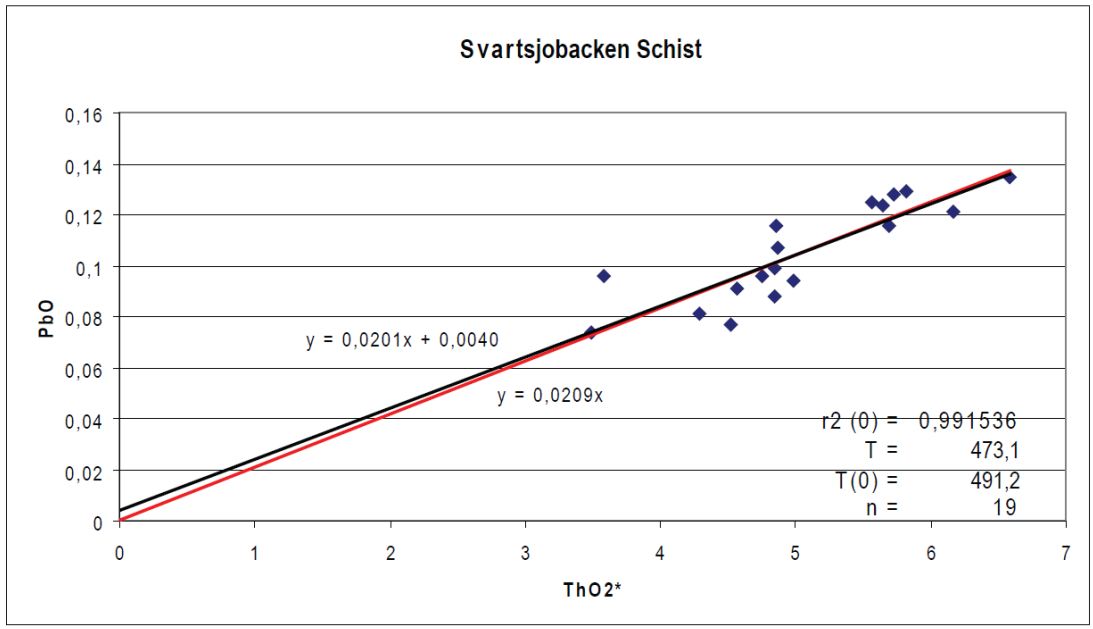

Figure 8-8 Isochron plot of the Svartsjöbäcken schist with corresponding ages, number of measurements and certainty level. Formulas correspond to the corresponding trend lines.

8.1.5 Standard monazite

In order to get control on the stability of the EMP equipment during the time consuming EMP monazite analyses each session was started and ended with the analyses of a standard monazite (appendix 1.5 for method and method section 5.3 for a brief explanation). The results are shown below (figure 8-9). The mean apparent age is 1132.7 +/- 10 Ma which is within the margin of 1125 Ma +/- 10 Myr. The spread is less than seen in the other graphs because the PbO values of the standard are significantly larger (average 0.7 wt % PbO) than the analyzed monazites of the Seve Nappe (average 0.11 wt % PbO), and thus the precision is larger. Resulting in a relative PbO error of 6.8 % for the analyzed monazites of the Seve Nappe and a relative PbO error of 1.3% for the standard monazite (both percentages calculated by the monazite age dating program designed at the EMP lab of Utrecht University). This average PbO value of the standard monazite gives an uncertainty interval of 10 Myr. This is also seen in the r^2 value (figure 8-10). Two lines are plotted in figure 8-10 (based on methods described in chapter 5). The red line gives the age (T_0) assuming no initial Pb was present. In this graph (figure 8-10) the slope of the red line is flatter, which means a younger age than the black line (T). Resulting in T_0=1132.7 +/- 10 Ma, T=1144.5 +/- 10 Ma.

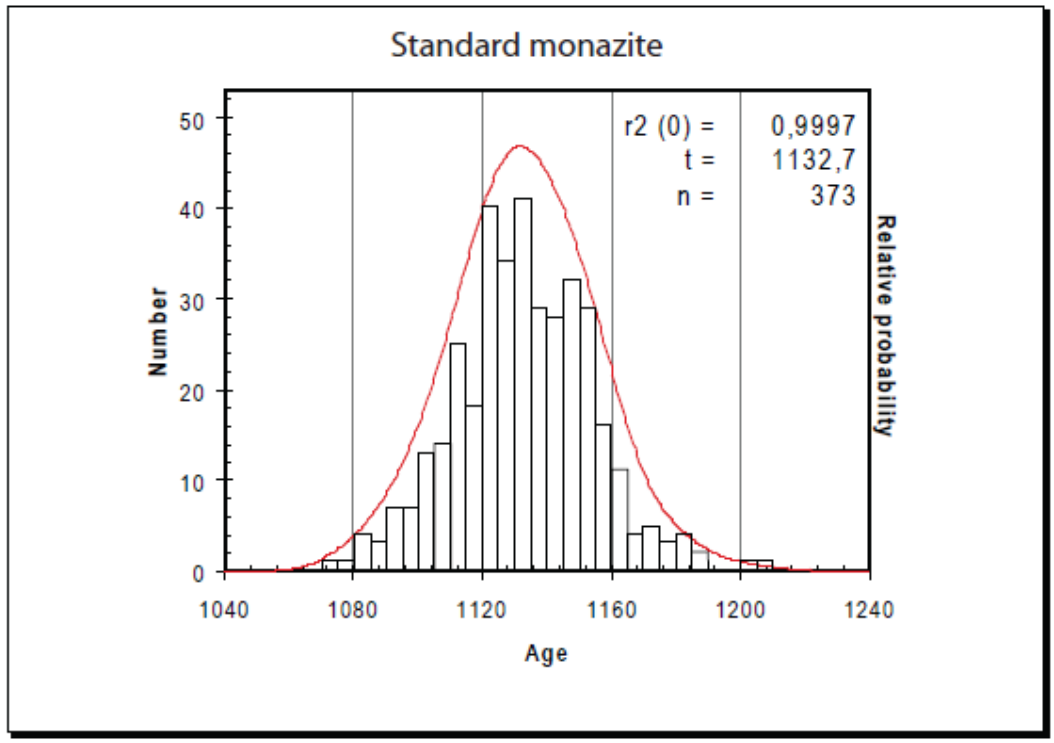

Figure 8-9 Cumulative EMP Monazite age diagram of the standard monazite. The peak of the probability curve corresponds to the mean apparent age (t). Also r^2 and number of analyses (n) are given.

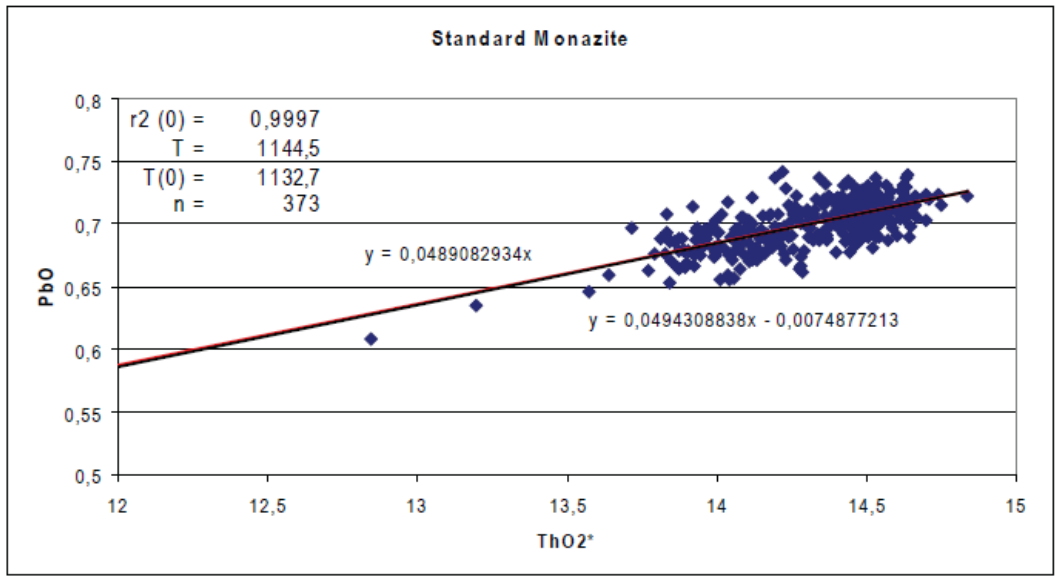

Figure 8-10 Isochron plot of the standard monazite with corresponding ages, number of measurements and certainty level. Formulas correspond to the corresponding trend lines.

8.1.6 Discussion results monazite ages

The low precision (+/- 20 Myr) of the mean apparent age (t) plots is caused by the low PbO values in the analyzed monazites of the Seve Nappe. All measured PbO values in the monazites range between 0.04 and 0.18 wt % PbO (see appendix 1.8 – 1.10). Resulting in a relative PbO error of 14.6% for the lowest wt % PbO and 4.1 % for the highest wt% PbO. This means that the uncertainty is relatively large. For example: the monazite with lowest PbO concentration gives an uncertainty of +/-50 Myr, the mean uncertainty of the monazites is +/- 20 Myr. This results in low precision of the curves in the age diagrams. However the accuracy is good when enough measurements are performed (figure 8-2, 8-4, 8-6 and 8-8). For the measurements of the standard monazite the PbO concentrations are higher, ~0.70 wt% PbO. This gives an uncertainty of +/- 10 Myr. This results in the higher precision for the standard monazite (smaller age range in the age diagrams).

To see the influence of the low wt % PbO, all low PbO values (<0.01 wt % PbO) are deleted from the starting data set used to calculate the cumulative diagram and isochron age of all monazite analyses of the Lillfjället gneiss (figure 8-11). Results are illustrated in figure 8-11 and 8-12. This is performed for the Lillfjället gneiss (figure 8-11). It gives a lower T (361 Ma vs. 454 Ma) an equal T_0 (503 Ma vs. 497 Ma), t (506 vs. 503) and r^2 (0,983 vs. 0,979). For the Lillfjället gneiss with low PbO values the uncertainty is 20 Myr and for the Lillfjället gneiss without low PbO values it is 18 Myr. The only real difference between the two plots (figure 8-2 vs. 8-12) is the formula with whom T is calculated which results in an age difference of 93 Myr. According to the formulas there is now 0.0356 PbO at the start versus the 0.0105 in the original graph with the low PbO values. Assuming that there is no PbO at the start and the original T is closer to T_0 the original data, with the low PbO concentrations, is used. The graphs for the Avardo gneiss and Lillfjället + Avardo gneiss show equal results and are shown in appendix 1.11. From the Svartsjöbäcken schist there was not enough data left to show a reasonable graph without the low PbO values.

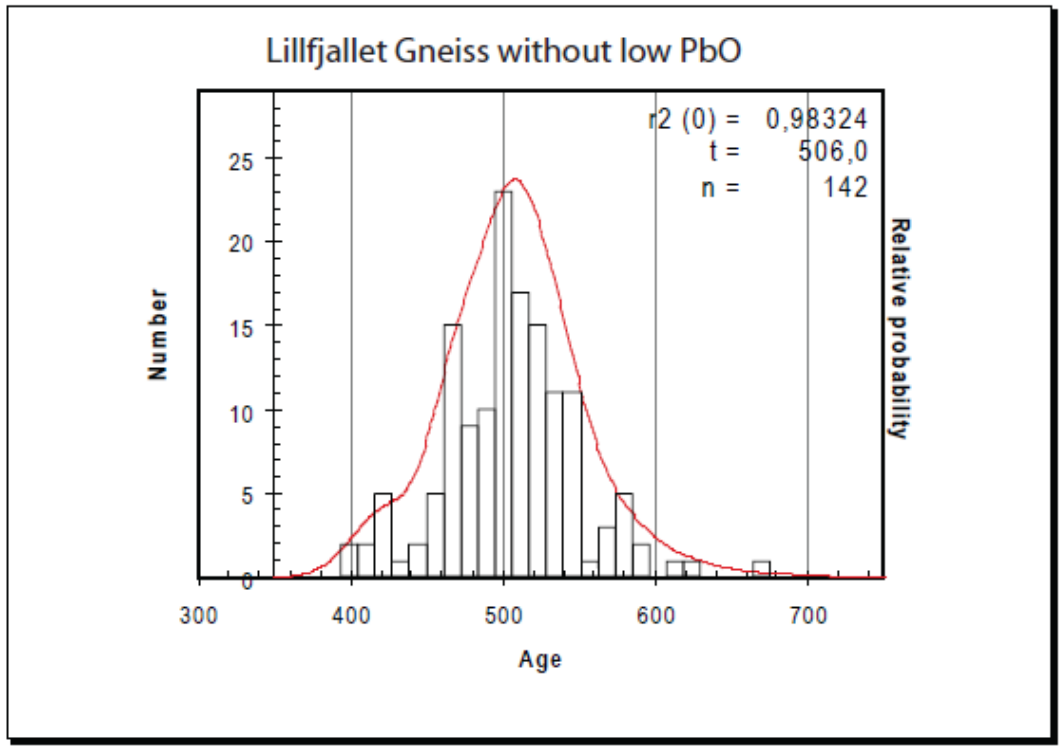

Figure 8-11 Cumulative EMP Monazite age diagram of the Lillfjället gneiss. All low PbO values (<0.01 wt % PbO) are deleted. Number of analysis and relative probability is plotted against different age ranges. The peak of the probability curve corresponds to the mean apparent age (t). Also the r^2, T, T(0) and n are given.

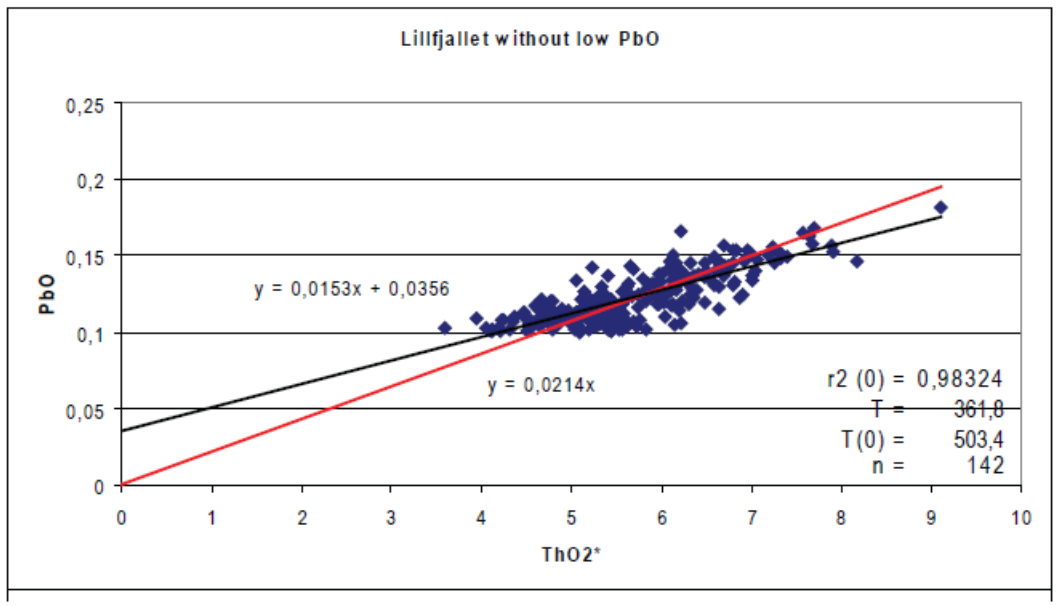

Figure 8-12 Isochron plot of the standard monazite with corresponding ages, number of measurements and certainty level. Formulas correspond to the corresponding trend lines.

8.1.7 Backscatter coefficient calculations

In BSE images most monazite grains reveal non-uniform grey levels (figure 8-13). This is the result of chemical zoning and related to differences in "mean atomic masses". A whiter shade represents a heavier mean atomic weight than a darker shade.

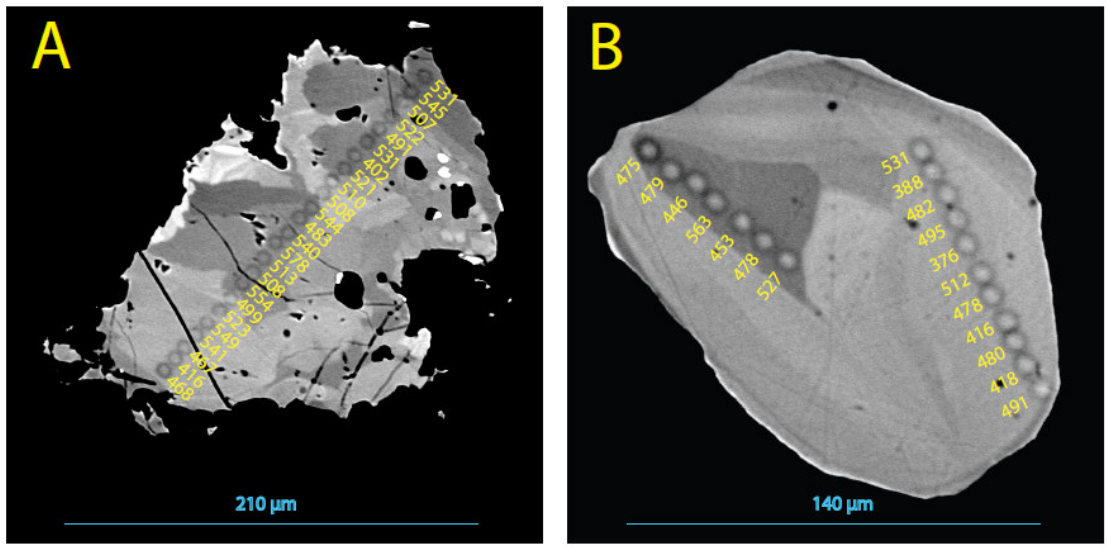

Figure 8-13 Monazites show analyzed spots and calculated ages. Both monazites do not show a relation between age and grey-level. Left picture is taken from sample 65, right picture is taken from sample 17.

The backscatter coefficients are calculated according to the formulas described in the methods section. This is applied to all monazite EMP analyses given in appendix 1.8 – 1.10. When the calculated Backscatter Coefficients (BSC) are ordered in terms of magnitude a continuous graph can be seen defining a range between 0.233 and 0.255 (figure 8-14a). This defines the horizontal numbering system used in figure 8-14 B-F. All other graphs in figure 8-14 are ordered according to this BSC-magnitude system. Out of figure 8-14 it can be concluded that, in general, the wt % CaO and wt % ThO_2* decrease with increasing BSC. The wt % CaO decreases with 0.006 wt% CaO and ThO_2 decreases with 0.038 wt% ThO_2. The opposite trend is seen for the REE (REE is here defined as the sum of the oxide wt % of La, Ce, Pr, Nd, Sm, Gd and Dy), which increase with 0.050 wt% REE. Si and P show no trend. Therefore must be concluded that the zoning in the monazites are predominately formed by the monazite substitution reaction (figure 8-14 B-D):

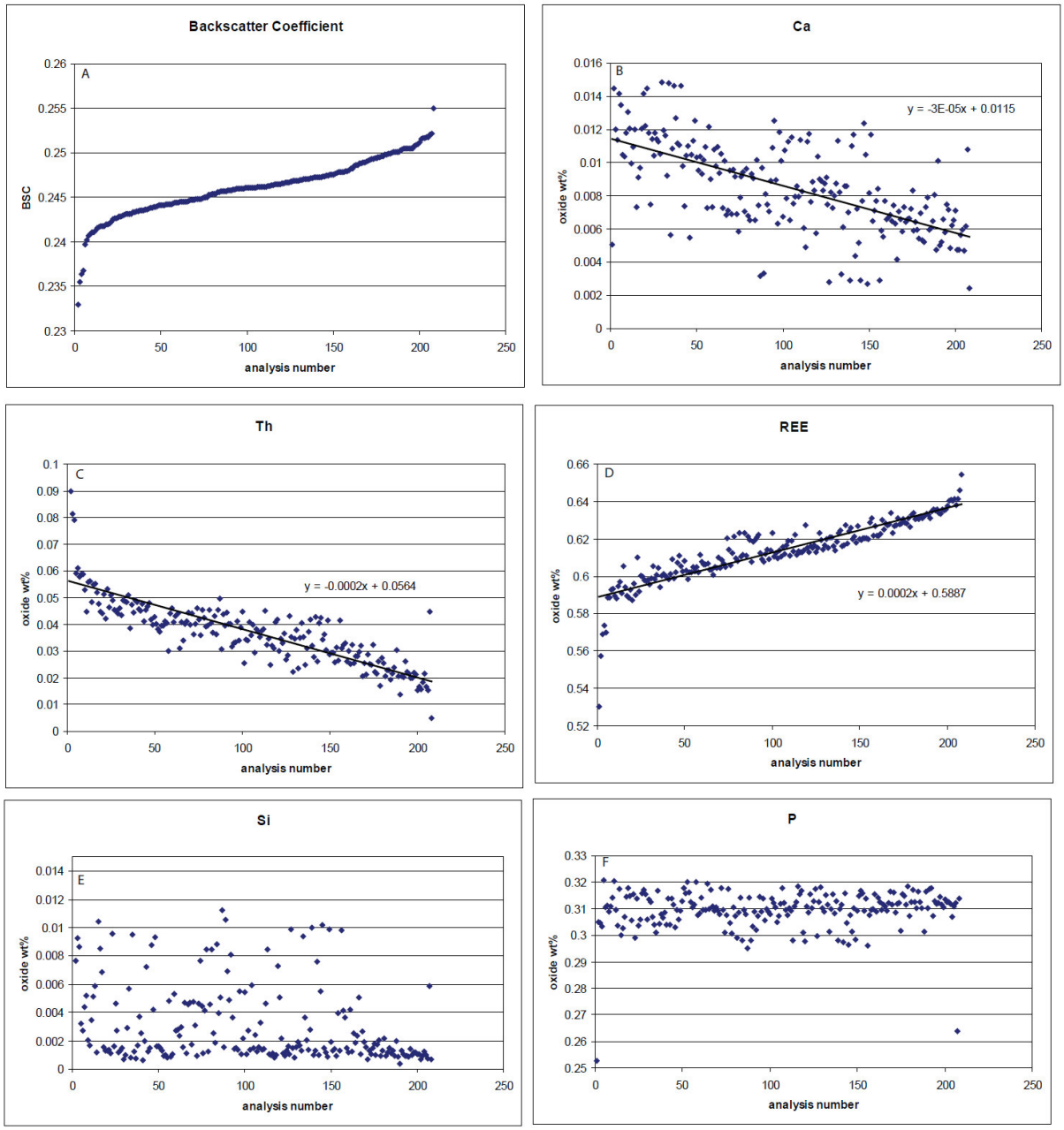

Figure 8-14 In all diagrams the monazite analyses of the Lillfjället gneiss are sorted on the horizontal axis according to a calculated BSE system (see text for further info). A. samples ordered on ascending BSC; this horizontal numbering is also used in B - F. B. Ca generally decreases when the backscatter coefficient increases. C. Th generally decreases when the backscatter coefficient increases. D. REE (REE is here defined as the sum of the oxide wt % of La, Ce, Pr, Nd, Sm, Gd and Dy) generally increases when the backscatter coefficient increases. E-F Si and P show no correlation with the backscatter coefficient.

$$2REE^{3+} \longleftrightarrow Ca^{2+} + Th^{4+} \quad (1)$$

And not by the monazite substitution reaction (figure 8-14 E-F):

$$P^{5+} + REE^{3+} \longleftrightarrow Si^{4+} + Th^{4+} \quad (2)$$

According to formula (1) the amount of CaO and ThO_2 should be equal. According to the measured wt% it is not (0.006 vs. 0.038). Since the EMP age dating method is specified for the elements U, Th and Pb and the ages are interpreted to be correct, the measurements on the standard monazite are within the uncertainty interval, the biggest error must be on the wt% CaO. This is also the element with the lowest amount of wt% on which the error of the EMP is larger since the EMP is especially accurate for major elements.

Figure 8-15 shows the age versus the same horizontal numbering system as used in figure 8-14. This figure shows that there is no correlation between the age and zoning of the monazite.

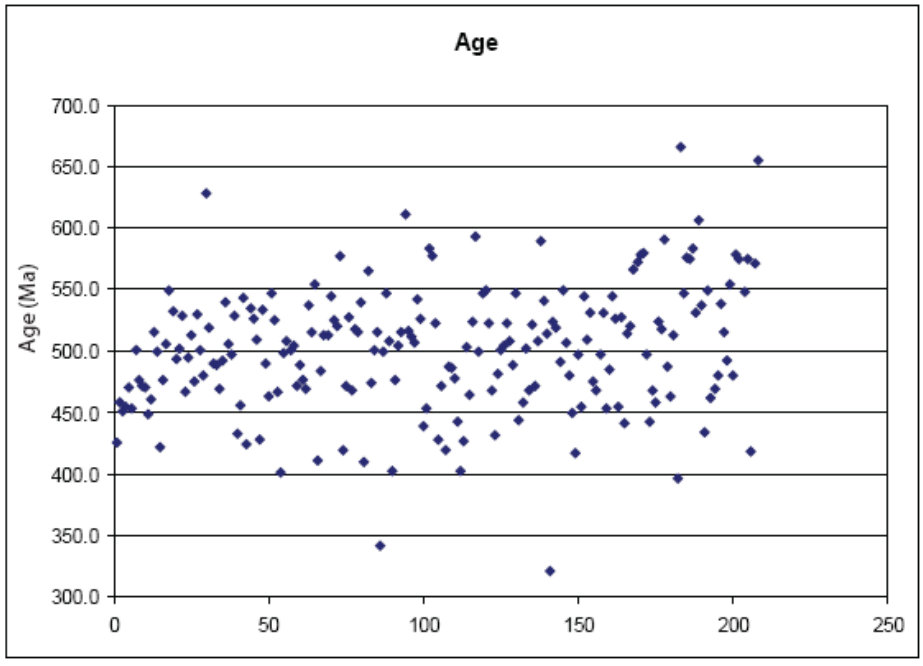

Figure 8-15 All monazite age analyses of the Lillfjället gneiss sorted against calculated backscatter coefficient in the same way as in figure 8-14. The horizontal numbering is sorted on ascending BSC. Y-axis shows the age in Ma. No trend can be seen between age and backscatter coefficient.

8.2 Metamorphism

The range of PT conditions defined in chapter 6 is further specified here to define the PT conditions more precisely. The PT conditions are determined using two samples of the Lillfjället gneiss (sample 42 and 54, figure 5-1 and 5-2 and appendix 1.2). Three methods will be used to do this: a) thermobarometry and b) computer program Domino.

8.2.1 Thermobarometry

The input for the thermometer calculations are data from the mineral analyses produced by EMP (see appendix 1.12). In figure 7-3, 7-4, 7-5 and 7-6 the locations of the mineral analyses are shown. All analyses are performed from top to bottom. The calculations below are performed with minerals from the same metamorphic event. The thermometer used is that of Ferry and Spear (1978), T_{FS}.

$$T_{FS}(°C) = \left\{ \frac{(3890 + 9.56P(kbar))}{2.868 - \ln K_D} \right\} - 273$$

Where $$K_D = \frac{(Fe/Mg)^{Bt}}{(Fe/Mg)^{Grt}}$$

Where $(Fe/Mg)^{Bt}$ is the FeO/MgO ratio in biotite and $(Fe/Mg)^{Grt}$ is the FeO/MgO ratio in garnet. Resulting in:

$K_D = \frac{20.00/9.26}{29.87/2.72} = 0.1970$ using the appropriate values of sample 42 (appendix 1.12).

The analyses are performed on M1 biotites and on M1 garnets which where least chemically zoned.

This results in (table 8-1):

P	T
5	603.536
6	605.664
7	607.792
8	609.92
9	612.048
10	614.176
11	616.304
12	618.432
13	620.56
14	622.688
15	624.816
16	626.944
17	629.072
18	631.2
19	633.328
20	635.456

Table 8-1 Result of the Thermometer of Ferry and Spear (1978).

These temperatures are just inside the stability field of monazites, higher temperatures are expected. The low temperatures are probably due to the restrictions on garnet and biotite compositions outlined by Ferry & Spear. They are:

$$\frac{(Ca+Mn)}{(Ca+Mn+Fe+Mg)} = 0.2 \qquad \text{(1) for garnet and:}$$

$$\frac{(Al^{VI}+Ti)}{(Al^{VI}+Ti+Fe+Mg)} \leq 0.15 \qquad \text{(2) for biotite.}$$

Where Al^{VI} is half of the total Al_2O_3 wt % in biotite minus 1 (Ferry and Spear 1978). According to the restriction on the biotite composition (2) this thermometer can not be used as out EMP analyses indicate (appendix 1.12).

$$\frac{(Al^{VI}+Ti)}{(Al^{VI}+Ti+Fe+Mg)} = \frac{(8.28+2.40)}{(8.28+2.40+20.00+9.26)} \approx 0.26$$

The analysis of sample 54 gives the same discrepancy.

8.2.2 Domino

Another way to specify the PT conditions is with the program Domino (Wei and Powell (2004, 2005); method section 5.5). This is performed on samples 42 and 54. The input for Domino comes from the XRF analyses performed on samples 42 and 54 (results XRF are given in appendix 1.6). Using these bulk rock compositions different Pseudosections can be produced for different H_2O contents (not determined by XRF) (figure 8-13). The H_2O content varies because the XRF can not measure the amount of H and O. Since there are hydrous minerals present the samples must have contained H_2O to some extend. The maximum OH ratio (figure 8-13a) results in a relatively large proportion of hematite (Fe_2O_3). In hematite the iron oxidation state is Fe^{3+}, corresponding to a Fe:O ratio of 1:1,5. This is necessary to compensate for the high OH ratio. When there is a relative high OH ratio it results in low abundances of garnet and biotite where Fe has an oxidation state of Fe^{2+}, corresponding to a Fe:O ratio of 1:1. In figure 8-13b hematite is replaced by magnetite (Fe_3O_4, corresponding to a Fe:O ratio of 1:1,3) this results in the presence of garnet in the pseudosection and the large stability field of biotite. All other fields are more or less the same. The garnet stability field keeps growing when more Fe^{3+} is replaced by Fe^{2+} (see figure 8-13c) until all Fe^{3+} is replaced by Fe^{2+} (figure 8-13d). There all magnetite is completely replaced by Ilmenite ($FeTiO_3$) and the garnet stability field has expanded to a maximum.

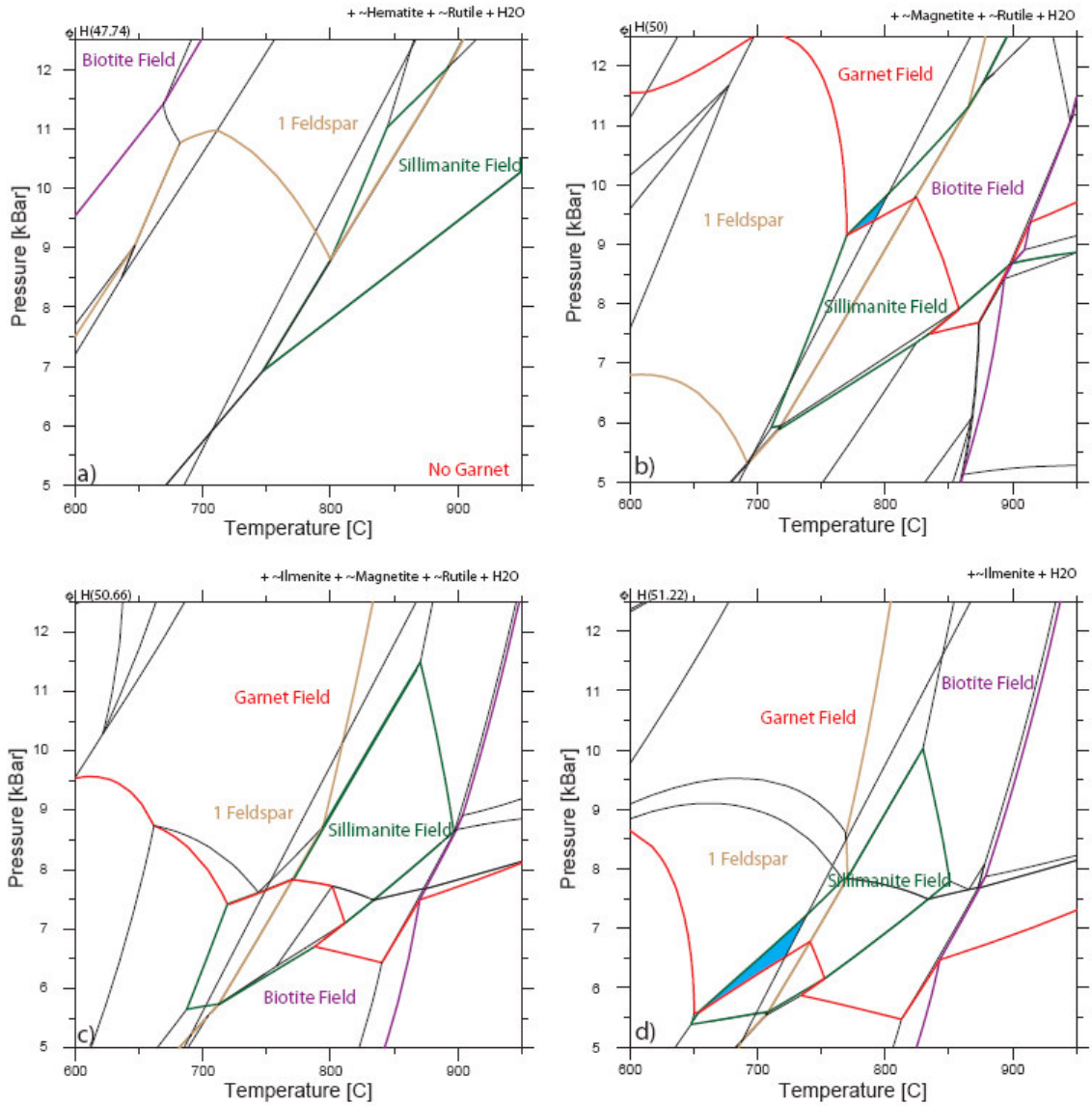

Figure 8-16 Results for different inputs of H_2O content (given at top left side of each diagram) in the Domino program applied to sample 42. Variable is the ratio between O and H. a) Shows the maximum OH ratio without free O_2. b) and c) show expected ratios, somewhere in between the maximum and minimum ratios. d) Shows the minimum OH ratio without free H_2. Blue areas correspond to calculated PT conditions.

Under the EMP it can be seen that there is some iron oxide and titanium oxide (rutile). Whether the iron oxide is hematite or magnetite is not measured. Also some iron-titanium oxide is found, which should be ilmenite, but in smaller amounts. In figure 8-17d relative

large amount of ilmenite (~2%) is found. The results illustrated in figure 8-17b are chosen above those in figure 8-17d because the percentages are better corresponding to the percentages estimated from EMP images. Figure 8-17a has not the right mineral assemblage (garnet is missing) and figure 8-17c has no area where the M1 mineral assemblage, found in the thin section and corresponding hand specimen is stable. Figure 8-17b is enlarged in figure 8-18.

The same procedure is performed for sample 54. The result is given in the pseudosection (figure 8-19).

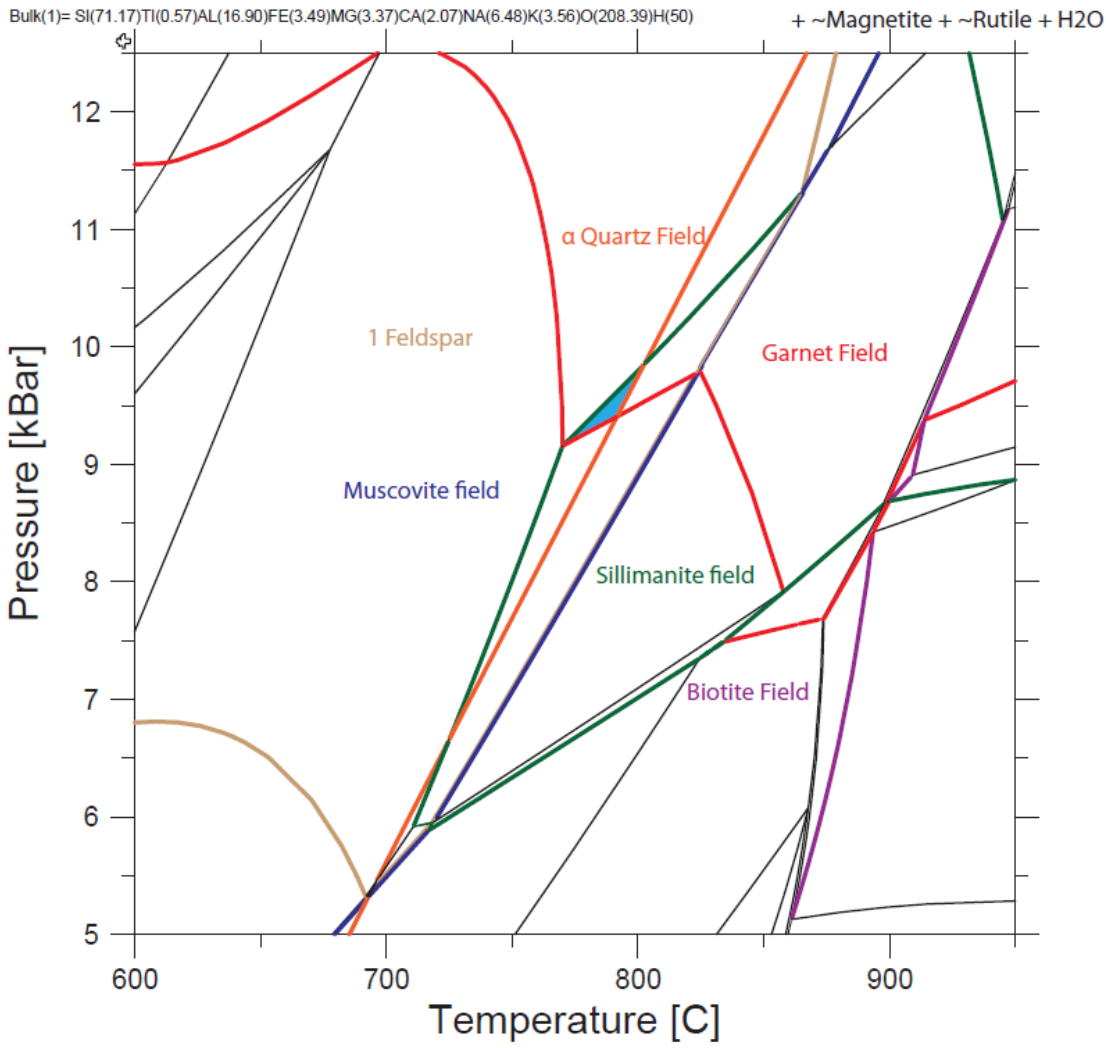

Figure 8-17 Pseudosection of sample 42. Blue area indicates the PT conditions calculated for the mineral assemblage seen in the handspecimen/thin section of the sample.

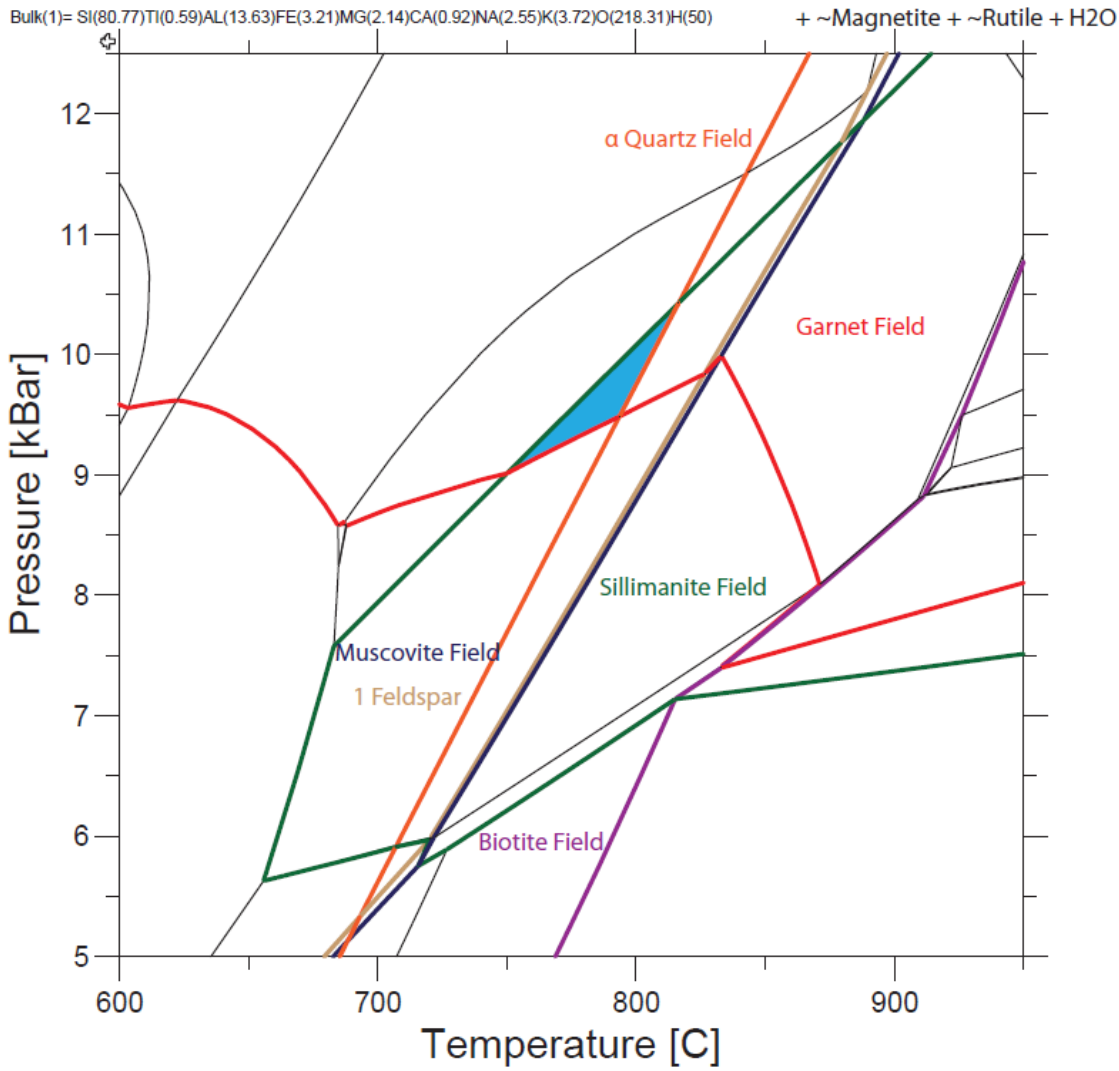

Figure 8-18 Pseudosection of sample 54. Blue area indicates the PT conditions calculated for the mineral assemblage seen in the handspecimen/thin section of the sample.

8.2.3 Conclusion PT conditions

Sample 42 gives a temperature range of 750 – 800 ºC and a pressure range of 9 – 10 kbar and sample 54 gives 725 – 825 ºC and 9 – 10.5 kbar. Both PT ranges overlap with each other defining one PT range for the Lillfjället gneiss. The overall PT range for the Lillfjället gneiss should have a temperature between 750 – 800 ºC and a pressure between 9 – 10 kbar. These PT condition needs to be specified. This is tried with combining the results of Domino and the results of the mineral analysis with the EMP. The mineral analysis obtained by EMP gives specific results about mineral end member compositions

present in the sample. Domino is also able to calculate the relative proportions of the end members. These results can thus be compared as a final check.

To determine the exact PT conditions the garnet field is expressed in percentages of pyrope, grossular and almandine by Domino (figure 8-20 and 8-21); other garnet endmember compositions such as spessartine (Mn endmember) are not calculated by Domino. This representation is called an isoplot graph (figure 8-20 and 8-21).

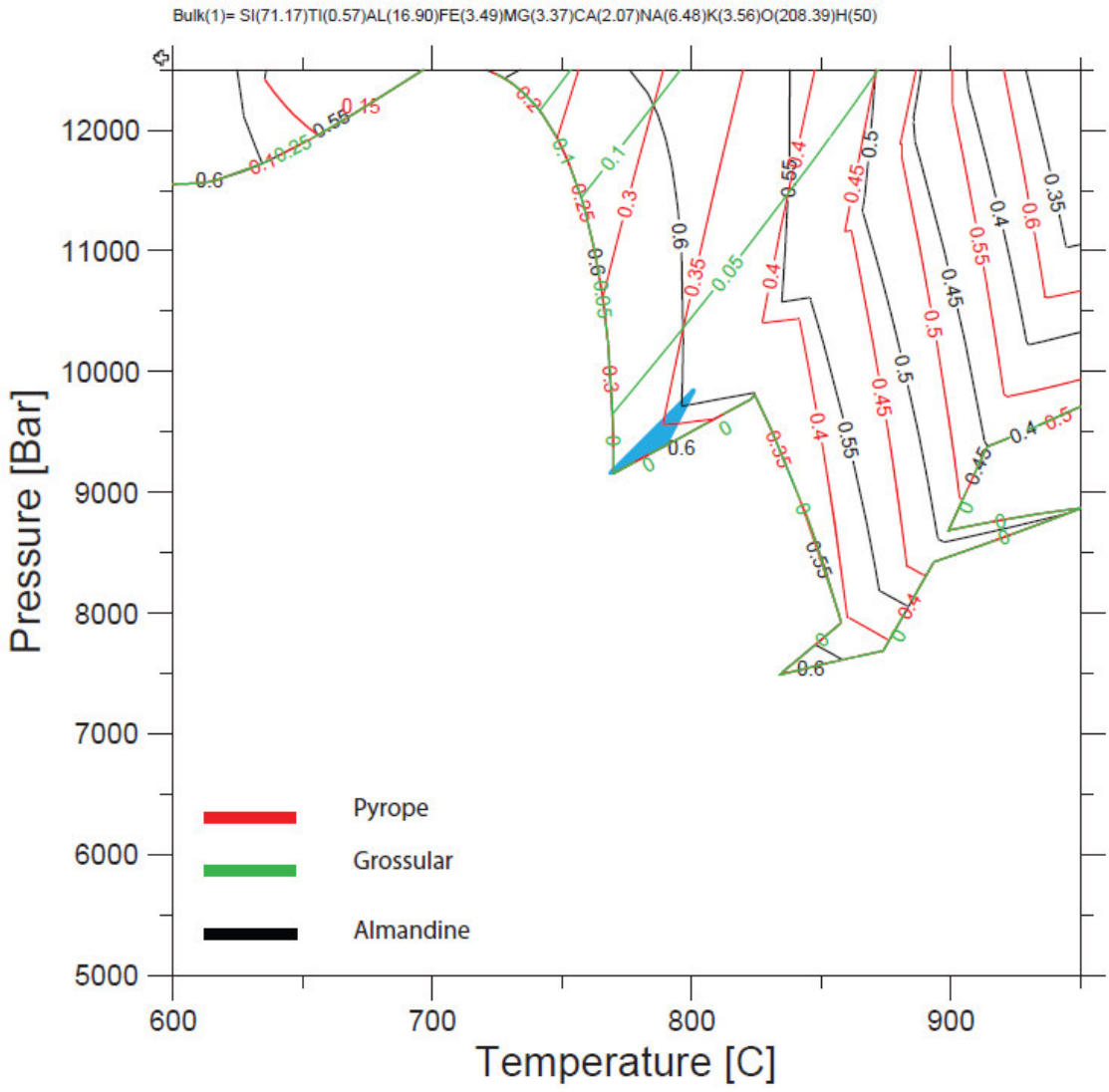

Figure 8-19 Isoplot graph of garnet from sample 42. All numbers refer to the relative percentages of the endmember compositions listed at the bottom left. Blue area is the PT condition found above.

These graphs are compared with the mineral analysis performed with the EMP (table 8-2; see method section for the calculation procedure)

	Almandine	Pyrope	Grossular
Sample 42	81,7163	13,2659	5,01789
Sample 54	75,8614	12,1372	12,0014

Table 8-2 Mean values of garnet analysis performed with EMP.

The maximum percentage of the almandine endmember component in garnet according to Domino (within the found PT condition described above; blue area in figure 8-20 and 8-21) is between 60 and 65 % for samples 42 and 54 while the measured percentage by EMP for almandine is 75 respectively 81 % for samples 42 and 54 (figure 8-20 and 8-21). For the pyrope endmember component in garnet it is the opposite, the maximum percentage by Domino is much higher than the measured percentage by EMP, 30 – 35 % in comparison with 12 – 13 %. The percentages for the grossular endmember component in garnet are between the 5 and 10 % according to Domino (figure 8-20 and 8-21) and 5 respectively 12 % according to the results of the EMP. This means that the percentage grossular is more or less the same in both methods. EMP mineral analysis of biotite, white mica and feldspar is also compared with the results of the pseudosections. Again there is no correspondence. This means that this method does not work (yet), and that it is not possible to specify the PT conditions by using the pseudosection made of the Domino program by combining both methods.

Combining all PT results described above the Lillfjället gneiss has undergone PT conditions ranging between 750 – 800 ºC and 9 – 10 kbar.

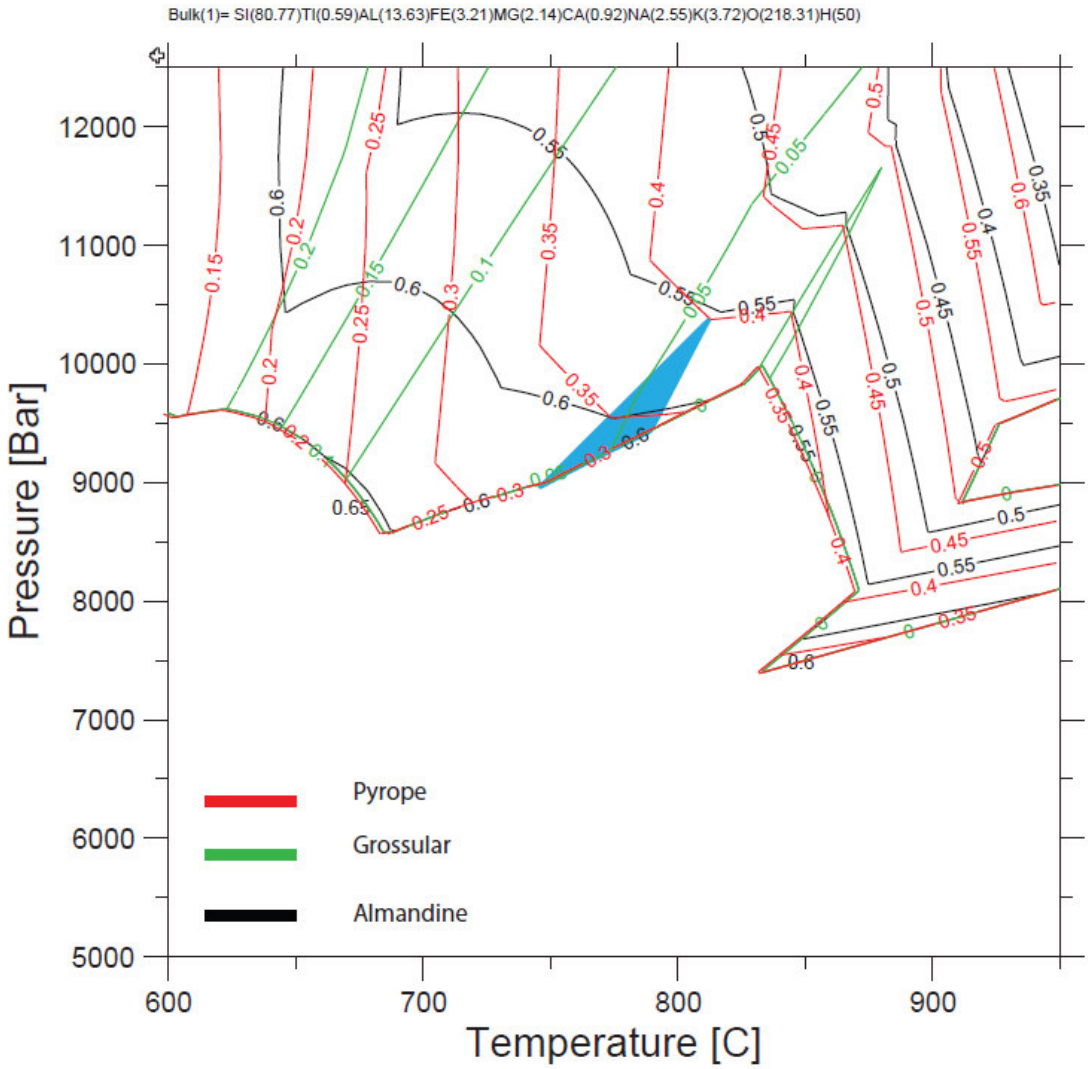

Figure 8-20 Isoplot graph of garnet from sample 54. All numbers refer to the relative percentages of the endmember compositions listed at the bottom left. Blue area is the PT condition found above.

9 Discussion

In this chapter all results presented in chapter 8 are discussed. This will results in a proposed geodynamic model presented in paragraph 9.3.

9.1 Ages

All monazites are interpreted to represent one tectonometamorphic event that occurred around 500 +/- 20 Ma (499.5 +/- 20 Ma is the T_0 of the combined data of the Lillfjället and Avardo gneiss). The cumulative EMP monazite age diagrams (figure 8-1 and 8-5) give one clear peak. The cumulative age diagram of the Avardo gneiss (figure 8-3) could be interpreted to contain more than one tectonic event but all peaks fall within the uncertainty level of +/- 20 Myr. Thereby the corresponding r^2 value (figure 8-3) is high enough to allow such an interpretation which is also supported by the curve which also gives one peak. In addition the age of the Lillfjället and Avardo gneiss give the same mean ages T_0 (497.9 and 502.3 respectively) within the uncertainty interval of +/- 20 Myr. From this it was concluded that the Lillfjället and the Avardo gneisses are affected by the same tectono-metamorphic event called M1. This is also in agreement with the corresponding r^2 values. The Svartsjöbäcken schists could be from the same tectono-metamorphic event also (T_0=491.2 +/- 20 Ma), although there are not enough measurements performed to be sure. Since there is no tectonic contact described between the Central belt (Lillfjället and the Avardo gneiss) and the Western belt (Svartsjöbäcken schist) it seems a reasonable assumption. Also the Marsfjället gneiss gives 507.2 +/- 20 Ma monazite ages (modified from dated monazites of M.A. Hogerwerf (Msc thesis 2010)). This makes it even more acceptable that all monazites are formed during the same tectonometamorphic event at ~500 +/- 20 Ma.

It takes at least several million years to subduct a slab to depths where monazites start to grow. This means that it also takes at least several million years for a slab to educt back to the surface. Therefore it is likely that monazite does not grow at one particular moment in time but during a period in time. This is probably the case here also because of the wide spread in the ages found (figure 8-1, 8-3, 8-5 and 8-7). This period could not be very long because the zoning in monazites is not linked with age as shown in chapter

8.1.7. Therefore it is not likely that it is one continuous metamorphic event that takes place from ~500 Ma – 400 Ma. This also means that other younger events did not affect the monazites. This could have several reasons. The first reason can be that temperatures were not high enough (550 ºC) (Wing et al. 2003) during the younger events or second that the monazites were not effected by a later metamorphic event and/or no new monazites grew.

The peak metamorphism does not have to be at 500 +/- 20 Ma. The monazites could start to grow before the peak metamorphism i.e. during the prograde path (1 in figure 9-1). They could also record ages after the peak metamorphism, when the temperature is still high enough (3 in figure 9-1). The three possibilities, called 1, 2 and 3 are shown in figure 9-1. The option given with number 1 in figure 9-1 is not very likely because the temperature at which monazite starts to grow should be (≥550 ºC) (Wing et al. 2003) to grow before the peak metamorphism. Since little is known about the exact growth conditions of monazites in comparison with peak metamorphism the ages are interpreted as peak metamorphic ages (Terry et al., 2000a; Carswell et al., 2003b; Bingen et al., 2003; Krogh et al., 2003.)

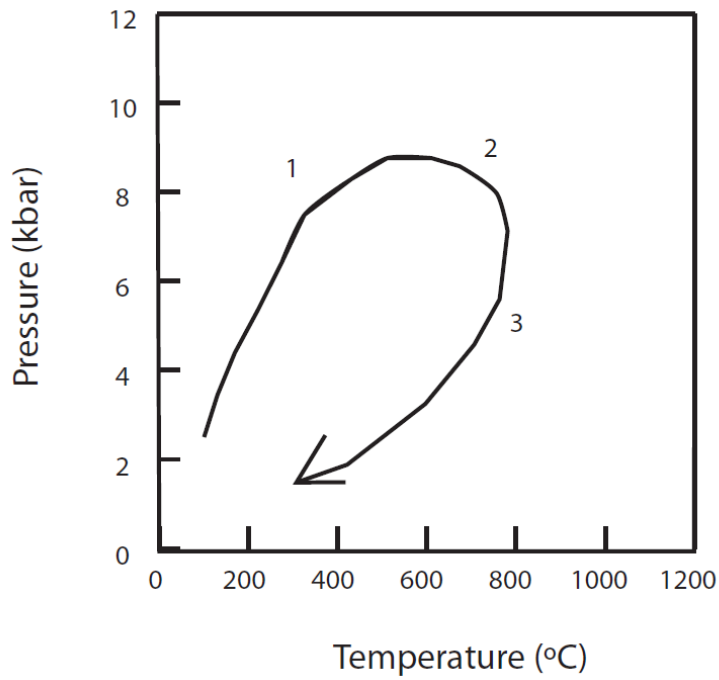

Figure 9-1 PT path from a subducting slab which returns to the surface. The numbers 1, 2 and 3 indicate moments where the monazite could start to grow.

As described above the tectonometamorphic event dated by the monazite (at ~500Ma) is the Finnmarkian event (chapter 4.5: Roberts 2003, Brueckner & Van Roermund 2004). For the Caledonides Roberts (2003) describes at this moment in time a collision between Baltica and a magmatic arc with Baltica (figure 4-9) subducting under the magmatic arc. According to Roberts (2003) the Middle Allochthonous Finnmarkian nappes tectonically on top of Baltica at the end of the Finnmarkian event (figure 4-9). According to Brueckner & Van Roermund (2004) the Virisen arc complex collide in Finnmarkian time with a microcontinent to form the Virisen/Norbotten composite terrane (VNCT see figure 4-6). The VNCT collides with mainland Baltica during the Jämtlandian (~450 Ma). Both models describe a magmatic arc that in one case is colliding with western Baltica (Roberts 2003) and in the other case collides with a microcontinent situated in front of the west coast of Baltica (Brueckner & Van Roermund 2004). Brueckner & Van Roermund (2004) do emphasize that the subducted/educted microcontinent has undergone HP metamorphic conditions (~15 kbar and ~700 °C), which means that the temperature is high enough to form monazites. Roberts (2003) shows (in figure 4-9) that there are eclogite facies conditions in the subducting slab but not that the exhumed nappes have undergone these conditions. Both models show that this event affected only a small area and not the whole Scandinavian Caledonides. The fact that the monazites dated in this thesis show only one tectonometamorphic event means that the other younger tectonometamorphic events, described by Brueckner & Van Roermund (2004) and Roberts (2003), have not affected the studied monazites. At least one more tectonic event should have happened to form the geological and tectonometamorphic setting shown in figure 4-2, 4-3 and 4-4.

9.2 Metamorphic facies

There are several reasons that can explain the difference in results obtained by the Domino program in comparison with results of the EMP (chapter 8.2). The input of the Domino program is the output of the XRF analysis. This is a whole rock analysis (M1+M2), while the measurement of the EMP is a mineral chemical analysis (M1),

which result in differences between the two methods. EMP mineral analysis is accurate in determining the major element components. Domino has to divide all elements, found by XRF whole rock analysis, over all possible minerals. Domino is able to do that but only with basic endmember mineral compositions (appendix 1.7). For example according to this table, there is no Ti incorporated in biotite while there is ~3% incorporated in biotite according to the EMP measurements. Another example is that Mn is not incorporated in garnet while there is ~7% incorporated in garnet according to the measurements by the EMP. Because of all these simplifications the ratio between different minerals is changed. Resulting in different endmember compositions between Domino and the EMP for garnet.

Another point of discussion is that the M1 and M2 mineral assemblages dated by the monazite are different for the Lillfjället and the Avardo gneisses. The monazites in the Lillfjället gneiss are incorporated in the M1 minerals quartz, garnet, muscovite, biotite, k-feldspar and plagioclase. While the monazites dated for the Avardo gneiss are included in quartz, muscovite and biotite (M1 minerals). The minerals muscovite and biotite are also interpreted as part of the metamorphic overprint M2. Nevertheless there are also two monazites found in garnet (sample 52d) (appendix 1.3) for the Avardo gneiss. These samples are not dated because the monazites where too small in size compared to monazites in other samples. If the monazites of sample 52d give older ages, the age described could be interpreted as a metamorphic overprint (M2). But the ages should be significantly older to conclude this because no significant number of analyses can be performed on these small monazites. Sample 37d (appendix 1.3) shows a monazite that is dated just outside a garnet; this is at this moment reason enough to interpret all monazite results to be the result of a same metamorphic event (=M1). Another reason to interpret that M1 and M2 are formed during the same tectonometamorphic event is that all monazites give the same age, also the monazites which are no inclusions in other minerals. Therefore M1 and M2 are interpreted to be formed during the Finnmarkian orogeny.

9.3 Geodynamic model

The model described below is a possible geodynamic reconstruction that can explain the local tectonometamorphic events described in this thesis. The focus of the model is to try to explain the different metamorphic units (Avardo-, Lillfjället-, Marsfjället gneiss and Svartsjöbäcken schist) next to each other despite the large differences in metamorphic pressure (figure 4-3). It is therefore a model that emphasizes the regional tectonics (size of Marsfjället to Lillfjället ~100 km) and is not representative for the whole Scandinavian Caledonides.

The starting configuration is based on the model of Brueckner & Van Roermund (figure 9-2) except for the microcontinent, which is not needed here because there is no tectonometamorphic event, at 454 Ma, according to the geochronological data presented in this thesis. Hereby is the anticlockwise rotation of Baltica with respect to Laurentia (Roberts, 2003; Torsvik, 1996, 1998; Torsvik and Cocks, 2005) neglected to simplify the model i.e. the model is independent of the fact that Laurentia or Siberia is facing Baltica. Neither does it matter, for the model, what kind of sea/ocean is situated between the colliding continents (Iapetus vs. Aegir).

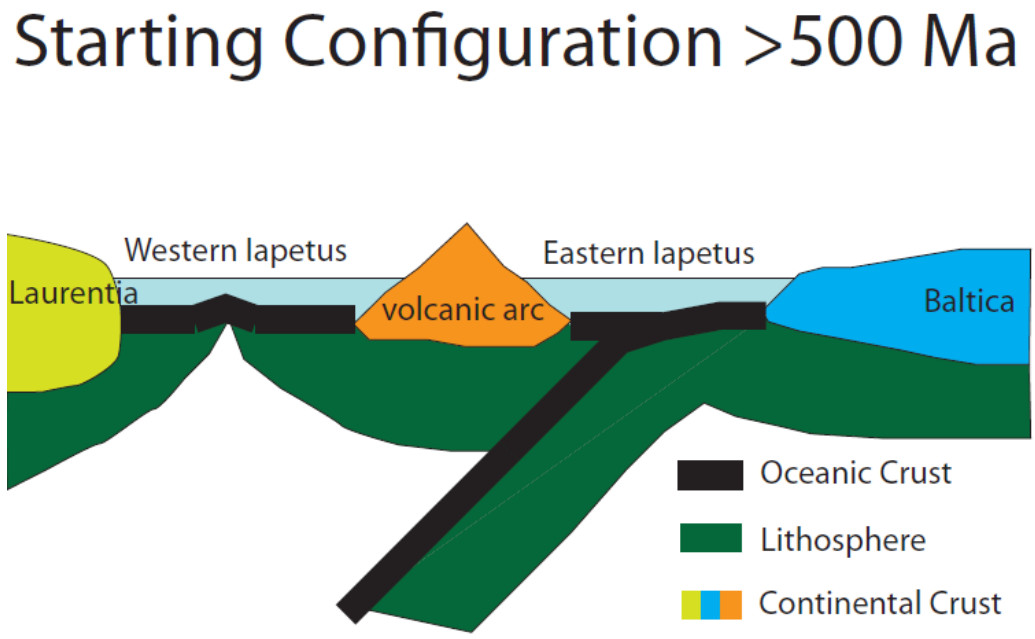

Figure 9-2 Starting configuration at >500 Ma. Based on the model of Brueckner & Van Roermund (2004).

Figure 9-2 illustrates the starting geometry of the model in which an island arc is formed when Eastern Iapetus becomes subducted below Western Iapetus. Subsequently Baltica is starting to subduct under the Virisen volcanic arc at ~500 Ma (figure 9-3 configuration A). At this moment in time it is possible for garnet peridotite to intrude into the subducting continental slab. This slab underwent eclogite facies metamorphism. At this moment in time monazites start to grow and record the peak metamorphic conditions at ~500 Ma. This collisional event is called Finnmarkian. The difference between the model of Brueckner & Van Roermund (2004) and this model is that the Western Belt (Svartsjöbäcken schist) and the Central Belt (Lillfjället, Avardo and Marsfjället gneiss) find their origin and peak metamorphism during the Finnmarkian orogeny (and not during the Jämtlandian =454 Ma, Brueckner & Van Roermund, 2004). Another difference is that the microcontinent introduced by Bruckner & van Roermund (2004) is not needed in the starting configuration because there is no Jämtlandian orogeny.

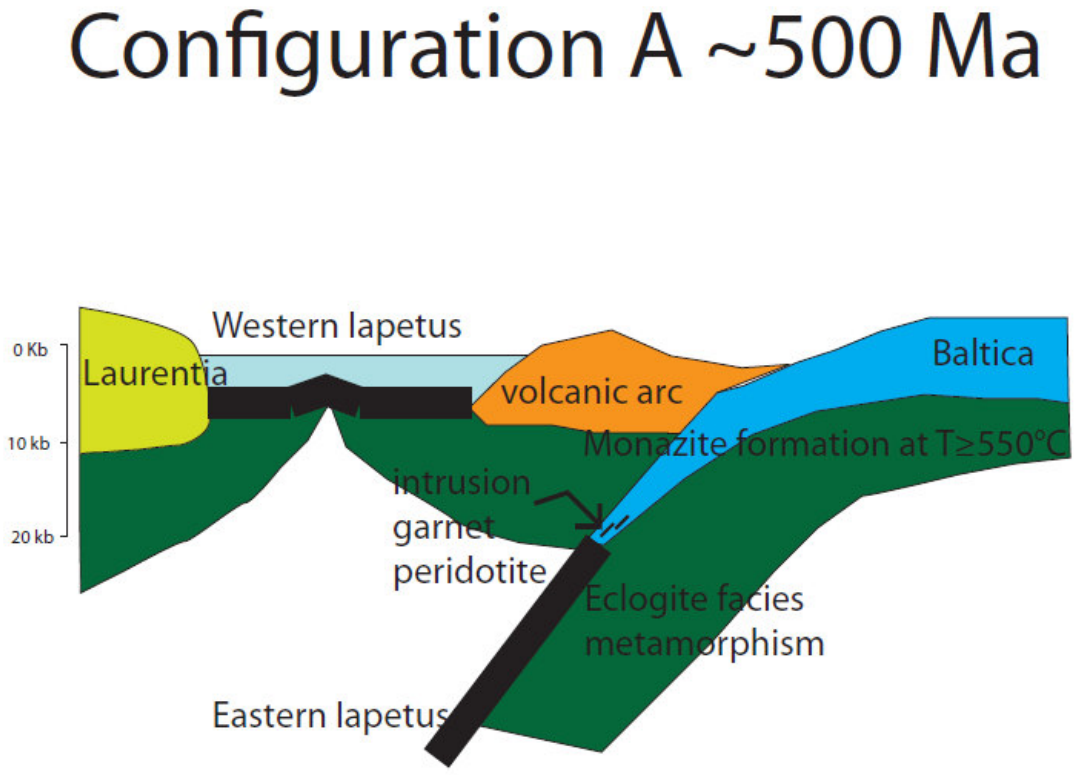

Figure 9-3 Configuration at ~500 Ma. Baltica is subducting under a volcanic arc. This is the moment in time where the monazites start to grow and the garnet peridotites are intruded in the subducted continental crust

Consequently after the Finnmarkian collision the subducted oceanic slab (i.e. Eastern Iapetus) breaks off and the subducted continental crust of Baltica starts to educt (figure 9-4 configuration B). The relative spatial positions of the tectonometamorphic units from the Central Belt are indicated in figure 9-5 (configuration C). In a 3D view (figure 9-6) it can be seen how the Svartsjöbäcken schist, Marsfjället- and Avardo gneiss are positioned in the subducting slab. In contrast the Lillfjället gneiss is interpreted based on metamorphic criteria to be part of the overriding subcontinental crust, not in the subducting slab (figure 9-5). At the end of the Finnmarkian orogeny, after eduction, the units are tentatively situated as illustrated in figure 9-7. The Svartsjöbäcken schist, Marsfjället gneiss and Avardo gneiss are educted to almost the same depth level as the Lillfjället gneiss (figure 9-7). Also the relative motions between the tectonometamorphic units are indicated.

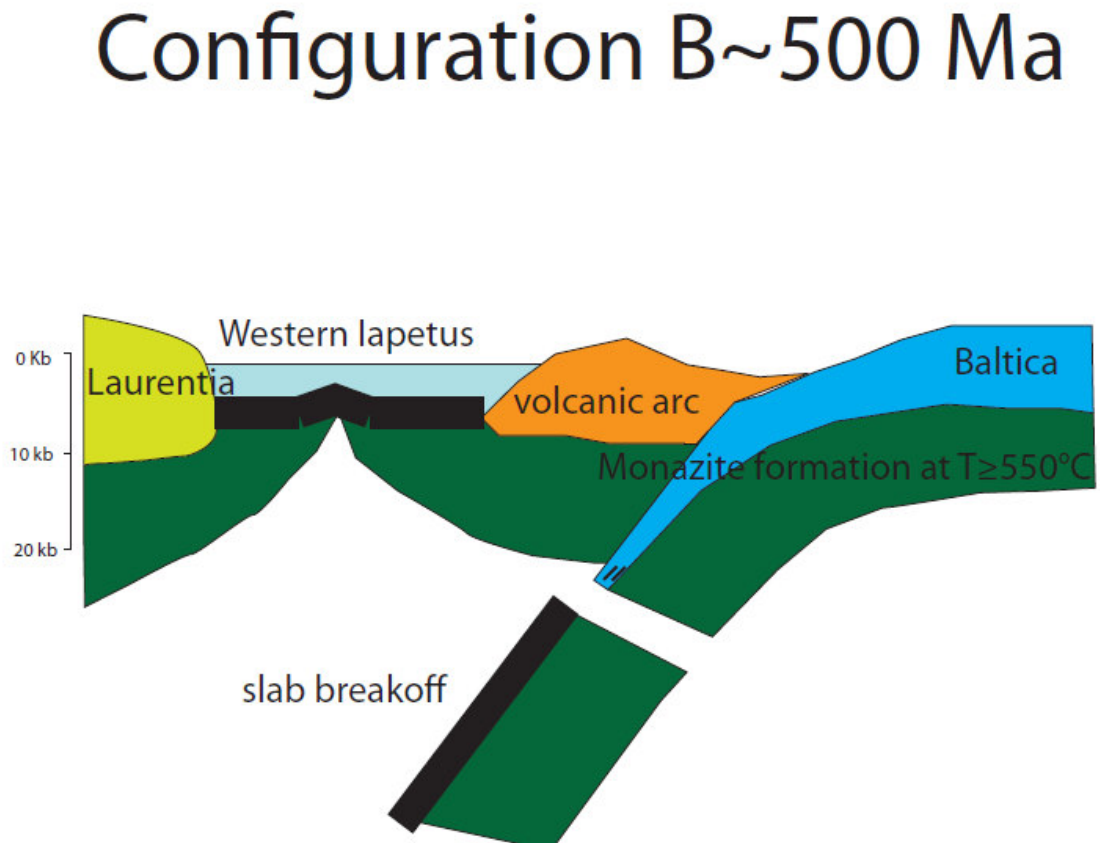

Figure 9-4 Configuration B at ~500 Ma just after slab break off.

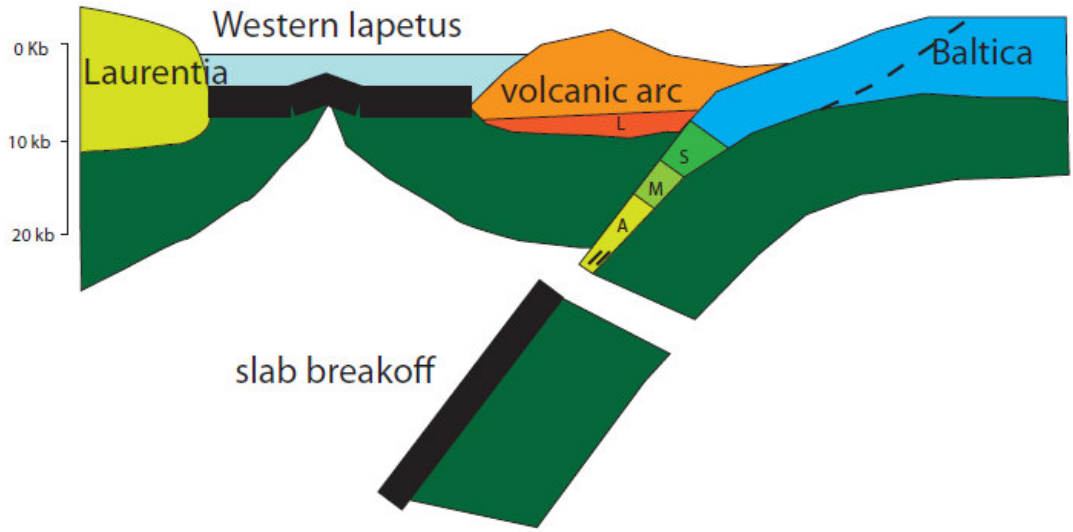

Figure 9-5 Configuration C at ~500Ma just after slab break off. In the configuration the different tectonometamorphic units, studied in this thesis, are illustrated with different colours and symbols. L=Lillfjället gneiss, S=Svartsjöbäcken schist, M=Marsfjället gneiss and A=Avardo gneiss. Dashed line becomes future thrust plane.

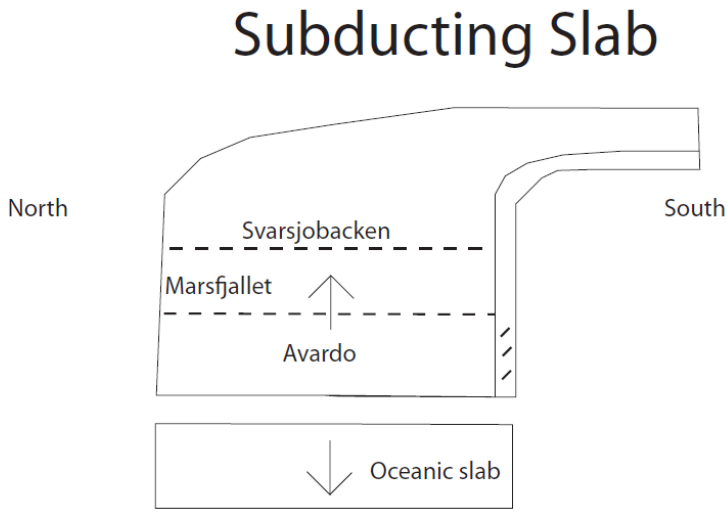

Figure 9-6 Front view of the subducting continental slab. Arrows indicate the relative movement directions of slab break off. The tectonometamorphic units are indicated according to their relative position in the subducted slab.

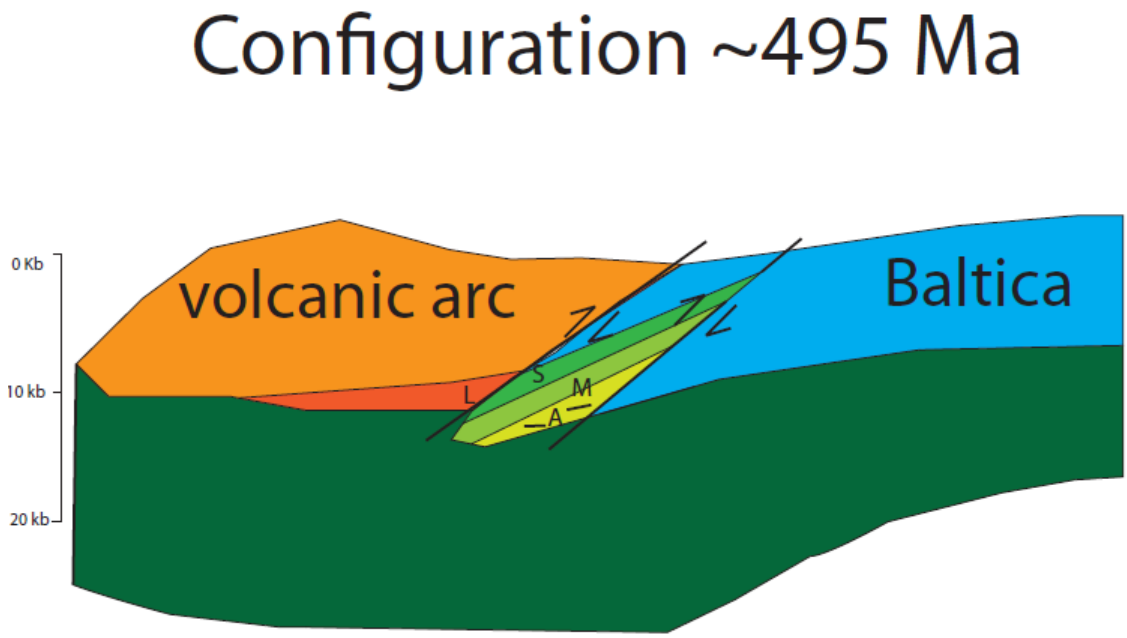

Figure 9-7 Eduction of the subducted continental slab. L=Lillfjället gneiss, S=Svartsjöbäcken schist, M=Marsfjället gneiss and A=Avardo gneiss.

After figure 9-7 the Finnmarkian orogeny was finished, but the overall convergence between Laurentia and Baltica did not stop yet (figure 9-2). Onwards convergence will result in subduction of Baltica underneath Laurentia from ~420 – 400 Ma (Scandian Orogeny, see figure 9-8). During this collision Western Iapetus subduct below Laurentia and Laurentia collides with Baltica forming the nappe stacks seen today (see profiles in figure 4-4). The Köli nappe is material that is scraped off form the subducting oceanic crust (figure 9-8). The former volcanic arc, Avardo-, Lillfjället-, Marsfjället gneiss and Svartsjöbäcken schist are thrusted further eastwards onto Baltica as shown in figure 9-8. Part of the westernmost continental crust subducts under Laurentia. After slab break off the remaining part of the subducted continental crust of Baltica exhumes back to the surface to form the Western Gneiss Complex and other related (U)HP areas (Brueckner & Van Roermund, 2004). Figure 9-9 shows the configuration after eduction of Baltica, the figure is focused on the tectonometamorphic units described in this thesis. In reality more nappe stacks are formed next to each other. After exhumation of the whole Scandinavian Caledonides the configuration figure 9-10 is seen in the northern part where the Lillfjället gneiss is absent. The position of the structural profile AB is illustrated in

figure 9-10, figure 9-11 shows the same configuration but in the central part, where the Marsfjället gneiss and the Svartsjöbäcken schist are replaced by Avardo gneiss. Figure 9-12 shows the configuration in the southern part, only the Lillfjället gneiss remains.

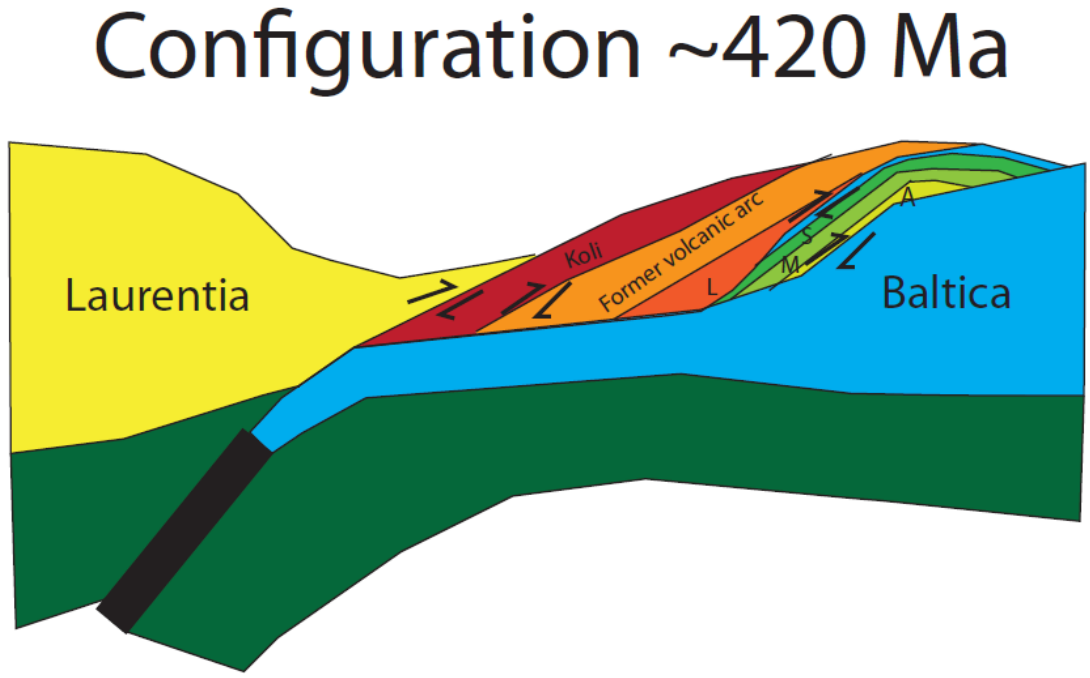

Figure 9-8 Collision of Baltica with Laurentia. Again intrusion of garnet peridotite in the downgoing slab is possible beneath Laurentia. L=Lillfjället gneiss, S=Svartsjöbäcken schist, M=Marsfjället gneiss and A=Avardo gneiss.

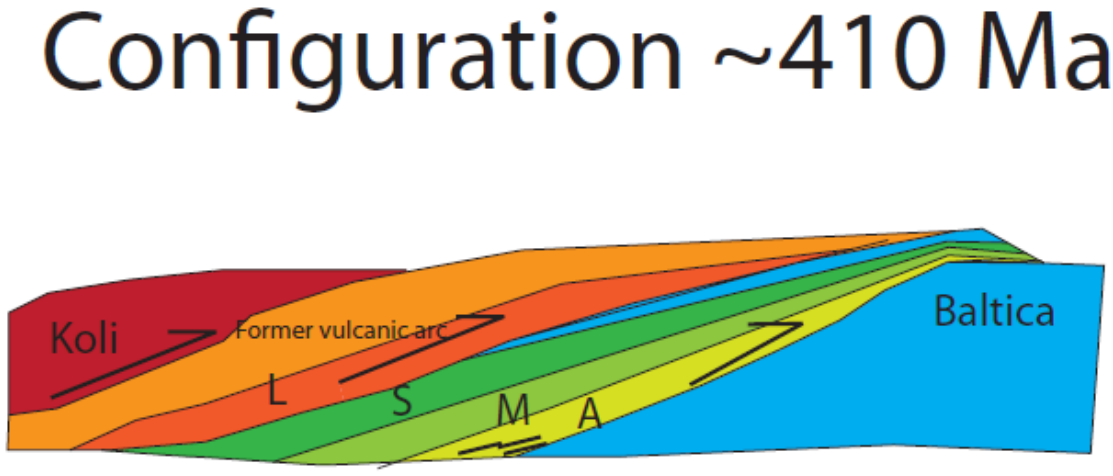

Figure 9-9 After exhumation of Baltica this configuration is recognized. L=Lillfjället gneiss, S=Svartsjöbäcken schist, M=Marsfjället gneiss and A=Avardo gneiss

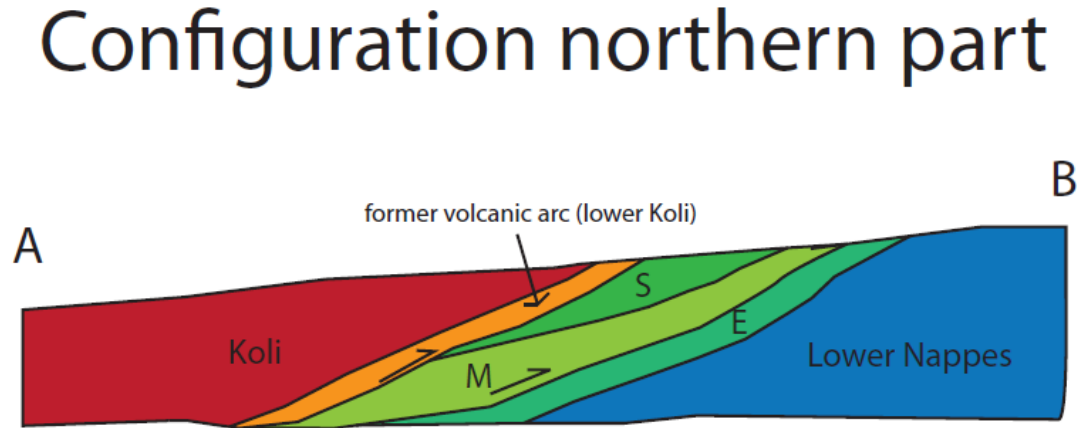

Figure 9-10 Simplified configuration as it is found nowadays in the northern area. S=Svartsjöbäcken schist, M=Marsfjället gneiss and E=Eastern Belt.

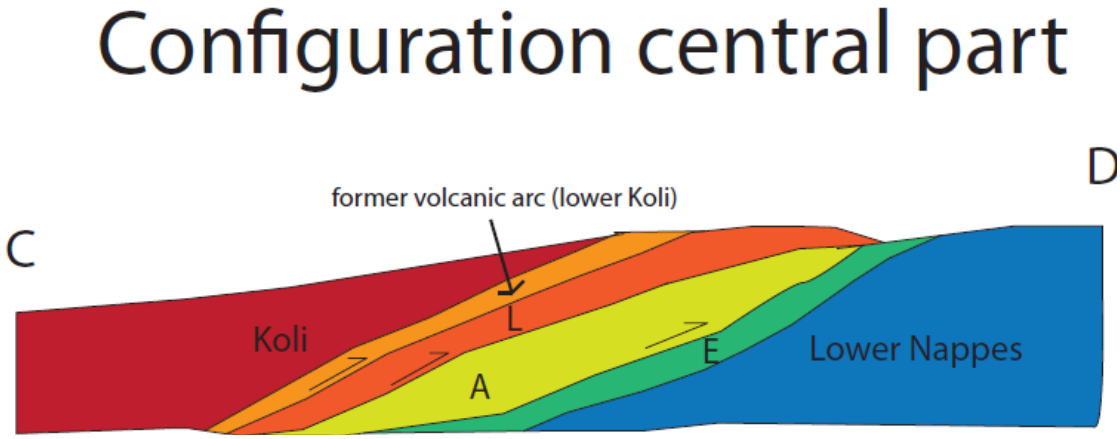

Figure 9-11 Simplified configuration as it is found nowadays in the Central area. At some places the Avardo gneiss is found at the surface, at other locations it is overlain by the Lillfjället gneiss. L=Lillfjället gneiss, A=Avardo gneiss and E=Eastern Belt.

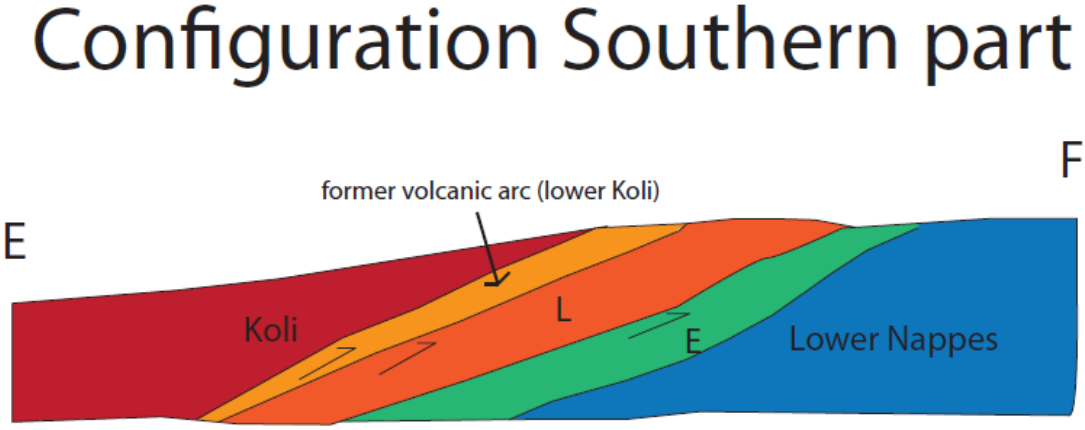

Figure 9-12 Simplified configuration as it is found nowadays in the Southern area. Only the Lillfjället gneiss is left in the southern part. L=Lillfjället gneiss and E=Eastern Belt.

10 Conclusion

- The high grade metamorphism of the Lillfjället gneiss is dated by the EMP monazite chemical age dating techniques. T=454.9 Ma, T_0=497.9 Ma and t=503.1 Ma with an uncertainty interval of +/- 20 Myr.
- The high grade metamorphism of the Avardo gneiss is dated by the EMP monazite chemical age dating techniques. T=409.3 Ma, T_0=502.3 Ma and t=512.7 Ma with an uncertainty interval of +/- 20 Myr.
- The high grade metamorphism of the Svartsjöbäcken schist is dated by the EMP monazite chemical age dating techniques. T=473.1 Ma, T_0=491.2 Ma and t=492.7 Ma with an uncertainty interval of +/- 22 Myr.
- All three units are interpreted to have formed during the same tectonometamorphic event. This is in agreement with the r^2 value.
- The high grade metamorphism of the Lillfjället and Avardo gneiss together is dated by the EMP monazite chemical age dating techniques. T=439.5 Ma T_0=499.5 Ma and t=507.2 Ma with an uncertainty interval of +/- 19 Myr.
- The monazites are interpreted to have formed during the Finnmarkian orogeny
- All ages are cross checked with a standard monazite where T_0=1132.7 Ma, t=1132.7 Ma and T=1144.5 Ma with an uncertainty interval of +/- 10 Myr. The standard monazite is dated 1125 Ma. So all monazite ages calculated are interpreted to be correct.
- The Lillfjället gneiss has undergone metamorphic conditions between 750 – 800 ºC and 9 – 10 kbar.
- The Lillfjället gneiss has two different mineral assemblages, M1 and M2: M1. garnet, muscovite, k-feldspar, biotite and plagioclase M2. muscovite and biotite.
- The stacking of the nappes is explained in a geodynamic model that shows two orogenic events, one stage at ~500 Ma and one stage at ~420 Ma.

11 Acknowledgement

This research was financially supported by Rinus Wortel/Ivau.

Second I want to thank Herman Van Roermund for all the help and support in the field and for the nice time we had there. I also want to thank Herman for paying all unexpected costs, for all help with the lab research, for leading me to the right direction in the research project, for all discussions about the results and for keeping me motivated.

I also want to thank Matthijs Hogerwerf for the support and nice time in the field and during the lab-research, especially during the lab-research we performed together at night. I also want to thank Matthijs for the good discussions and mental support when necessary.

Finally I want to thank all family, friends and roommates for the distraction, motivation and support when needed.

12 References

Bingen, B., H. Austrheim, M. Whitehouse, and W. Davis (2003), Geochronology of the Bergen Arcs eclogites, W. Norway: New SIMS zircon data and implications for Caledonian tectonic evolution, in The Alice Wain Memorial West Norway Eclogite Field Symposium, abstract volume, edited by E. A. Eide, Norg. Geol. Undersøk. Rep. 2003. 055, 15 – 16.

Bucher, K. & Frey, M. 2002. Petrgonesis of Metamorphic rocks, seventh edition, ISBN 3-540-43130-6

Brueckner, H.K. & Roermund, H.L.M. van, 2004. Dunk tectonics: a multiple subduction/eduction model for the evolution of the Scandinavian Caledonides. Tectonics 23; 1-20.

Brueckner, H.K. & Roermund, H.L.M. van, 2007. Concurrent HP metamorphism on both margins of Iapetus: Ordovician ages for eclogites and garnet pyroxenites from the Seve Nappe Complex, Swedish Caledonides. Journal of the Geological Society, London, Vol. 164, 2007, pp. 117–128

Carswell, D. A., H. K. Brueckner, S. J. Cuthbert, K. Mehta, and P. J. O'Brien (2003b), The timing of stabilization and the exhumation rate for ultrahigh pressure rocks in the Western Gneiss Region of Norway, J. Metamorph. Geol., 21, 601 – 612.

Cocherie A, Albarede F. 2001. An improved U-Th-Pb age calculation for electron microprobe dating of monazite. *Geochim. Cosmochim. Acta* 65:4509–22

Cocherie, A., Legendre, O., Peucat, J-J., and Kouamelan, A.N., 1998, Geochronology of polygenetic monazites constrained by in situ electron microprobe Th-U-total Pb determination: implications for lead behaviour in monazite. Geochimica Cosmochimica Acta, 62, 2475.2497.

Cocks, L. R. M. & Torsvik, T. H. 2006. European geography in a global context from the Vendian to the end of the Palaeozoic, European Lithosphere Dynamics. Geological Society, London, Memoirs, 32, 83–95.

Cressey G, Wall F, Cressey BA. 1999. Differential REE uptake by sector growth of monazite. *Mineral. Mag*. 63:813–28

Ferry, J.M., Spear F.S., 1978. Experimentental calibration of the partitioning of Fe and Mg between biotite and garnet, Contribution to Mineral Petrology 66:113-117

Förster H.J., Harlov D.E., 1999. Monazite-(Ce)-huttonite solid solutions in granulitefacies metabasites from the Ivera-Verbano Zone, Italy. *Mineral. Mag*. 63:587–94

Gaál, G., Gorbatscheb, R., 1987, An Outline of the Precambrian Evolution of the Baltic Shield, Precambrian Research 35, p. 15-52

Gee, D.G., Fossen, H., Henriksen, N., Higgins, A.K., 2008, From the Early Paleozoic Platforms of Baltica and Laurentia to the Caledonide Orogen of Scandinavia and Greenland, Episodes, Vol. 31, No. 1

Gee, D.G., Juhlin, C., Pascal, C., Robinson, P., 2010, Collisional Orogeny in the Scandinavian Caledonides (COSC), GFF, 132: 1, 29 — 44.

Jenkins, R., X-Ray Fluorescence Spectrometry. 1988, John Wiley & Sons, Inc. QD96.X2J47 ISBN 0-471-83675-3.

Jercinovic M.J., Williams ML. 2005. Analytical perils (and progress) in electron microprobetrace element analysis applied to geochronology: background acquisition interferences, and beam irradiation effects. Am. Mineral. 90:526–46

Krogh, T., P. Robinson, and M. P. Terry (2003), Precise U-Pb zircon ages define 18 and 19 m. y. subduction to uplift intervals in the Averøya-Nordøyane area, Western Gneiss Region, in The Alice Wain Memorial West Norway Eclogite Field Symposium, abstract volume, edited by E. A. Eide, Norg. Geol. Unders. Rep., 2003. 055, 71 – 72.

Ludwig, K.R., 1993. A Computer Program for Processing Pb-U-Th Isotope Data, United States Geological Survey Open-File Report 88-542.

Montel, J.M. Foret, S. Veschambre, M. Nicollet C.and Provost A., 1996, Electron microprobe dating of monazite, Chem. Geol. 131 pp. 37–53.

Parrish RR. 1990. U-Pb dating of monazite and its application to geological problems. *Can. J. Earth Sci. J. Can. Sci. Terre* 27:1431–50

Pyle J.M., Spear F.S. 1999. Yttrium zoning in garnet: coupling of major and accessory phases during metamorphic reactions. *Geol. Mat. Res*. 1:1–49

Reed, S.J.B. 1996. Electron microprobe analysis and Scanning Electron Microscopy in Geology. Cambridge University press. 2nd Edition

Roberts, D. 2003. The Scandinavian Caledonides: Event chronology, paleogeographic settings and likely modern analogues, Tectonophysics, 365, 283 – 299.

Roberts, D. & Gee, D.G. 1985. An introduction to the structure of the Scandinavian Caledonides. In: Gee, D.G. & Sturt, B.A. (eds) The Caledonide Orogen—Scandinavia and Related Areas. Wiley, Chichester, 55–68.

Roermund, H.L.M. van & Bakker, E., 1984: structure and metamorphism of the Tången-Inviken area, Seve Nappes, Central Scandinavian Caledonides. Geologiska Föreningens I Stockholm Förhandlingar, Vol. 105[for 1983], Pt. 4, pp. 301-319. Stockholm. ISSN 0016-786X

Roermund, H. L. M. van (1989), High-pressure ultramafic rocks from the allochthonous nappes of the Swedish Caledonides, in The Caledonide Geology of Scandinavia, edited by R. A. Grayer, pp. 205 – 219, Graham and Trotman, Norwell, Mass.

Roermund, H.L.M. van, 2009, Mantle wedge garnet peridotites from the northernmost ultra-high pressure domain of the Western Gneiss Region, SW Norway, European Journal of Minerology.

Spear F.S., Kohn M.J., Cheney, J.T. (1999) P-T paths from anatectic pelites. Contirbution to Mineral Petrology 134:17-32.

Suzuki K. & Adachi M. 1991. The chemical Th-U-total Pb Isochron Ages of zircon and monazite from the Gray Granite of the Hida Terrane, Japan. J.Earth Sci. Nagoya Univ., 38; 11-38.

Sveriges Geologiska Undersokning Berggrundskartan (1991). C 689, 1-155.

Ten Grotenhuis S.M., Passchier C.W., Bons P.D., 2002, The influence of strain localization on the rotation behaviour of rigid objects in experimental shear zones, Journal of Structural Geology, 24:485-501.

Terry, M. P., P. Robinson, M. A. Hamilton, and M. J. Jercinovic (2000a), Monazite geochronology of UHP and HP metamorphism, deformation and exhumation, Nordøyene, Western Gneiss Region, Norway, Am. Mineral., 85, 1651 – 1664.

Torsvik, T.H., 1998. Palaeozoic palaeogeography: a North Atlantic viewpoint. Geol. Foren. Stockh. Forh. 120, 109–118.

Torsvik, T.H., Smethurst, M., Meert, J., Van der Voo, R., McKerrow, W.S., Brazier, M., Sturt, B.A., Walderhaug, H., 1996. Continental break-up and collision in the Neo-proterozoic and Palaeozoic—a tale of Baltica and Laurentia. Earth-Sci. Rev. 40, 229– 258.

Torsvik, T. H. & Cocks, L. R. M. 2005. Norway in space and time: a centennial cavalcade. Norwegian Journal of Geology, 85, 73–86.

Trouw, R.A.J., 1973, Structural Geology of the Marsfjällen area Caledonides of Västerbotten Sweden, Sveriges Geologiska Undersökning, årsbok 67 nr 7.

Voegelé V., Ando J.I., Cordier P., Liebermann RC. 1998a. Plastic deformation of silicate garnet I. High pressure experiments. Phys Earth Planet In, 108:305-318.

Wang Z, Ji S. 1999. Deformation of silicate garnets: Brittle ductile transition and its geological implications. Can Miner. 37:525-541.

Wei, C. J., Powell, R. 2004. Calculated phase relations in high-pressure metapelites in the system NKFMASH. Journal of Petrology 44, 183–202.

Wei, C. J., Powell, R. 2005. Calculated Phase Relations in the System NCKFMASH (Na2O–CaO–K2O–FeO–MgO–Al2O3–SiO2–H2O) for High-Pressure Metapelites, Journal of Petrology Advance Access published October 21, 2005

Williams ML, Jercinovic MJ, Goncalves P, Mahan KH. 2006. Format and philosophy for collecting, compiling, and reporting microprobe monazite ages. *Chem. Geol*. 225:1–15

Williams, L.M., Jercinovic, M.J. and Hetherington, J.C; 2007; Microprobe Monazite Geochronology: Understanding Geologic Processes by Integrating Composition and Chronology; Annual review of Earth Planetary sciences; 35:137-175.

Wing BA, Ferry JM, Harrison TM. 2003. Prograde destruction and formation of monazite and allanite during contact and regional metamorphism of pelites: petrology and geochronology. *Contribut. Mineral. Petrol*. 145:228–50

Wortel, M. J. R., and W. Spakman (2000), Subduction and slab detachment in the Mediterranean-Carpathian Region, Science, 290, 1910 – 1917

Zwart, H.J. 1974. Structure and metamorphism in the Seve–Köli Nappe Complex (Scandinavian Caledonides) and its implications concerning the formation of metamorphic nappes. In: Bellière, J. & Duchesne, J.C. (eds) Géologie des Domains Cristallins. Centenaire de la Société Géologique de Belgique, Liège, 129–144.